

**35<sup>th</sup> Conference on Radar Meteorology**  
**Short Course on Millimeter Wavelength Radars**  
**Spaceborne Cloud and Precipitation Radar Applications**

S. Tanelli - Jet Propulsion Laboratory, California Institute of Technology

Pittsburgh PA, Sept 2011

© 2011 California Institute of Technology. Government sponsorship acknowledged.



# Outline



- Millimeter Wavelength nadir-pointing Cloud Radars in space
  - The fundamental differences between spaceborne and ground/airborne.
  - CloudSat's Cloud Profiling Radar
  - Products and their use
  - EarthCARE's Cloud Profiling Radar
- Peculiarities of the spaceborne configuration.
  - Multiple Scattering (6 min)
  - Doppler measurements (6 min)
  - Non-Uniform Beam Filling
  - Pointing (6 min)
- Concepts for future spaceborne Atmospheric Radars
  - Dual Phase Center Antenna (3 min)
  - Geostationary applications (3 min)
  - Electronically scanning radars (3 min)



# Passive and Active Remote Sensing of the Atmosphere



## •Passive Systems

- Weighting functions derived from radiative transfer model equations applied to clear air atmospheric profiles lose validity in cloudy conditions.

$$B_t(\nu) = \int_0^{\infty} \alpha(\nu, z) \cdot B[\nu, T(z)] \cdot e^{-\tau(\nu, z)} dz + B_s[\nu, T(z)] \cdot e^{-\tau(\nu, 0)}$$

$$\tau(\nu, z) = \int_z^{\infty} \alpha(\nu, \xi) d\xi$$



## •Active Systems

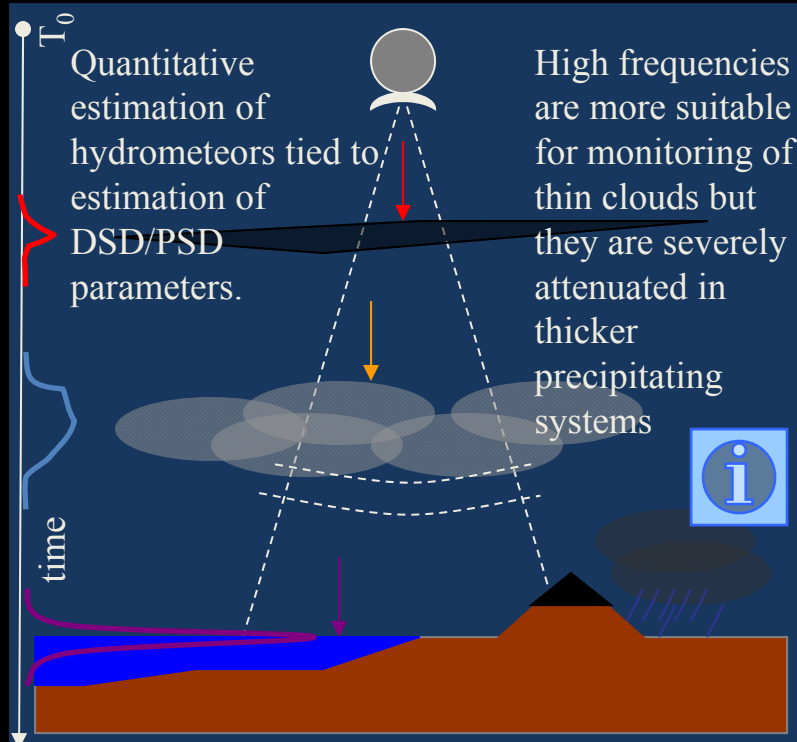
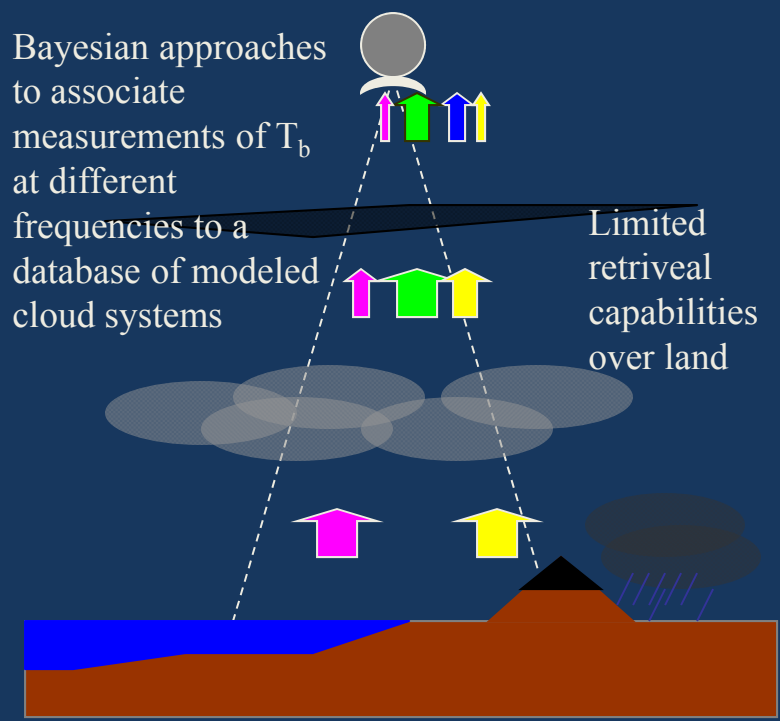
- ‘Attenuating frequencies’ are used for spaceborne applications
- Rayleigh scattering approximation almost never valid

$$P(t, \nu) = \frac{1}{2} \sum_{i,k} A_i A_k^* W_i W_k^* e^{-j4\pi \frac{(r_i - r_k)}{\lambda}}$$



Bayesian approaches to associate measurements of  $T_b$  at different frequencies to a database of modeled cloud systems

Limited retrieval capabilities over land





# Basics: Spectral Radiance and Brightness Temperature



- Microwave emission from atmospheric gases follows the Rayleigh-Jeans approximation of Planck's Law
- for Blackbody spectral radiance (good within 1% for Earth's atmosphere under 100GHz)

$$B(\nu, T) = \frac{2h}{c^2} \frac{\nu^3}{e^{h\nu/(kT)} - 1} \xrightarrow{h\nu \ll kT} B(\nu, T) \cong \frac{2kT\nu^2}{c^2}$$

$$h = 6.6262 \cdot 10^{-34} \text{ J s}, k = 1.3807 \cdot 10^{-23} \text{ J K}^{-1}, c = 2.99792458 \cdot 10^8 \text{ m s}^{-1}$$

related quantities and expressions

$$B(\lambda, T) = \frac{\lambda^2}{c} B(\nu, T) : \text{spectral radiance in waven gth}; S = \pi B : \text{spectral emittance}$$

The Rayleigh-Jeans approximation is commonly used to convert spectral radiance measurements into the 'equivalent' Brightness Temperatures.

$$(T_a, T_s) \rightarrow B_a(\nu) + B_s(\nu) \cdot e^{-\tau_a(\nu)} = B_t(\nu) \xrightarrow{R-J} \tilde{T}_t(\nu)$$

Almost all profiling algorithms based on Passive Remote Sensing Systems operate on brightness temperatures: consistency between the retrieval model and forward model must be checked.

$$T_t(\nu) = T_a(\nu) + T_s(\nu) \cdot e^{-\tau_a}$$

$$T_a(\nu) = \int_0^{\infty} W(\nu, z) T(z) dz; \quad W(\nu, z) = \alpha(\nu, z) \cdot e^{-\int_z^{\infty} \alpha(\nu, z') dz'}$$





# Basics: Reflectivity to Equivalent Reflectivity Factor...and back



$$P_{Rx}(t) = \frac{\lambda^2 P_{Tx}}{(4\pi)^3} \int_V \frac{G^2(\Omega) \eta(r, \Omega) e^{-2\gamma(r, \Omega)}}{r^2} |u(t - 2r/c)|^2 d\Omega dr$$

## •Equivalent Reflectivity Factor

- Which reflectance was used in Level 0 processing?
  - At Ku band and below, water,  $0.93 \pm 0.01$  for all temperatures
  - At Ka band, water,  $0.91 \pm 0.01$  for non supercooled water
  - At W band, water, 0.68 at 0C, 0.75 at 10C, 0.81 at 20C, 0.85 at 30C
  - All bands, ice, 0.176

$$Z_e = \frac{\lambda^4}{\pi^5 |K_w|^2} \eta$$

$$\eta = \int_0^{D_{\max}} \sigma_b(D) N(D) dD$$

$$\sigma_b(D) = \frac{\pi^5}{\lambda^4} D^6 |K_{\#}|^2 \text{ i}$$

$$\sigma_b(D) = \frac{\lambda^2}{2\pi} \left| \sum_{m=1}^{\infty} (2m+1)(-1)^m (a_m - b_m) \right|^2$$





# Basics: Index of Refraction to Reflectance



- Relative dielectric constant of water:  $\epsilon_r = \epsilon/\epsilon_0$
- Index of refraction:

$$n^2 = \frac{c^2 k^2}{\omega^2} = \epsilon + \frac{4\pi\sigma}{\omega} i$$

$$n = \begin{cases} \frac{c}{v_{phase}} & v_{phase} = \frac{\omega}{k}; k = \frac{2\pi}{\lambda} \text{ (usually!) wavenumber} \\ \sqrt{\epsilon\mu} = \sqrt{\epsilon_r\mu_r} & \begin{cases} \omega = 2\pi f \text{ angular frequency} \\ \epsilon = \epsilon_0\epsilon_r \text{ electric permittivity (MKS)} \\ \mu = \mu_0(1 + \chi_m) \text{ magnetic permeability (MKS)} \\ \epsilon_r = \text{(relative) dielectric constant} \\ \mu_r = (1 + \chi_m) = \text{relative permeability} \end{cases} \end{cases}$$

Maxwell's relation for the Index of refraction (assumes  $\mu=\mu_r=1$ ):

$$n \cong \sqrt{\epsilon} \cong \sqrt{\epsilon_r}$$

Reflectance of water in air  
(from Fresnel equations):

$$|K|^2 = \left| \frac{(n^2 - 1)}{(n^2 + 2)} \right|^2 = \left| \frac{(\epsilon_r - 1)}{(\epsilon_r + 2)} \right|^2$$





# Basics: Gaseous absorption by H<sub>2</sub>O and O<sub>2</sub> in the microwave region



- Liebe's forward model of resonant and non-resonant gaseous absorption is valid up to 1THz.
- HITRAN and other databases report all known molecular absorption lines and their characteristics. Doppler broadening and collisional broadening are calculated through standard models

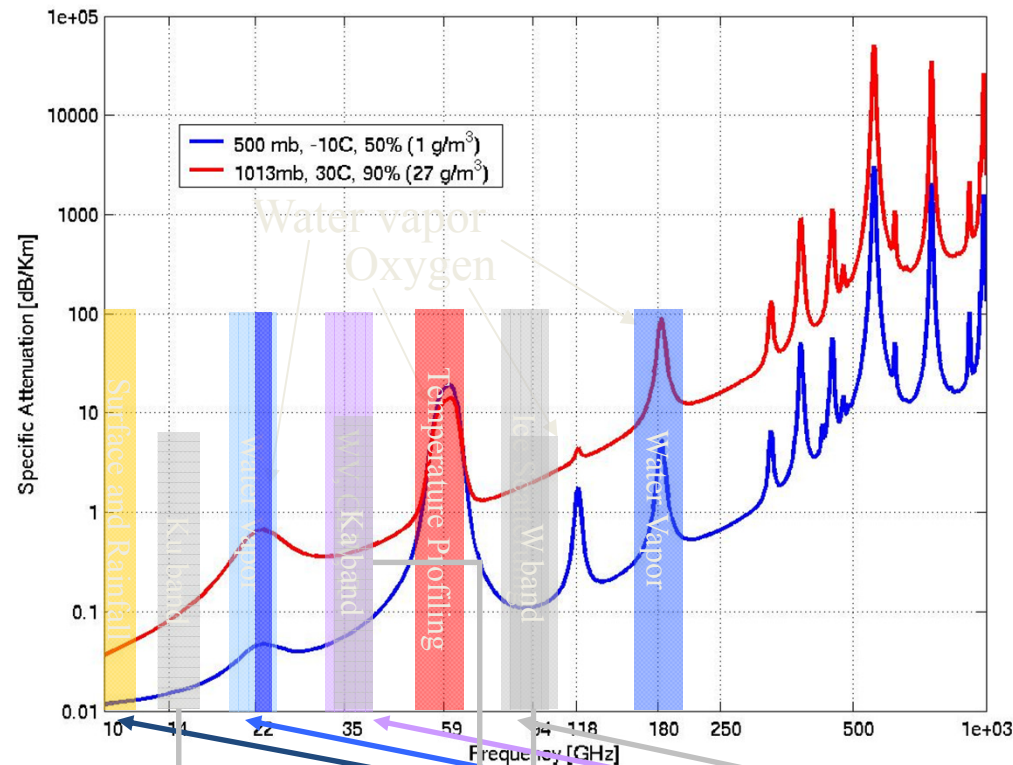


Table 1. AMSR-E PERFORMANCE CHARACTERISTICS

CENTER FREQUENCIES (GHz)	6.925	10.65	18.7	23.8	36.5	89.0
	350	100	200	400	1000	3000
	0.3	0.6	0.6	0.6	0.6	1.1
(km)	56	38	21	24	12	5.4
	74 x 43	51 x 30	27 x 16	31 x 18	14 x 8	6 x 4
SAMPLING RATE	10 x 10	10				0.5 x 0.5
	2.6					1.3
	95.3					96.0
	2.2	1.4	0.8	0.9	0.4	0.18

Rainfall: light to strong

Snowfall: strong

Clouds: embedded hydrometeors

Rainfall: very light to moderate

Snowfall: light to strong

Clouds: optically thick

Rainfall: drizzle to light

Clouds: optically thin





# Frequency Bands for Passive Remote Sensing



Frequency band (GHz)	Instrument	Measurement use
6.6–6.9	ADEOS-II AMSR	Sea surface temperature, rainfall
10.5–10.9	TRMM-TMI, ADEOS-II, AMSR, EOP-PM AMSR-E	Sea surface temperature, surface winds, precipitation
18.5–19.	5 SSM/I, TRMM-TMI, ADEOS-II AMSR EOP-PM AMSR-E	Surface winds, cloud water, rain, water vapor
21.3–24	SSM/I, TRMM-TMI, ADEOS-II AMSR AMSU-A EOP-PM AMSR-E	Water vapor line, integrated water vapor
31–34	Up-looking radiometric profilers	Water vapor line, water vapor profiling
36.5–37.2	SSM/I, TRMM-TMI, ADEOS-II AMSR EOP-PM AMSR-E	Cloud water, rainfall
50.0–50.4	ADEOS-II AMSR AMSU-A, SSM/T1	Oxygen absorption line, temperature
52.6–59.3	AMSU-A, SSMI/S	Oxygen absorption line, temperature
85.5–89.0	SSM/I, TRMM-TMI, AMSU-B, ADEOS-II AMSR AMSU-A, EOP-PM AMSR-E	Rainfall—particularly over land areas, clouds, ice and snow
115.25–122.25		Oxygen absorption line, temperature
150	SSM/T2, AMSU-B	Snow and other surface parameters, cloud parameters, water vapor sounding
155.5–158.5	MHS	Water vapor and cloud parameters for water vapor sounding
164–168		Cloud water, rain ice
174.8–191.8	SSM/T2, AMSU-B, MHS	Water vapor line, water vapor profiling
220, 340, 440	Geostationary sensors	Radiative balance, cirrus particle sensing

ADEOS—Advanced Earth Observing Satellite AMSR—Advanced Microwave Scanning Radiometer EOP-PM—Earth Observing System-P.M. ESTAR—Electronically Scanning Thinned Array Radiometer MHS—Microwave Humidity Sounder SSM/I—Special Sensor Microwave/Imager SSM/T1—Special Sensor Microwave/Temperature SSM/T2—Special Sensor Microwave/Water Vapor Profiler TRMM—Tropical Rainfall Measuring Mission TMI—TRMM Microwave Imager



# Frequency Bands for Active Remote Sensing



Band name	Nominal frequency range	Effective frequency range
L	1 ÷ 2 GHz	1.215 ÷ 1.4 GHz
S	2 ÷ 4 GHz	2.3 ÷ 2.5 GHz, 2.7 ÷ 3.7 GHz
C	4 ÷ 8 GHz	5.25 GHz ÷ 5.925 GHz
X	8 ÷ 12 GHz	8.5 ÷ 10.68 GHz
K <sub>u</sub>	12 ÷ 18 GHz	13.4 ÷ 14 GHz, 15.7 ÷ 17.7 GHz
K	18 ÷ 27 GHz	24.05 ÷ 24.25 GHz
K <sub>a</sub>	27 ÷ 40 GHz	33.4 ÷ 36 GHz
mm	40 ÷ 300 GHz	

Attenuating Frequencies





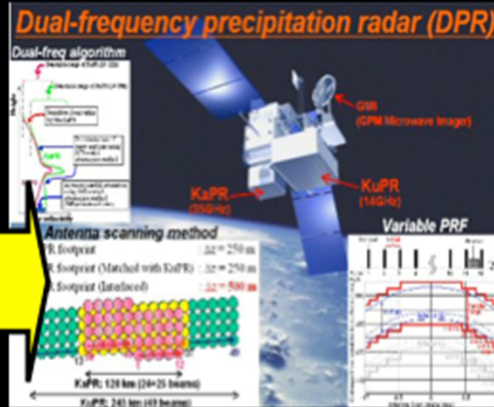
# Cloud and Precipitation Radars in Space



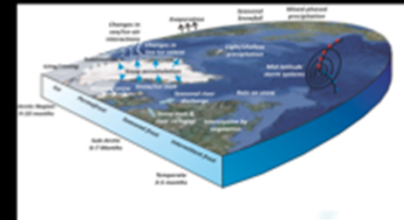
**TRMM/PR – NICT/JAXA**  
Ku, Scanning, Tropical Rain



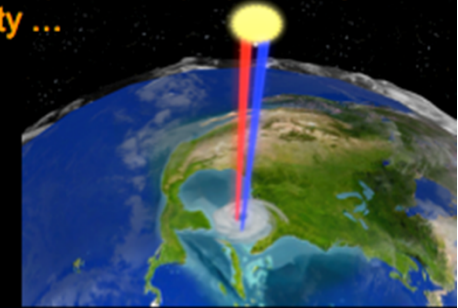
**GPM/DPR – NICT/JAXA**  
Ku/Ka, Scanning, Precipitation



Some concepts under development or proposed by the international community ...



**SnowSat / PPM**  
W/Ka, (Doppler)



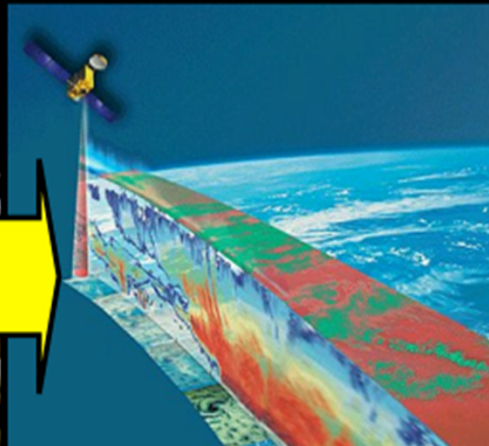
**NIS**  
W/Ka, Scanning,  
Doppler, GEO

**CloudSat/CPR – JPL/NASA/CSA**  
W, -30dBZ, Clouds

2006 -Today

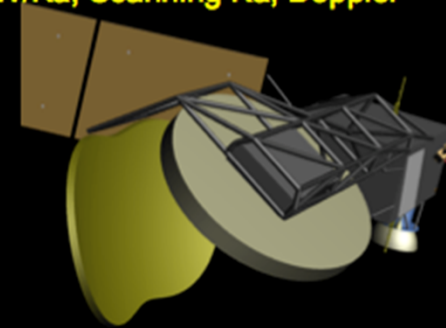


**EarthCARE/CPR – NICT/JAXA**  
W, Doppler, Clouds

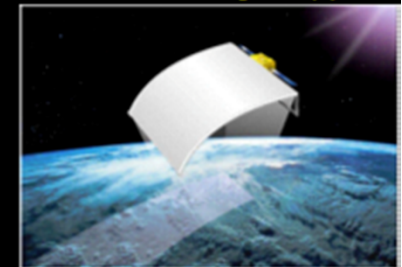


**ACE Radar**  
W/Ka, Scanning, Doppler

**ACE – ACERAD concept**  
W/Ka, Scanning Ka, Doppler

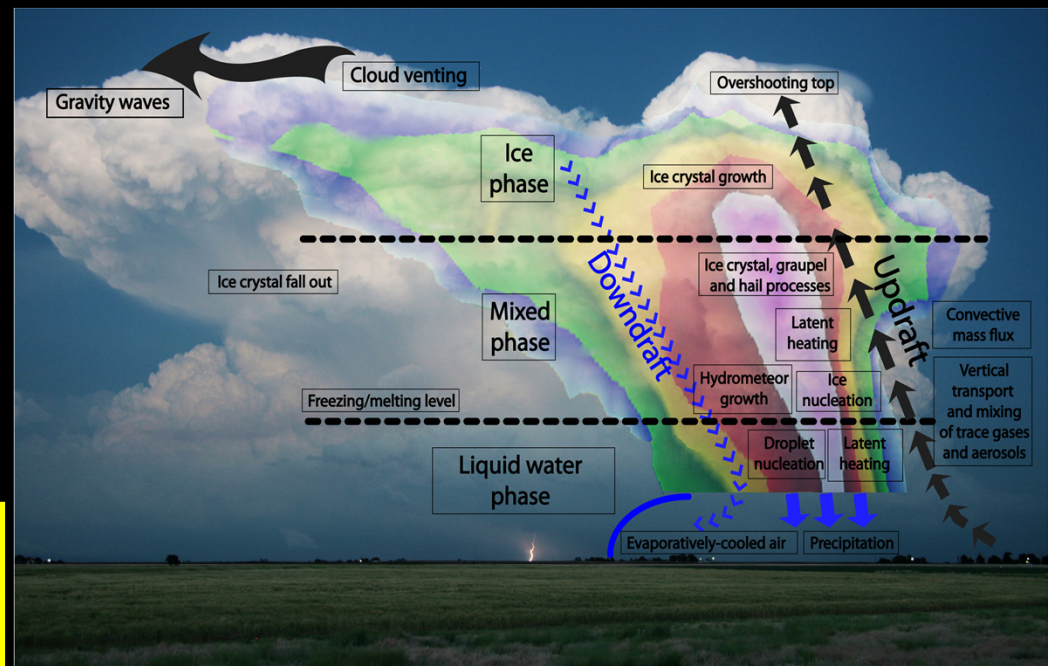


**ACE – Phased Array concepts**  
W/Ka, Scanning, Doppler





# Science Driver – Process Study



**Consistent with the findings of the US Earth Science Decadal Survey Report, 2007.**

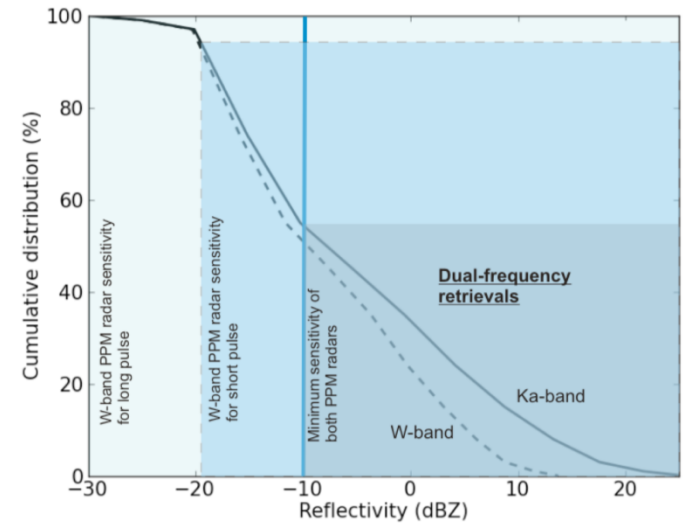
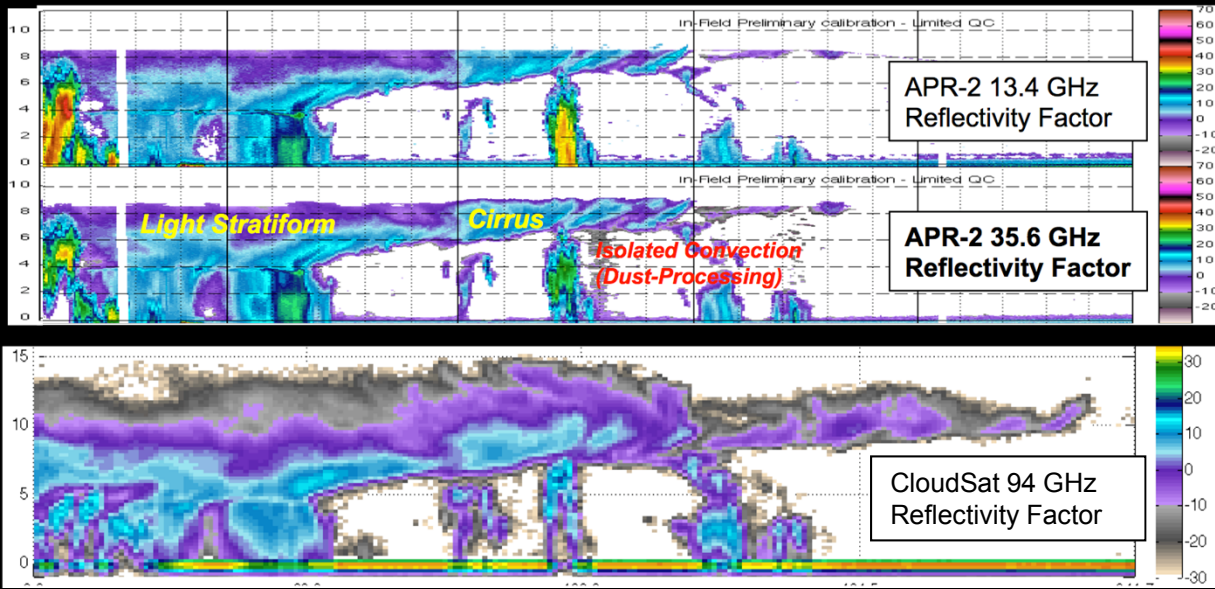


# Choices of Radar Frequencies (1)





# Choices of Radar Frequencies (2)





# Millimeter wave cloud radars in space



## The two fundamental differences wrt ground and airborne applications



- Distance from nearest target is at least 300 km
  - In radar Equation terms this is a whopping -109 dB hit to the sensitivity, at least.
  - Refer to the radar equation, how to mitigate this problem?
    - Larger antenna (limited by costs and feasibility of large antennas with accurate surface)
    - More power (limited by the power available on the spacecraft and by thermal dissipation, this can be achieved by means of higher peak powers or higher duty cycles)
    - Lower losses (limited by technology and engineering)
    - Higher frequency (impacts all the above)
  - No blind range problems
    - The last generation of ground and airborne cloud radars employ a mix of long and short pulses to optimize coverage of range between 0 and maximum distance. This is not necessary for spaceborne radars.
  - Mm-wave radars are not particularly affected by this (wrt lower frequency radars)
    - this distance is in near vacuum
    - However, the resulting large footprints are more prone to second order effects such as Non-Uniform Beam Filling and Multiple Scattering
- In LEO (formally 160-2000 km, in practice for Earth Remote Sensing platforms 300-1400 km) the platform moves at 7 to 7.6 km/s.
  - Integration times tend to be much shorter
    - Scanning exacerbates this problem
  - Platform movement introduces significant broadening and/or biasing in Doppler measures
  - Given a cloud system of 1000 km, a ground based radar requires at least 6 hours to capture its structure, an airborne radar at least 1 hour, a LEO radar less than 3 minutes.

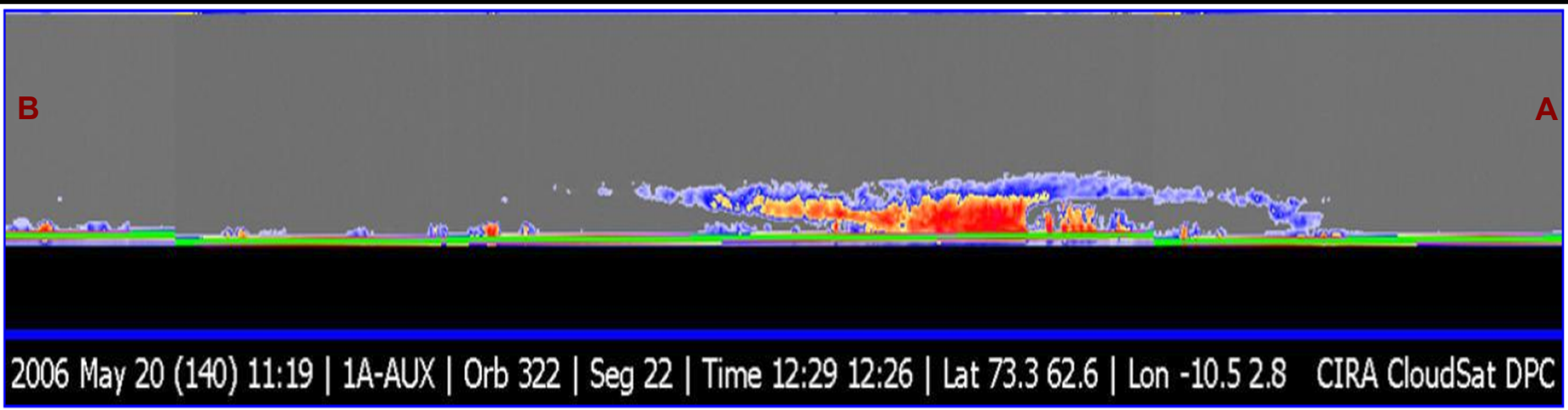
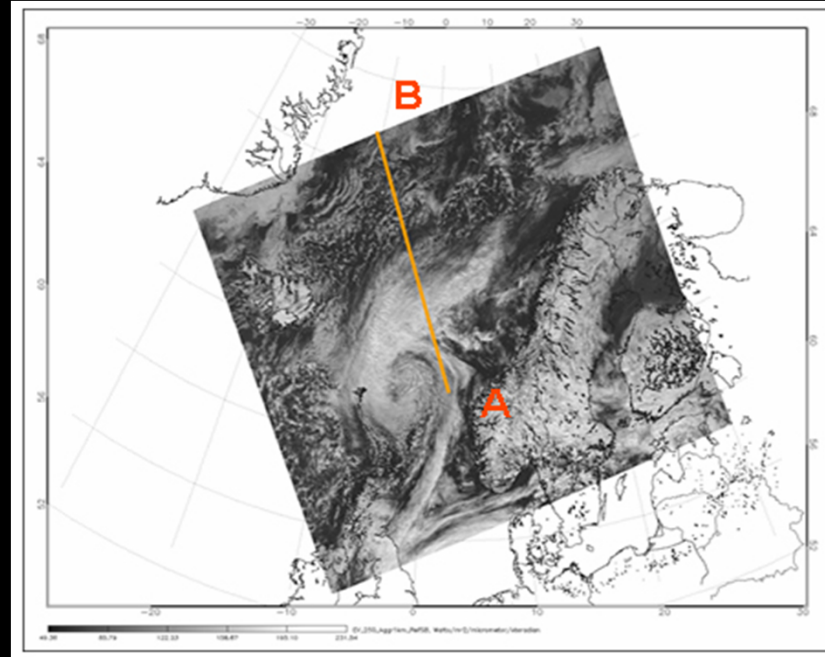


# First Images of CPR on May 20, 2006 (1)



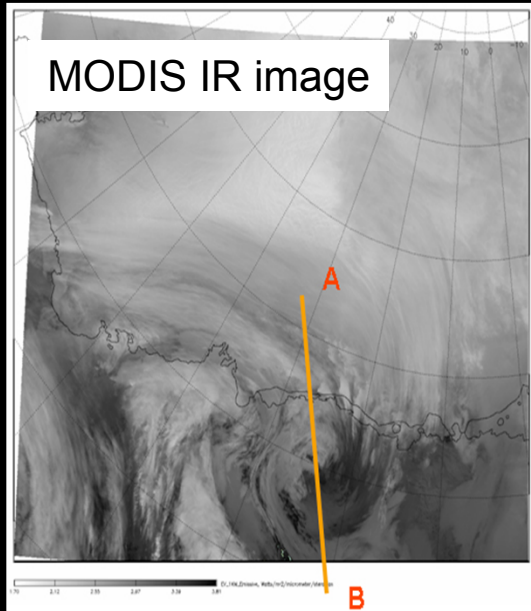
## Warm Front Storm Over the Norwegian Sea: 12:26-12:29 UTC

MODIS Visible image



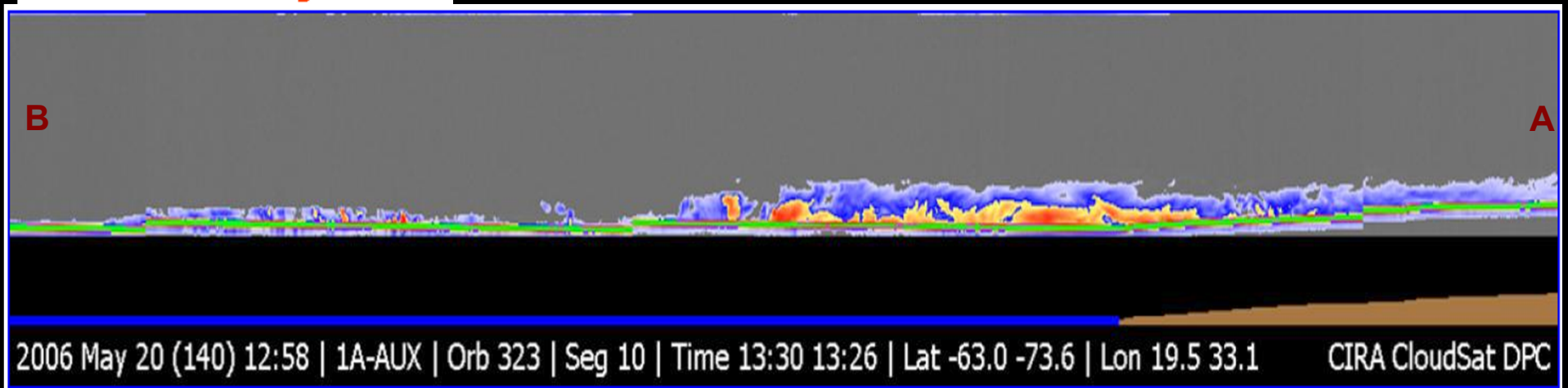


# First Images of CPR on May 20, 2006 (2)



## Polar Night Storm Near Antarctica: 13:26-13:30 UTC

CloudSat image of a horizontal cross-section of a polar night storm near Antarctica. Until now, clouds have been hard to observe in polar regions using remote sensing, particularly during the polar winter or night season.





# CloudSat Mission

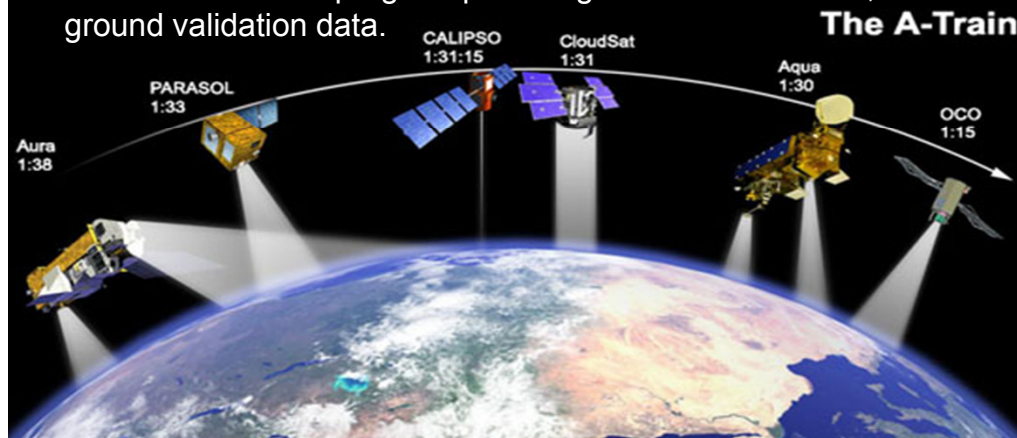


## Mission Features

- First spaceborne 94-GHz Cloud Profiling Radar (CPR)
- Ball Aerospace's RS-2000 spacecraft bus
- Flies in the A-Train formation with EOS Aqua and Calipso (705 km altitude, sun sync orbit)
- Launch date: April 28, 2006
  - Successfully completed Prime Mission in Feb 2008
- CloudSat Mission PI: Graeme Stephens (CSU)
- CPR is jointly developed by NASA/JPL and CSA
- USAF Kirtland AFB provides Missions Operations
- CSU's Cooperative Institute for Research in Atmosphere (CIRA) processes CloudSat science data
- ECMWF and ARM program provide global forecast fields, and ground validation data.

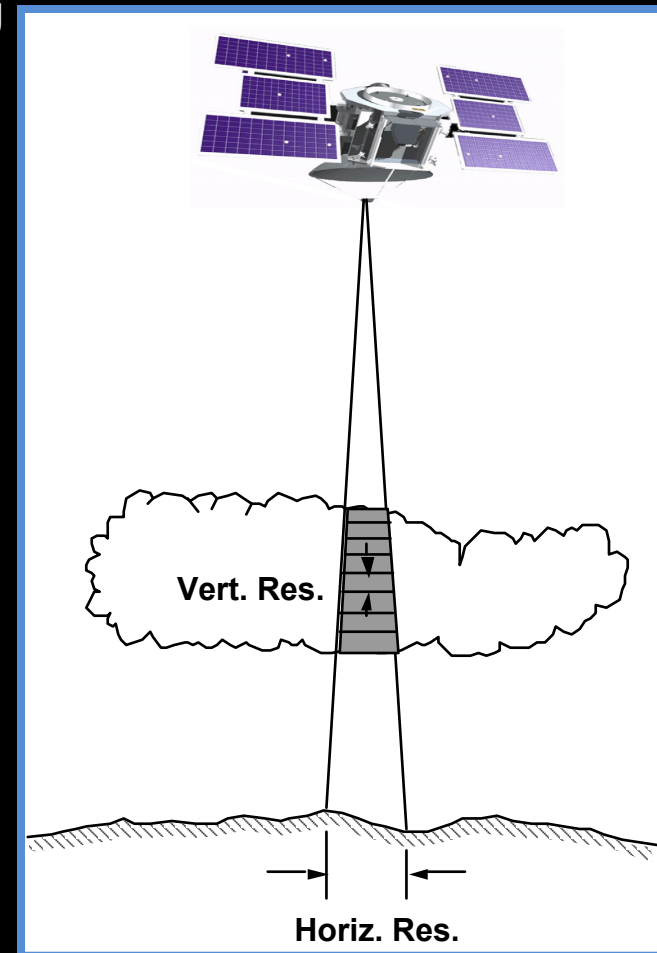
## Objectives

- Measure vertical structure of clouds and quantify their ice and water content
- Improve weather prediction and understanding of climatic processes
- Investigate the effect of aerosols on clouds and precipitation
- Investigate the utility of 94 GHz radar for spaceborne remote sensing





- Nadir-pointing 94-GHz radar
  - Measure cloud reflectivity vs. altitude profile along nadir track
- One science operation mode
  - Vertical resolution  $\sim 500$  m
    - Transmits  $3.3\text{-}\mu\text{s}$  monochromatic pulses
  - Horizontal resolution  $\sim 1.4$  km
    - Uses 1.85-m dia. antenna
- Sensitivity of  $-28$  dBZ (nominal) is achieved by:
  - High peak power, large antenna, low-noise receiver, and pulse-averaging
- Dynamic range: 80 dB
  - To capture low reflectivity clouds and surface return
  - Height window: 25 km
- Technical resource allocations:
  - Mass: 250 kg
  - Power: 230 W
  - Data rate: 25 kbits/sec
  - Share with spacecraft within DPAF envelope





## 2: CPR's heritage



- Scientifically, CloudSat CPR demonstrated that:
  - We can profile clouds from Space
  - Such profiles contain information that cannot be obtained otherwise on a global scale and is critical for weather and climate modeling (e.g., precipitation efficiency, heating budget of multi-layer clouds, frozen precipitation over polar regions).
- Technologically, CloudSat CPR demonstrated
  - Use in space of W-band High Power Amplifiers (EIK and related HVPS)
    - Miniaturization of HVPS could provide significant benefits for multi-frequency, or multi-polarization missions in terms of instrument size and mass.
    - Improved efficiency of HPA could also benefit such missions.
    - Increase in EIK RF Peak power is unlikely to be a major driver.
    - Increased lifetime is more interesting.
    - The EarthCARE mission is addressing some of these points.
  - Use of low-loss QOTL and high-efficiency antenna at W-band
    - Larger antenna is key to improved resolution, sensitivity and Doppler accuracy.
    - Scanning capability is requested, but very challenging at W-band.
    - Multi-frequency operation is also requested.
    - The ACERAD IIP (S. Durden PI) is addressing these points.



## CPR's heritage: the highest priority improvements

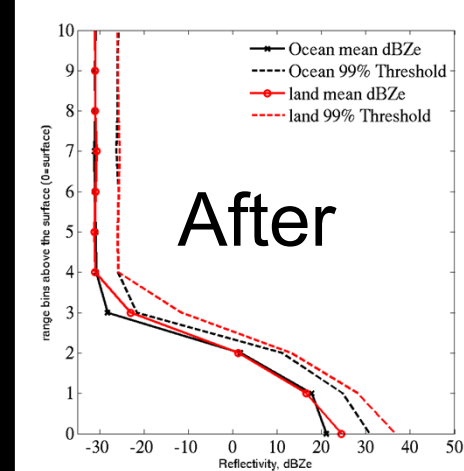
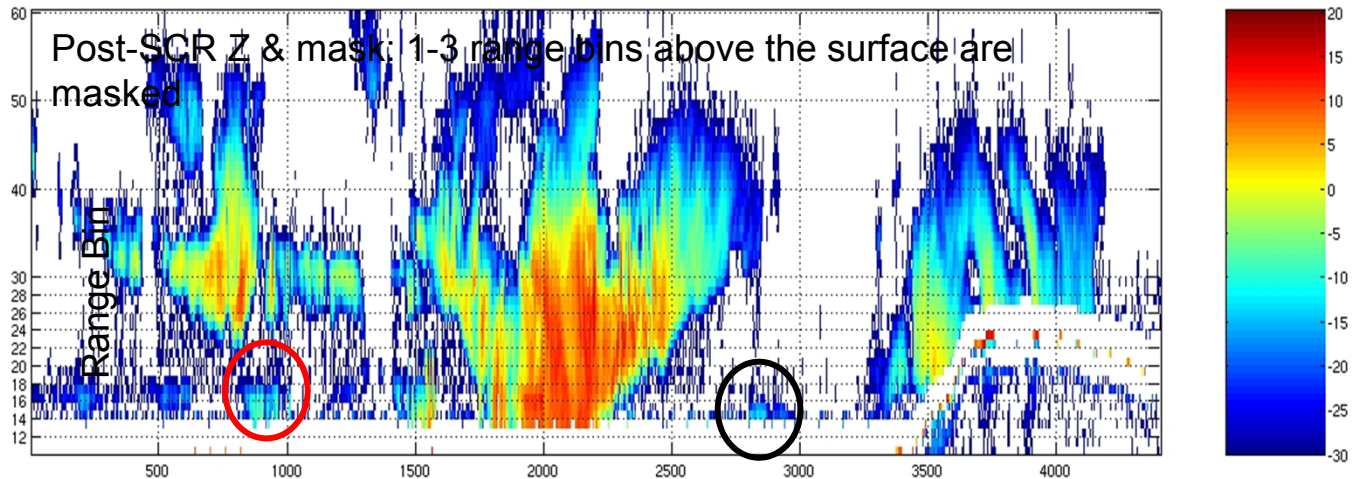
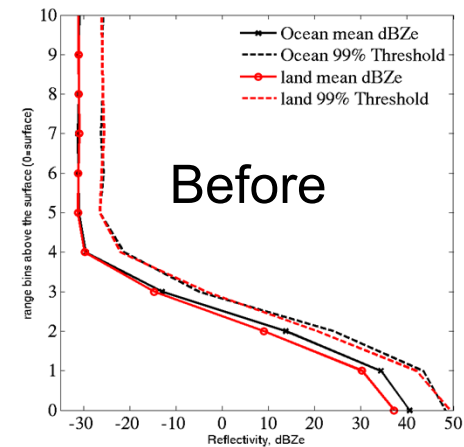
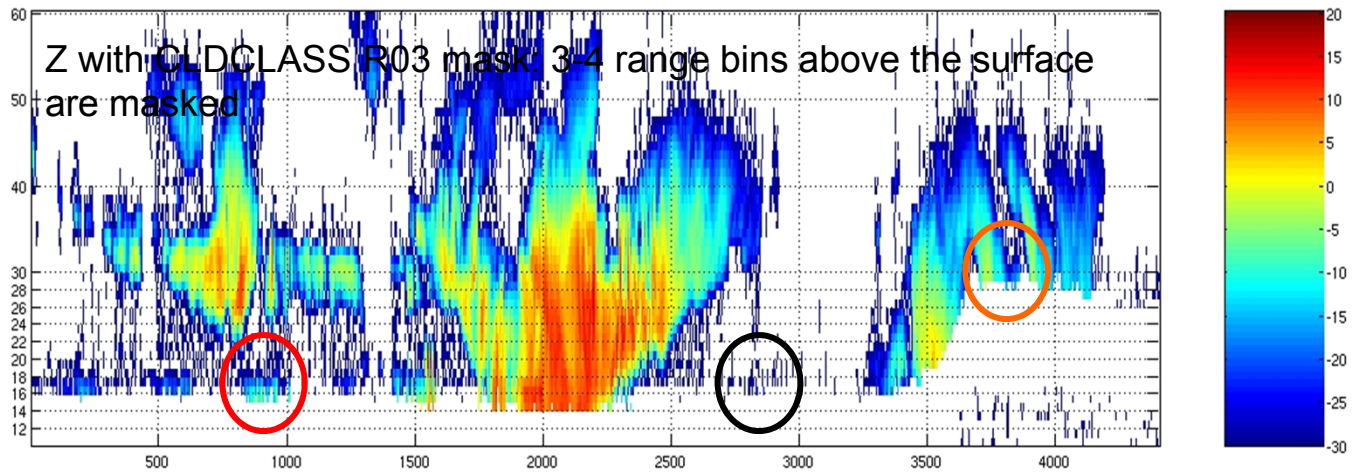


A few selected topics:

- ① CloudSat's sensitivity is adequate to observe a large portion of earth's clouds, but the 500 m range resolution prevents observation of near surface precipitation and often cloud base.
  - ① EarthCARE CPR will mitigate the surface clutter problem but not enough to address this need.
  - ② GPM/DPR and TRMM/PR have a 250m range resolution but their sensitivity is limited to approximately +17 dBZ.
- ② **Lack of Doppler measurements hinders classification of precipitating vs non-precipitating clouds, snow vs rain, characterization of convection, etc.**
  - ① **EarthCARE will demonstrate**
- ③ **Single-frequency measurements**
- ④ **Scanning**



# 1: Range Resolution & Ground Clutter





## CPR status (1)



As of April 14, 2011 CPR was operating at better than required performance. It was properly commanded OFF by the Spacecraft Autonomous Fault Response on April 15. It is currently in Survival Mode, all temperatures are compliant with this configuration.

- April 2011 estimated MDR (Minimum Detectable Reflectivity):
  - -27.3 to -28.4 dBZ. BOL requirement: -28dBZ, EOL requirement: -26 dBZ.
- Losses from beginning of life, budget:
  - RF Output power (EIK aging): 1.6 dB
  - Reduced pulses: 0 to 1.1 dB
    - CPR minimum detectable sensitivity was reduced in Jan 2010, to compensate for a damaged element in the spacecraft battery. Reduction due to reduced number of integrated pulses. It is variable within an orbit and has been adjusted according to seasons and spacecraft status. It is reversible.
  - Receiver: gain loss ~0.1 dB (does not affect MDR), NF increase: < 0.1 dB.



## CPR status (2)



- High Power Amplifier (Still on primary side, redundant pair not used in orbit yet)
  - Extended Interaction Klystron (EIK):
    - Aging is progressing at (and beyond) 'best in class' expectations.
    - EIK switchover rule defined with STM and ADWG: whenever linear extrapolation will predict violation of EOL MDR requirement (-26 dBZ) within 6 months.
  - High Voltage Power Supply (HVPS):
    - Performed flawlessly: successfully exercised autonomous fault protection 11 times (the last one being August 25<sup>th</sup> 2009). No sign of thermal runaway or deterioration.
- Receiver is performing well beyond requirement, with the exception of the internal calibration source which has performed marginally vs requirement.
  - Marginal performance of calibration source did not affect end-to-end system stability assessment: 4 year analysis of Earth surface targets (ocean and deserts) indicates that estimated end-to-end stability is accurate within  $\pm 0.2$  dB.
- All other electronics & antenna: everything nominal, no impact on mission performance, no unexpected trends.



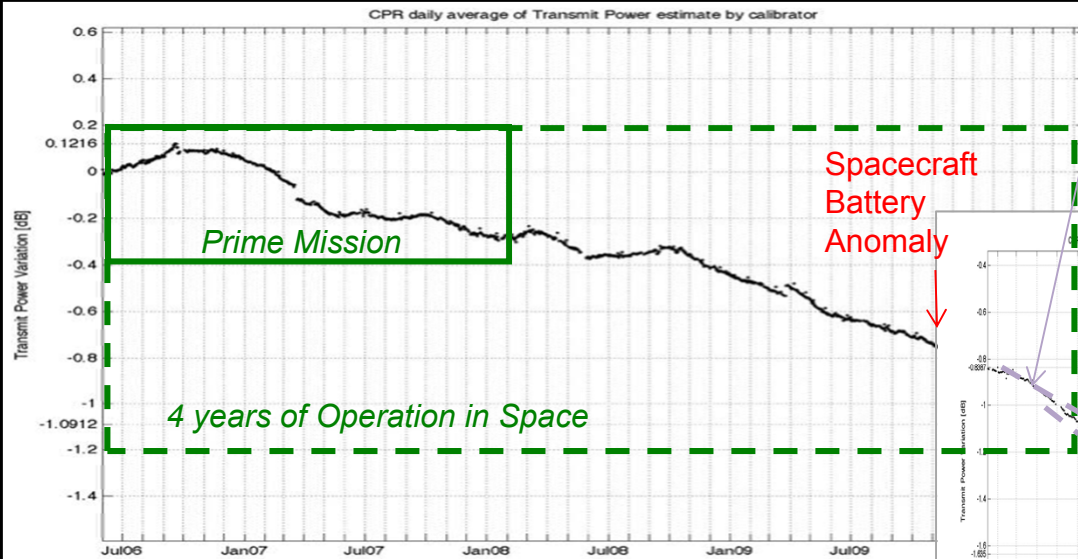
# CPR EIK performance and Minimum Detectable Reflectivity forecast



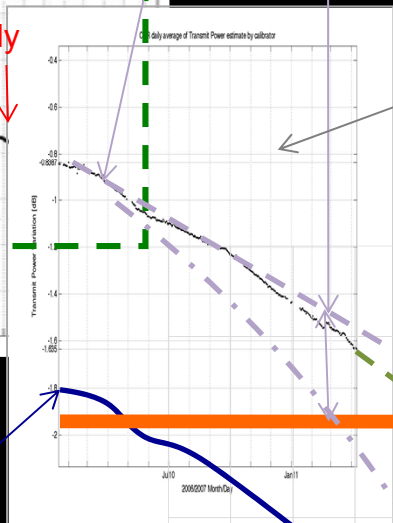
**March 2010 forecast of range of RF power reduction:**

- best case forecast (purple dash): ETA BOL MDR\* ~Nov 2011.
- worst case forecast (purple dot-dash) : ETA BOL MDR\* ~Feb 2011

\* Minimum detectable reflectivity (MDR): MDR' is calculated at orbital minimum number of integrated pulses before Dec 2009.



**March 2011 actuals:** in-flight data show MDR' close to the best case forecast. Orbit-Averaged Transmit power as measured by calibrator dropped ~1.6 dB (as of end of Mar 2011) corresponding to a MDR' of about -28.4 dBZ.



- Operations resumed with less pulses, adapting to season and battery status.
- MDR" (minimum number of integrated pulses adopted ever – i.e. during ~15% of each orbit in the Jan-Apr 2011 period) is ~1dB below MDR'.
- The radar sensitivity at any given time is between MDR' and MDR".

**APRIL 2011 FORECAST OF RADAR SENSITIVITY:**

- MDR" will reach EOL MDR requirement between Dec 2011 and summer 2012.
- EIK switchover planned for winter 2011/2012.

**-28 dBZ  
BOL MDR Req.**

**MDR' best case forecast**

**-26 dBZ  
EOL MDR Req.**

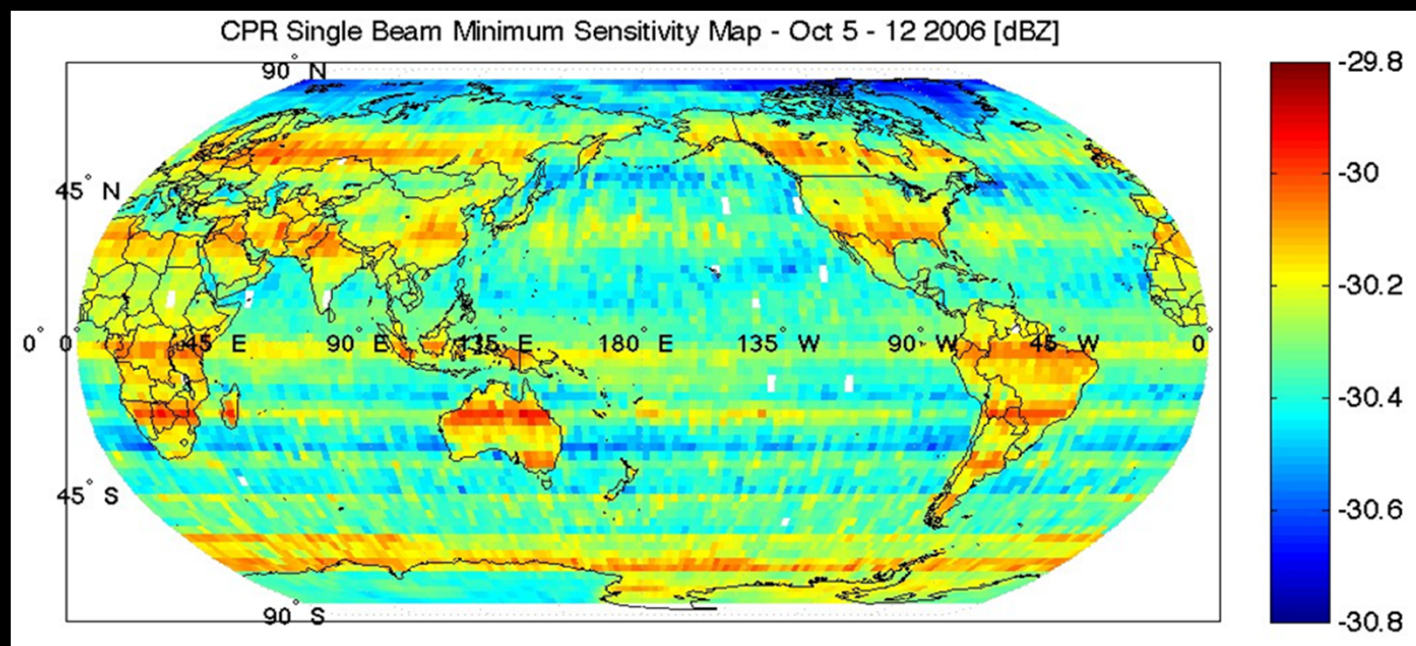
**MDR" worst case forecast**



# CPR Minimum Detectable Reflectivity Factor



- Minimum detectable Z is not constant over the globe and across the seasons. It depends on:
  - Radiometric temperature of the observed scene (~0.8 dB swing)
  - Algorithm used to estimate noise floor
  - Number of pulses per averaging period (latitude dependent)
  - System overall performance (no hardware degradation so far)
- Example: Pre-launch tuning & calibration coefficients, 0.16s along-track integration
  - Minimum detectable reflectivity in the -30 to -31 dBZ range

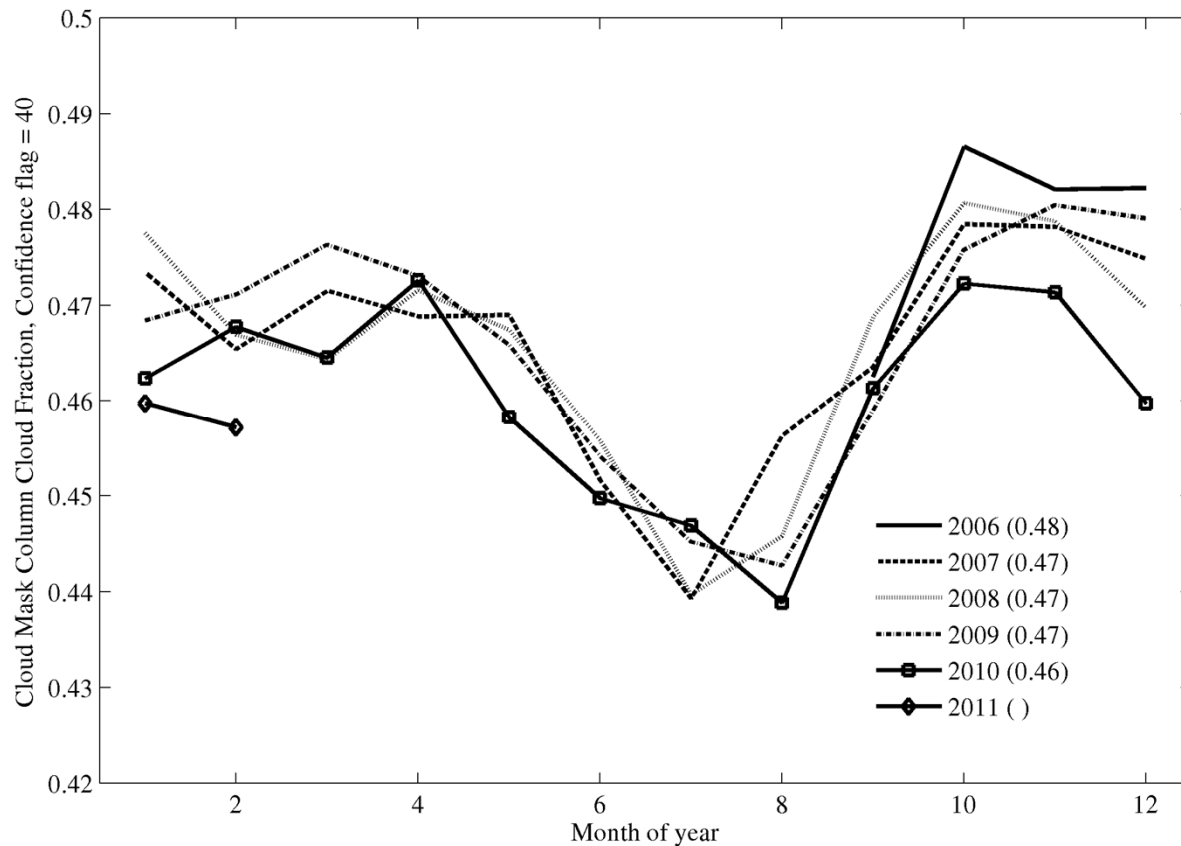




# Impact of changing sensitivity on long term climatological analyses

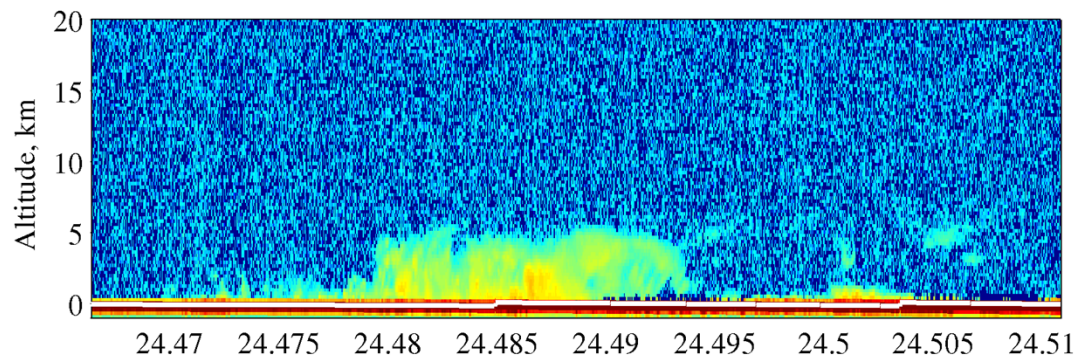


Cloud Mask confidence values depend on the Signal/Noise ratio. So cloud amount with respect to the confidence values will change over time !

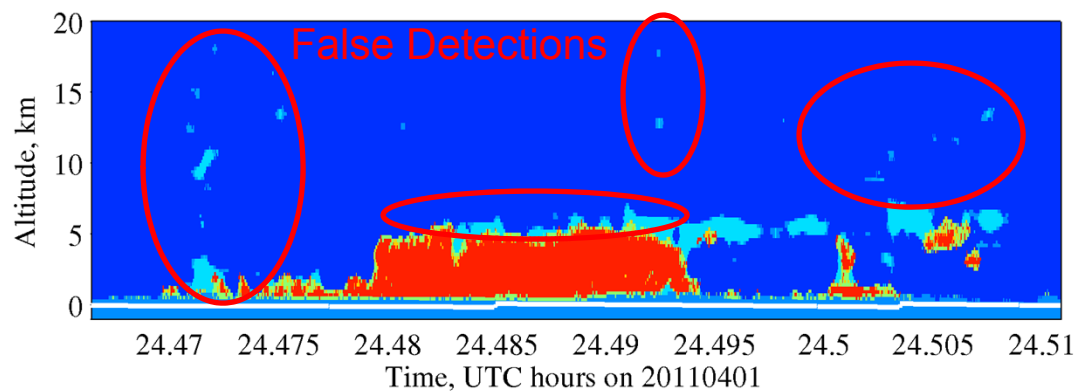




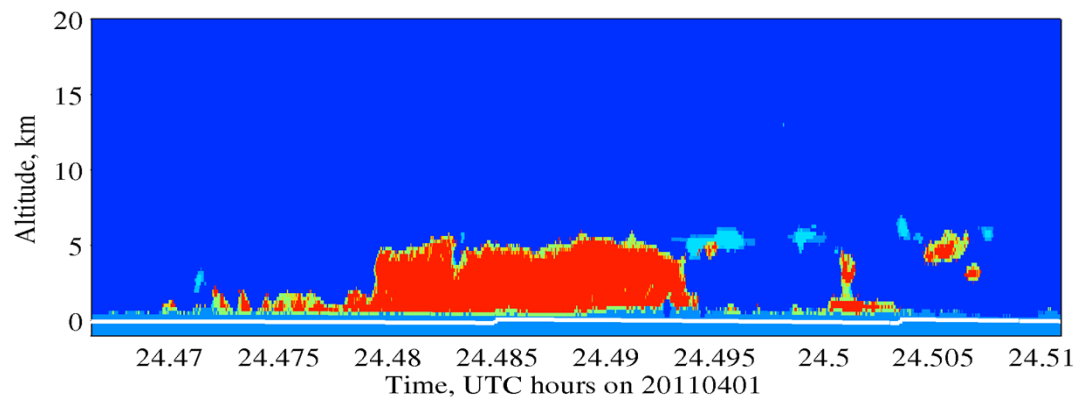
# Example of reduction in false detection rate



R04

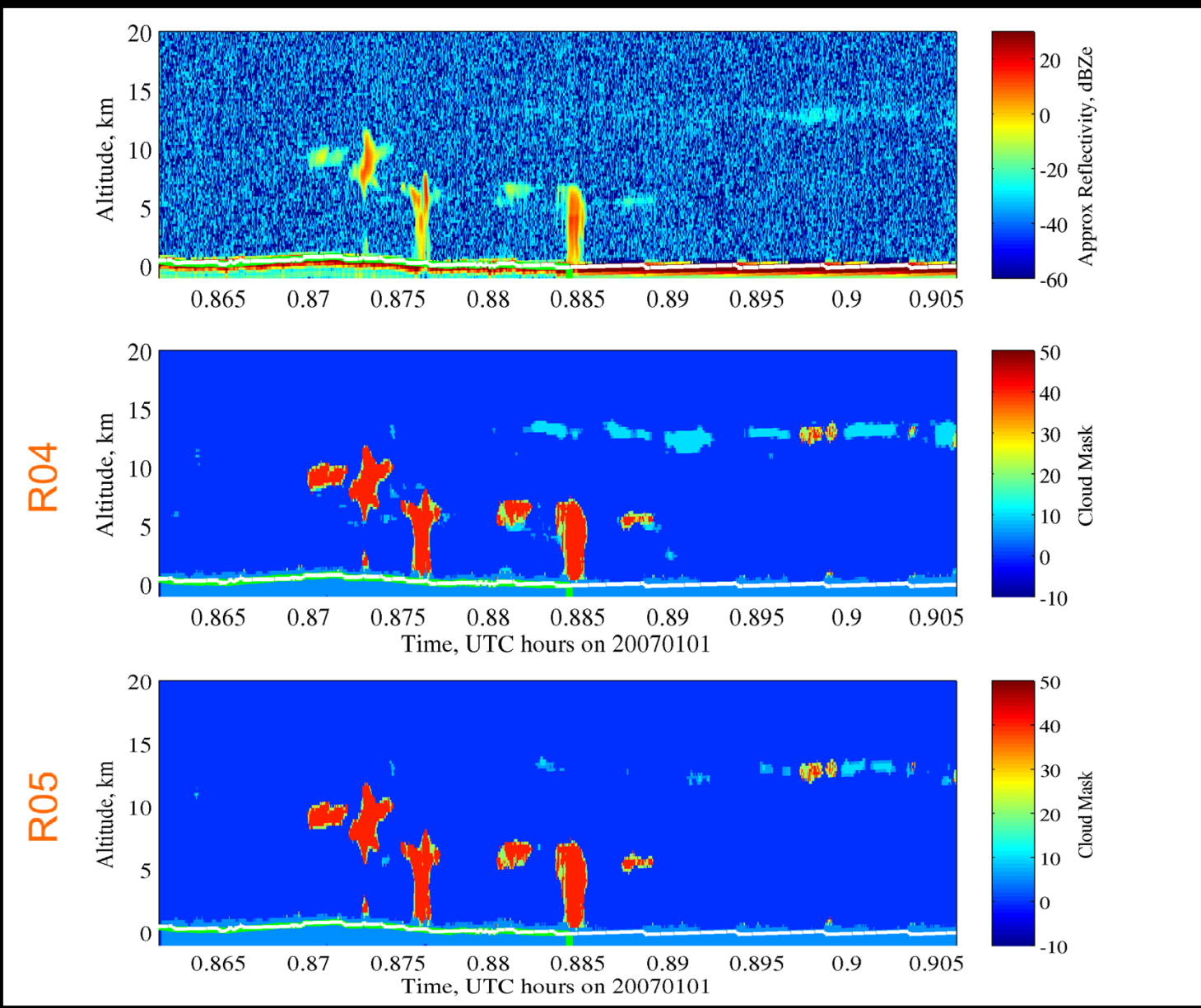


R05





# ... and reduction in good detections





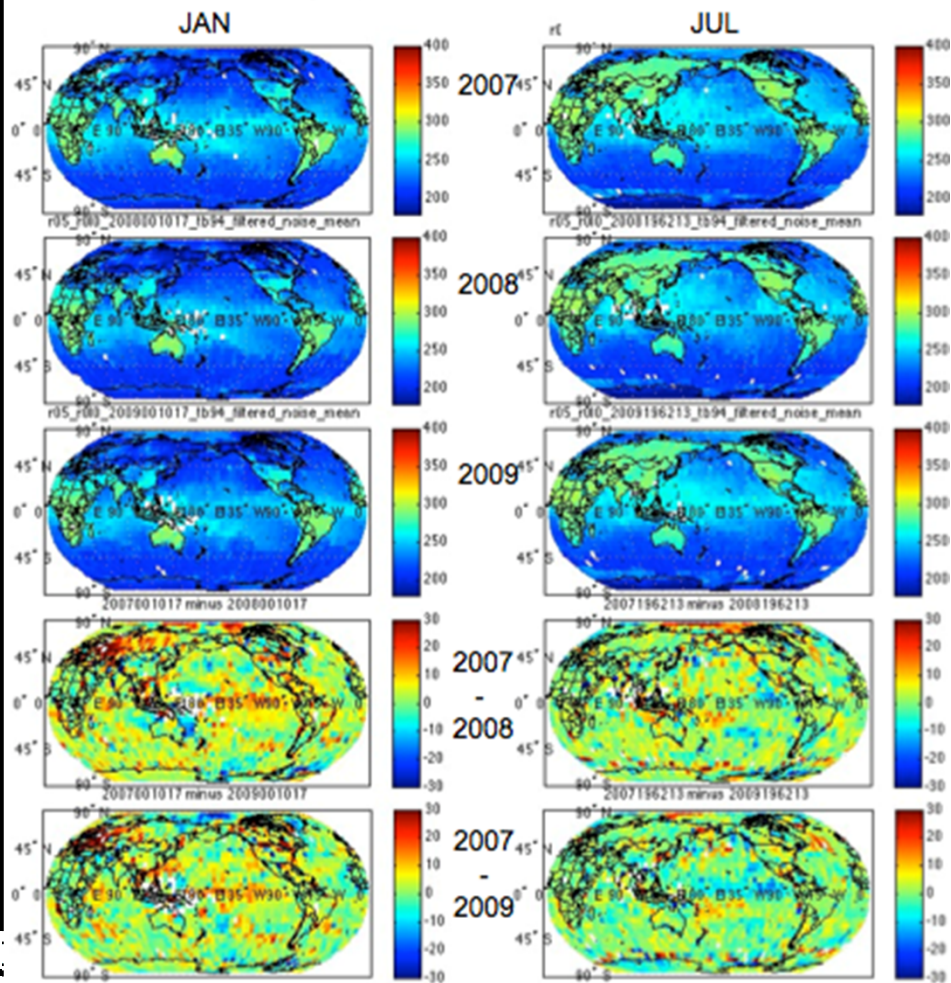
# New radiometric product in L2B



## New fields for L2B Brightness Temperature Product

- **tb94\_new\_sem\_NoiseFloor** - the new noise using as many clear bins as possible
- **tb94\_new\_sem\_NoiseFloorStd** - standard deviation of new noise
- **tb94\_new\_num\_bins** - number of clear bins used to calculate the new noise
- **tb94\_filtered\_noise** - new noise after it has been run through the dynamic window filter
- **tb94\_window\_size** - window size used for filtering a given ray

R05 Noise with brightness temperature coefficients applied. CPR and Lidar clear. Same color scale as R04 plots, 180 - 400.



### TB ESTIMATE ERROR BUDGET (K) FOR BEST AND WORST

Nwindows	Npulse	Nbins	Noise							
			Avg	Sigma	1	5	11	31	51	101
620	85	4.25	0.018513291	4.0	1.8	1.2	0.7	0.6	0.4	
				4.3	2.5	2.1	1.9	1.8	1.8	
520	20	4.5	0.04412613	9.5	4.2	2.9	1.7	1.3	0.9	
				9.9	5.1	4.0	3.3	3.1	2.9	



# EarthCARE CPR



EarthCARE CPR adopts a design philosophy very similar to CloudSat's CPR, and it employs similar key technologies and configuration.

The most significant changes in terms of the science that is expected from it come from:

-The larger Antenna Size (2.5 vs 1.85 m) combined with the lower orbital altitude (405 km vs 705 km) will provide:

- more than 7 dB improvement in minimum detectable reflectivity.
- improved horizontal resolution (~ 700 x 1400m), and consequent reduction in multiple scattering contamination

- The 2.5m Antenna combined on-board Pulse-Pair processing will provide:

**- The first ever Doppler measurements of Cloud and Precipitation vertical velocity from space**

- Other minor improvements are expected from the 100m sampling in range (the radar resolution is the same as CloudSat).

Table. 1 Major specifications of the CPR

Frequency	94.05GHz ± 3.5MHz
Polarization	circular (Tx: LHC, Rx: RHC)
Antenna aperture	2.5m
Antenna beam width	0.095 degrees
Antenna sidelobe level	less than -50dB (1< θ < 7 deg.) less than -56dB (> 7 deg)
Beam direction	nadir
Beam pointing error	less than 0.015 degrees rms
Peak transmit power	>1.43kW (BOL) >1.34kW (EOL)
Transmit pulse width	3.3+/-0.1µs
Pulse repetition frequency	6100Hz to 7500Hz (variable PRF)
Observation Altitude	-1km to 20km -1km to 16km -1km to 12km
Range resolution	less than 500m
Range sampling interval	100m
Dynamic range	>85dB
Radiometric error	less than 1.7dB
Doppler measurement range	±10m/s
Doppler measurement error	less than 1m/s (for reflectivity factor higher than -19dBZ)

From: Takahashi et al. 2009

(Takahashi, N.; Kimura, T.; Ohno, Y.; Horie, H.; Nakatsuka, H.; Sato, K.; Sakaide, Y.; Okada, K.; Kumagai, H.; , "Cloud profiling radar on earthcare satellite," ICCAS-SICE, 2009 , vol., no., pp.1328-1332, 18-21 Aug. 2009



# Peculiarities of the spaceborne configuration



# The relation between the natural hydrometeor spectrum and the spectrum observable by a spaceborne radar



$$f'(\theta, \phi) \approx qx$$

Doppler shift

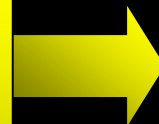
$$W(\mathbf{r}; \mathbf{r}_V) = \frac{C \cdot G_a^2(\theta, \phi) \cdot |G_r(r - r_V)|^2}{L(r) \cdot r^4}$$

Radar weighting factor

$$P(f; \mathbf{r}_V) = \int_{r_1}^{r_2} \int_0^\pi \int_0^{2\pi} \eta[\mathbf{r}, f - f'(\theta, \phi)] W(\mathbf{r}, \mathbf{r}_V) r \sin\theta \, d\theta \, d\phi \, dr$$

$\eta(\mathbf{r}, f)$ : natural rainfall spectrum in an elementary volume at  $(r, \theta, \phi)$

UBF (Uniform Beam Filling) conditions  
+  
Gaussian antenna pattern

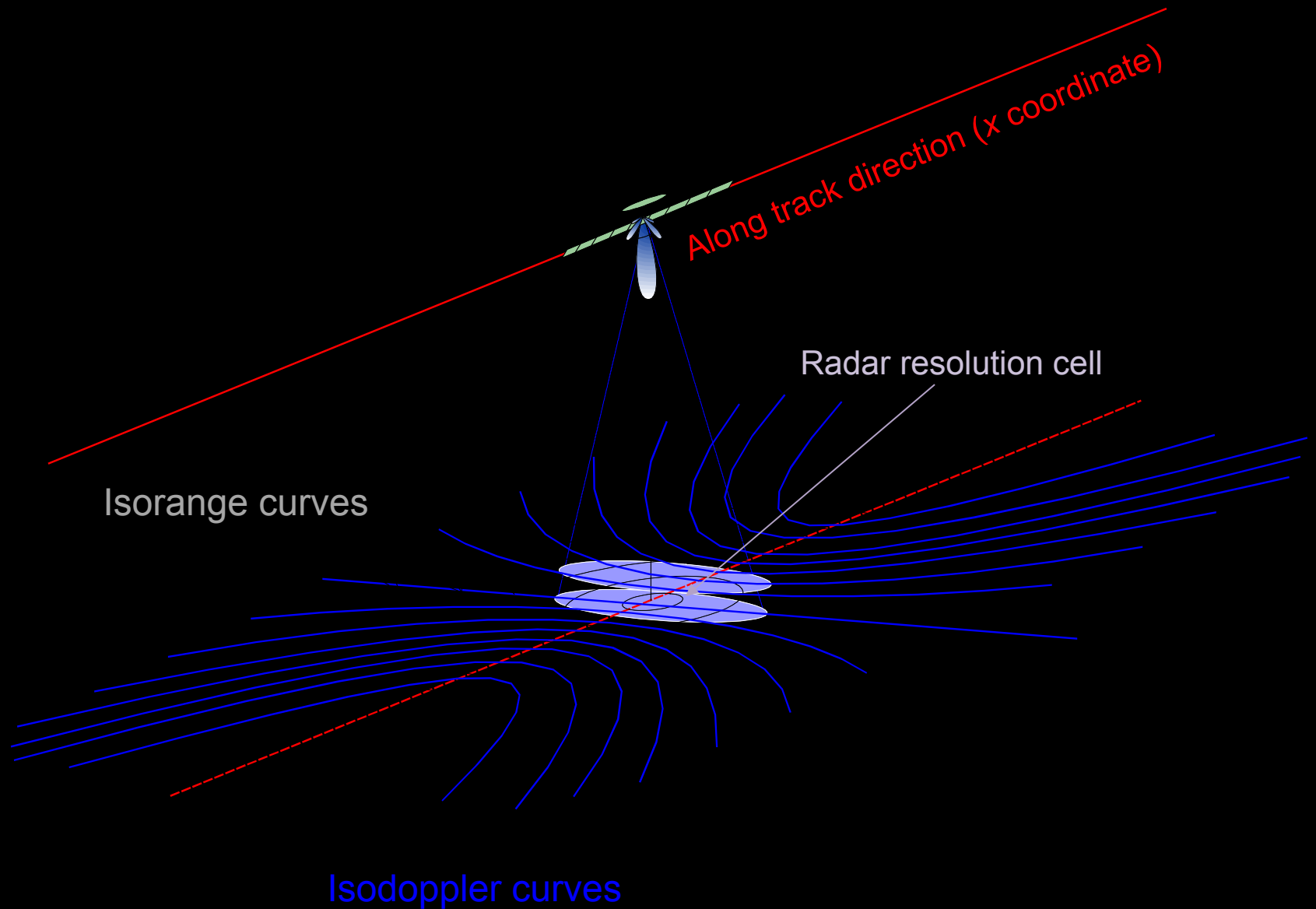


Gaussian spectrum with normalized width:

$$w_N = \frac{4}{\lambda PRF} \sqrt{\sigma_R^2 + \frac{\theta_{3dB}^2 V_S^2}{16 \ln(2)}}$$



# Rainfall Doppler measurements from space (nadir configuration)

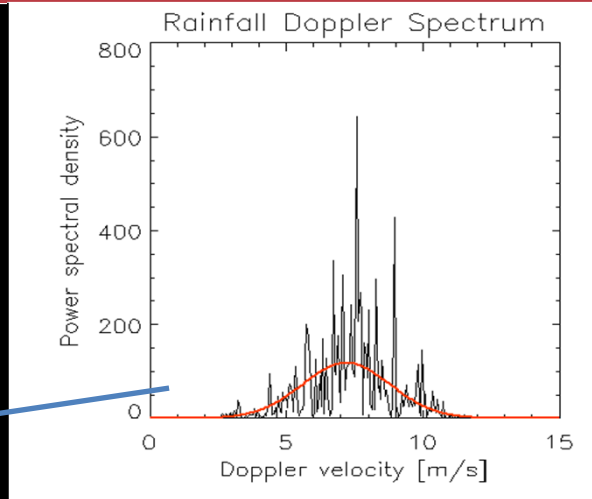
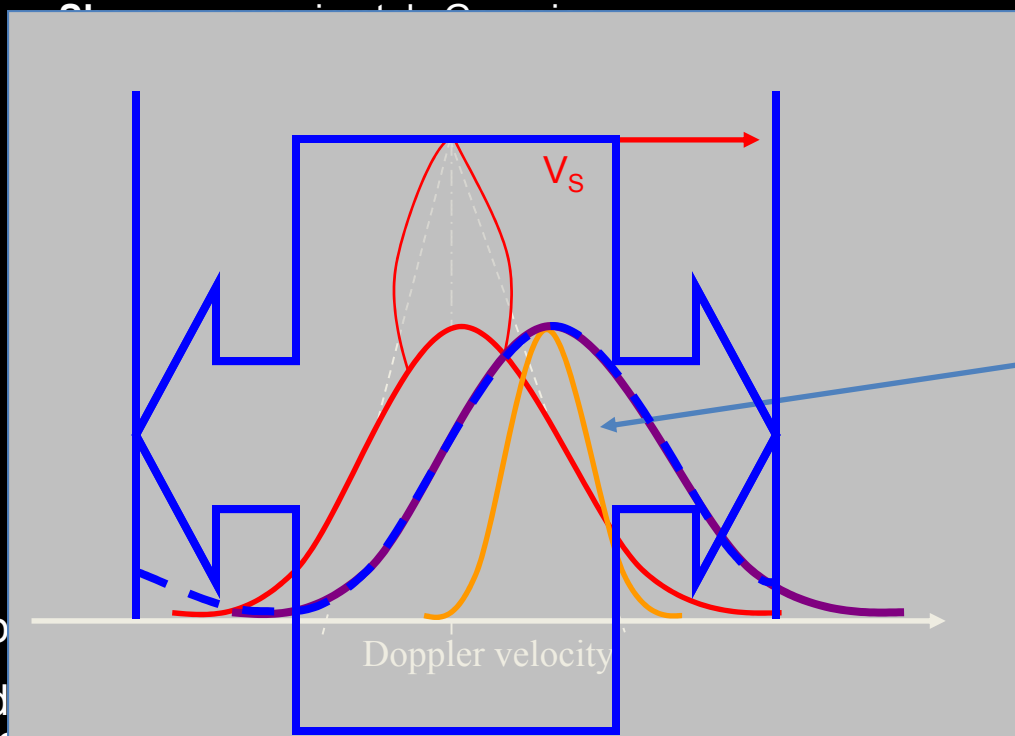




# Doppler radar measurements of hydrometeors



## Natural Doppler velocity spectrum of rainfall

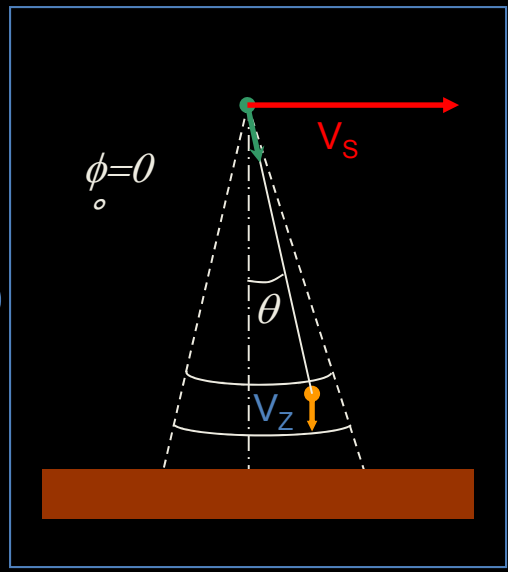


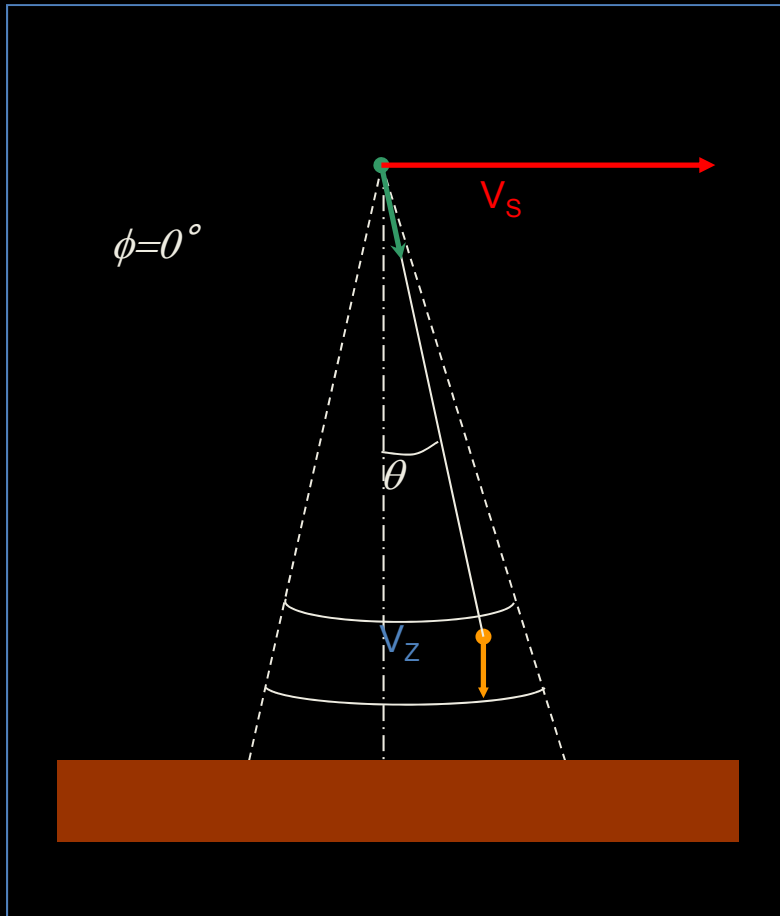
Dop  
Rad

an elementary volume at coordinates  $(r, \theta, \phi)$  with respect to the radar:

$$v_r = (v_x - v_s) \cdot \sin \theta \cos \phi + v_y \cdot \sin \theta \sin \phi + v_z \cdot \cos \theta$$

where  $v_x$ ,  $v_y$ , and  $v_z$  (i.e.,  $v = [v_x, v_y, v_z]$ ) are the particle velocity components in the along track, cross track and vertical direction respectively.  $V_s$  is the satellite speed (around 7 km/s)





The simplified diagram shown aside indicates only one velocity,  $v_s$  = the instantaneous tangential velocity of the spacecraft.

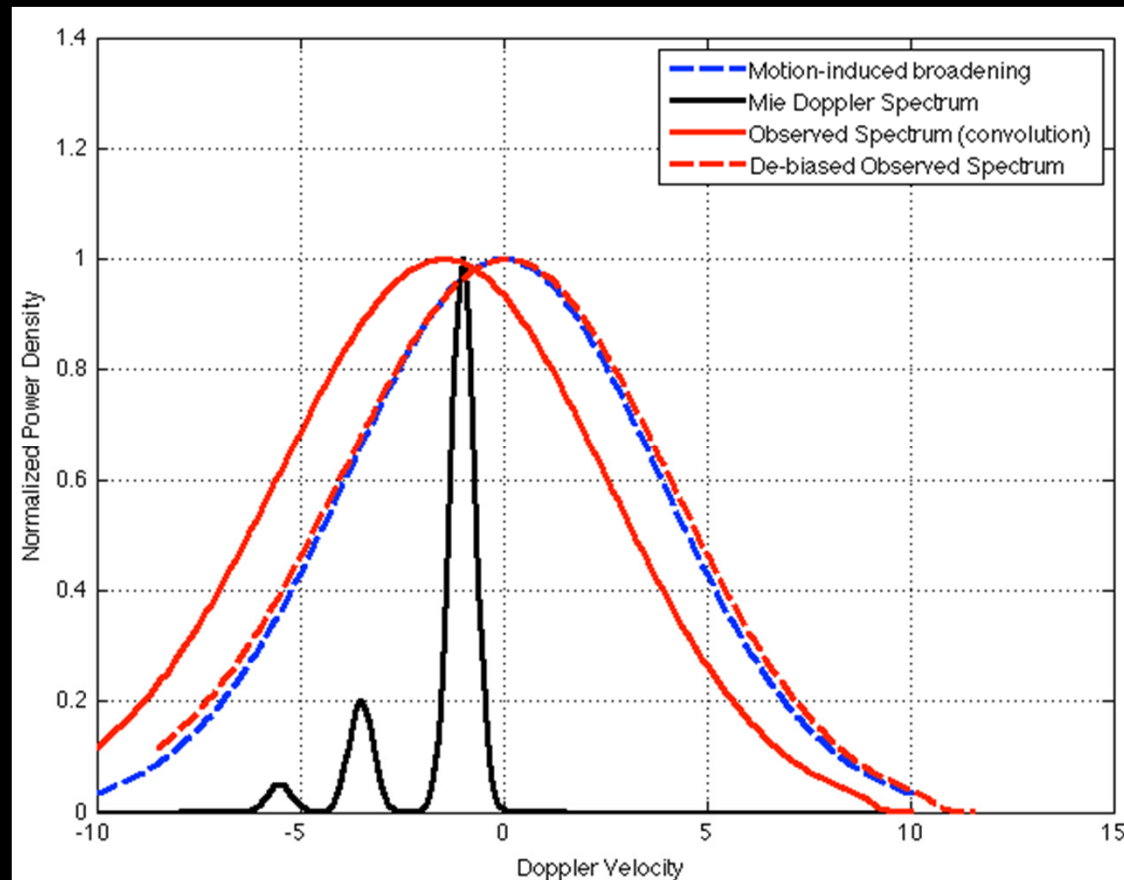
The same conceptual diagram can be used also when  $v_s$  is not parallel to the Earth's surface (see Tanelli et. al 2005 for the corresponding formulation).

The Earth not being flat, not only causes this diagram to be misleading if applied to long baselines, but it is also misleading at the short (footprint) scale when NUBF effects are estimated: in fact the instantaneous velocity of the sub-satellite point on the ground track is only a fraction of  $v_s$  (depending on the  $R_e + h_s / R_e$  ratio).

By the same token, while the tangential trajectory approximation is in general very good for LEO, it can lead to errors for other orbital configurations.



# Impact of non-Gaussian Doppler spectra



Even in the case of a very non-Gaussian spectrum (such as that observable from ground-based W-band Doppler radars because of the Mie resonance combined with particle fall speed) the broadening induced by the spacecraft motion combined with the antenna pattern generates an observed spectrum whose shape is mainly determined by the latter. For this reason, the requirements on antenna size or signal processing necessary to allow estimation of any spectral moment beyond the first (i.e., mean Doppler velocity) are one order of magnitude more demanding than those imposed by mean Doppler velocity alone.



# Antenna Size vs Spectra Width

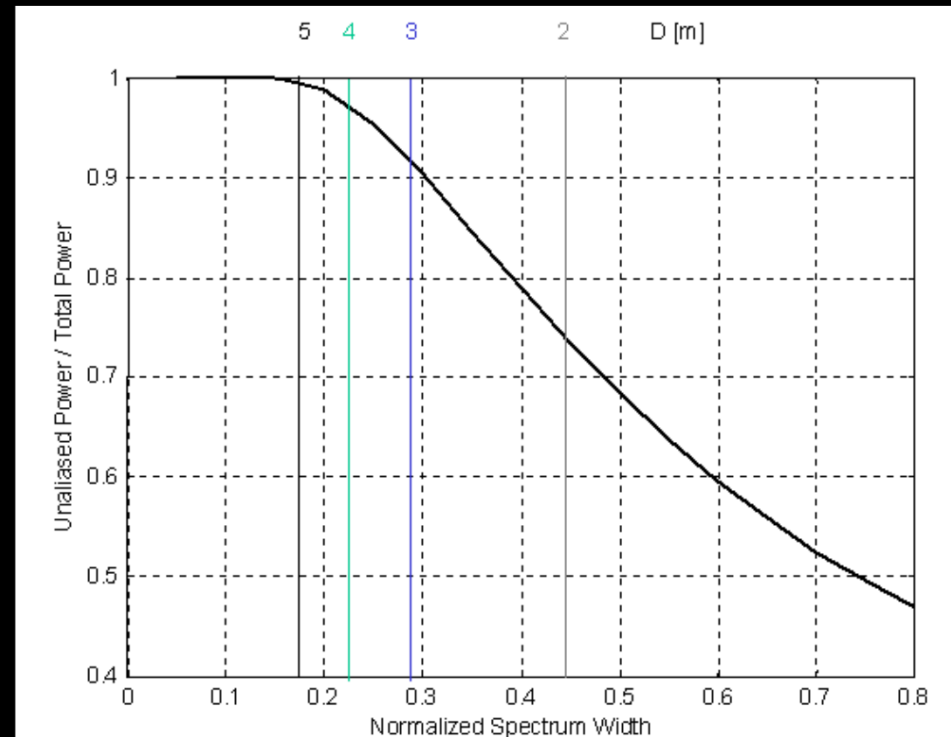


When the Doppler broadening induced by the satellite dominates over the width of the rainfall spectrum  $\sigma_R$ , the normalized Doppler spectral width is **inversely proportional to antenna size**

$D$ [m]	2	3	4	5	6	10
<b>PRF</b>						
<b>5000</b>	0.50	0.34	0.25	0.20	0.17	0.10
<b>6000</b>	0.42	0.28	0.21	0.17	0.14	0.09
<b>7000</b>	0.36	0.24	0.18	0.14	0.12	0.07
<b>8000</b>	0.32	0.21	0.16	0.13	0.11	0.06

Normalized spectral widths  $w_N$  as function of  $PRF$  and antenna diameter  $D$ , for  $v_s = 7000 \text{ m s}^{-1}$  and  $\sigma_R = 0$ .

The aliased portion of the Power spectrum **introduces a bias and increases the variance of estimates**

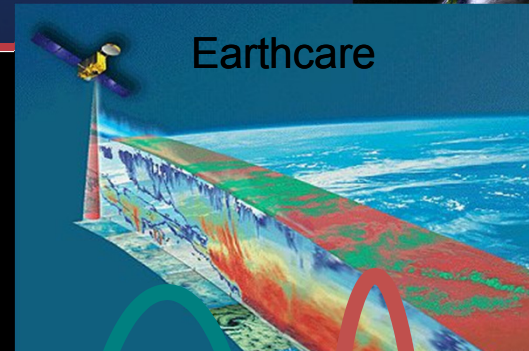
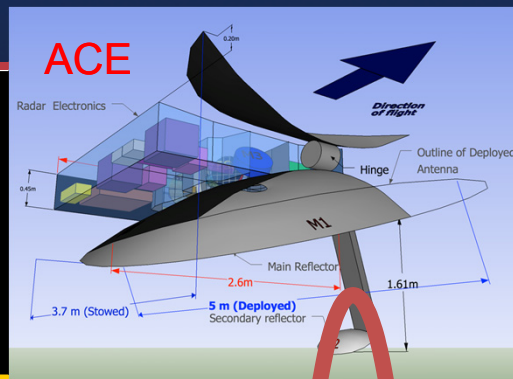




# Rainfall Doppler width from LEO



Normalized spectral widths for different radar configurations (Op.Freq., Antenna Size D (m) & PRF (Hz)) and 3 turbulence regimes ( $\sigma_R=1$  m/s mild,  $\sigma_R=3$  m/s moderate,  $\sigma_R=5$  m/s extreme)



$\sigma_R$	Ku band (13.6 GHz)							Ka band (35 GHz)							W band (94 GHz)													
	D	2	3	4	5	6	10	D	2	3	4	5	6	10	D	2	3	4	5	6	10							
	$\theta_{3dB}$	.76	.51	.38	.30	.25	.15	$\theta_{3dB}$	.29	.20	.15	.12	.10	.06	$\theta_{3dB}$	.11	.07	.05	.04	.04	.02							
PRF	5000	6000	7000	8000	5000	6000	7000	8000	5000	6000	7000	8000	5000	6000	7000	8000	5000	6000	7000	8000	5000	6000	7000	8000				
1	5000	.50	.34	.25	.20	.17	.10	5000	.51	.34	.26	.21	.17	.11	5000	.52	.36	.28	.24	.21	.16	5000	.63	.50	.45	.43	.41	.39
	6000	.42	.28	.21	.17	.14	.09	6000	.42	.28	.21	.17	.15	.09	6000	.43	.30	.23	.20	.17	.13	6000	.52	.42	.38	.36	.34	.32
	7000	.36	.24	.18	.14	.12	.07	7000	.36	.24	.18	.15	.12	.08	7000	.37	.26	.20	.17	.15	.11	7000	.45	.36	.32	.30	.29	.28
	8000	.32	.21	.16	.13	.11	.06	8000	.32	.21	.16	.13	.11	.07	8000	.32	.22	.18	.15	.13	.10	8000	.39	.32	.28	.27	.26	.24
3	5000	.51	.34	.26	.21	.18	.11	5000	.52	.36	.29	.25	.22	.17	5000	.63	.50	.45	.43	.41	.39	5000	.80	.71	.68	.66	.65	.63
	6000	.42	.28	.22	.17	.15	.10	6000	.44	.30	.24	.20	.18	.14	6000	.52	.42	.38	.36	.34	.32	6000	.67	.59	.56	.55	.54	.53
	7000	.36	.24	.18	.15	.13	.08	7000	.37	.26	.21	.18	.16	.12	7000	.45	.36	.32	.30	.29	.28	7000	.57	.51	.48	.47	.46	.45
	8000	.32	.21	.16	.13	.11	.07	8000	.33	.23	.18	.15	.14	.11	8000	.39	.32	.28	.27	.26	.24	8000	.50	.44	.42	.41	.41	.40
5	5000	.51	.35	.27	.22	.19	.14	5000	.56	.41	.34	.31	.29	.25	5000	.80	.71	.68	.66	.65	.63	5000	.80	.71	.68	.66	.65	.63
	6000	.43	.29	.22	.18	.16	.11	6000	.46	.34	.29	.26	.24	.21	6000	.67	.59	.56	.55	.54	.53	6000	.67	.59	.56	.55	.54	.53
	7000	.37	.25	.19	.16	.14	.10	7000	.40	.29	.25	.22	.21	.18	7000	.57	.51	.48	.47	.46	.45	7000	.57	.51	.48	.47	.46	.45
	8000	.32	.22	.17	.14	.12	.08	8000	.35	.26	.21	.19	.18	.16	8000	.50	.44	.42	.41	.41	.40	8000	.50	.44	.42	.41	.41	.40

**VERY BROAD**

Pulses are almost uncorrelated, Doppler spectrum is almost white

**BROAD**

Pulses are poorly correlated, Doppler ambiguity reduces the unbiased Doppler unambiguous range by > 40%

Pulses are moderately correlated, Doppler ambiguity reduces the effective Doppler unambiguous range by 5-40%

**NARROW**

All results obtained for ground based and airborne Doppler radars are valid



# Spectral Moment Estimators (SME)

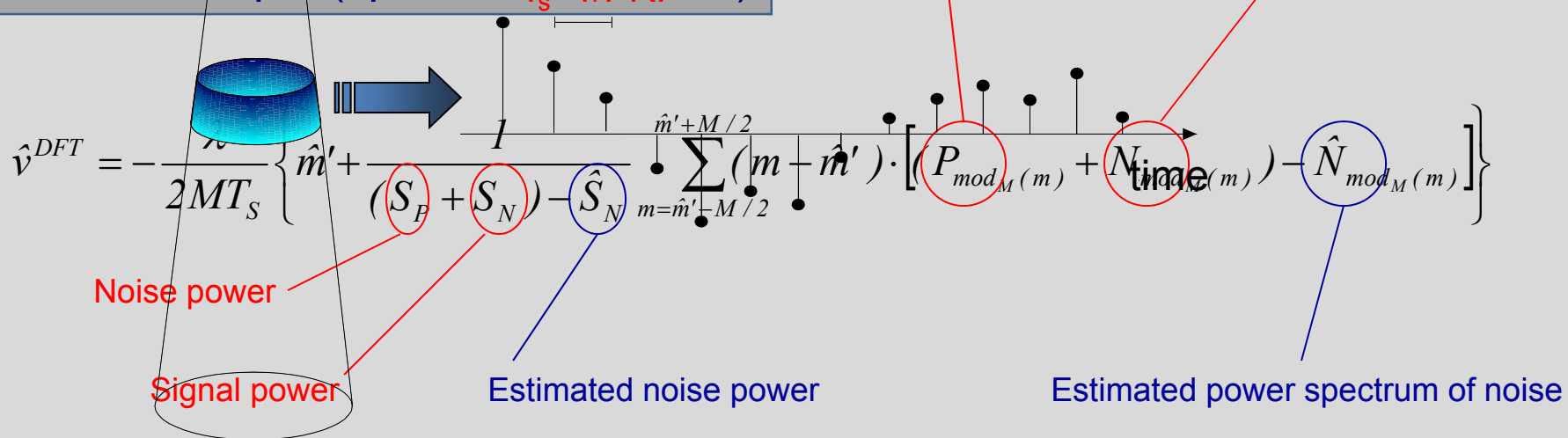


Given a sequence  $\{\tilde{s}_n\}$  of M complex radar samples in a resolution cell

## Pulse Pair (PP) technique (one-lag correlation)

$$\hat{v}^{PP} = -\frac{\lambda}{2} \frac{1}{2\pi T_s} \arg \left( \frac{1}{M-1} \sum_{n=-\frac{M-1}{2}}^{\frac{M-1}{2}-1} \tilde{s}_n^* \tilde{s}_{n+1} \right)$$

## DFT technique (spectral estimation)





# Expected performance: first assessment

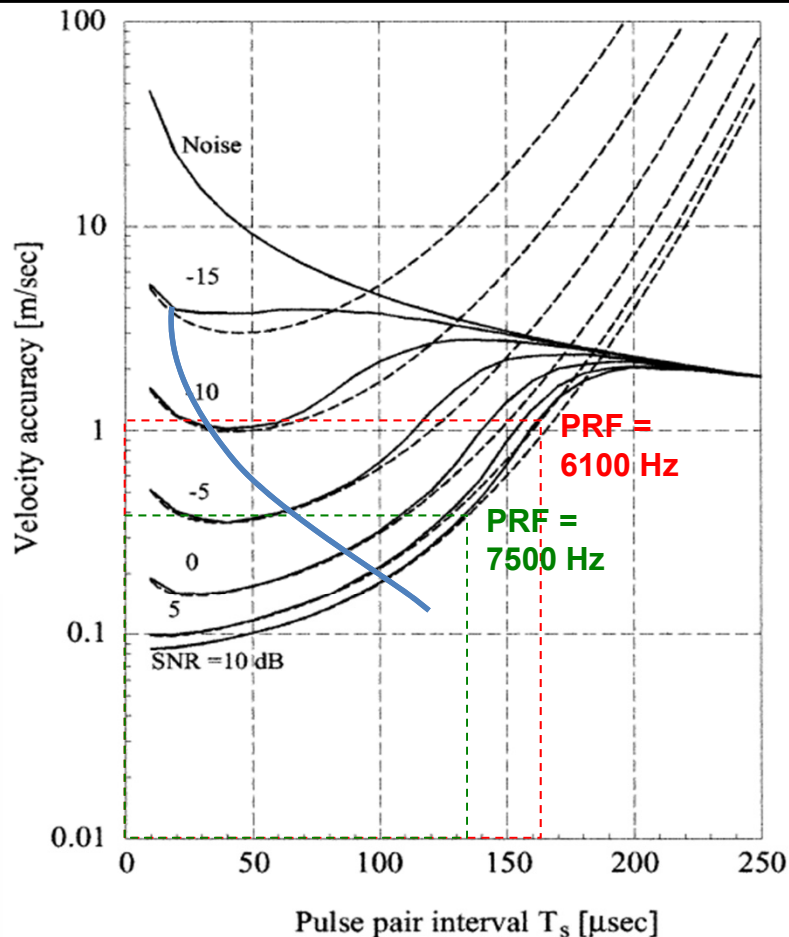


FIG. 3. Accuracy in Doppler velocity vs pulse-pair interval  $T_s$  for contiguous pulse-pair operation. The along-track integration and the spectral width of velocity are set at  $d = 1$  km and  $\sigma_v = 3.85$  m s<sup>-1</sup> ( $T_c = 93$  μs), respectively. The simulations are performed over 10 000 times, as described in section 2, for the parameters  $T_{it} = 10T_c$  and  $T_{is} = 2T_c$ . The noises superimposed on the data SNR = -15 to +10 dB have been assumed to be white. The broken lines are calculated by a perturbation formula of Doviak and Zrnić (1993).

First order assessment of Performance of Cloud Doppler radars is often described by a plot such as this: it highlights well the effects of SNR and decorrelation. In this simulation, however, the mean Doppler velocity is assumed to be zero, the most favorable situation in terms of aliasing. When the mean Doppler velocity approaches the Nyquist limit, additional uncertainty affects the measurements.



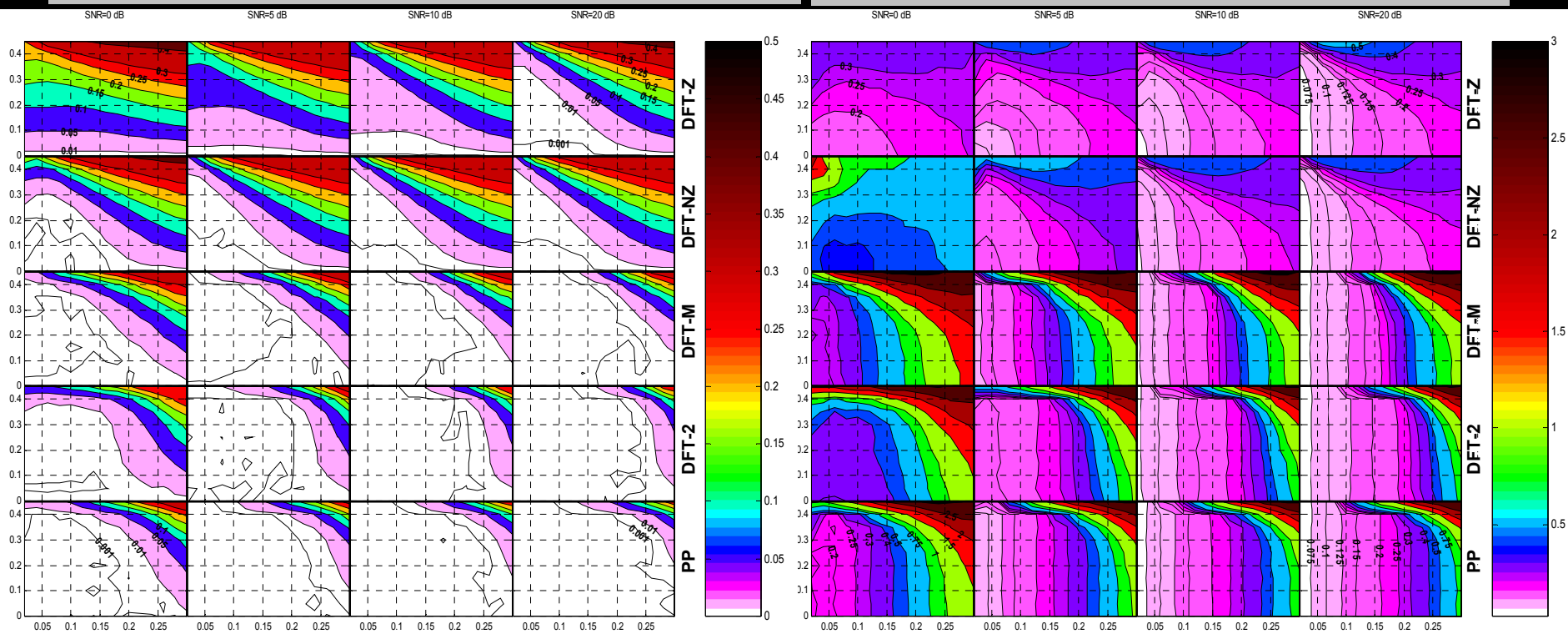
# SME performance in UBF conditions



- PP is best performing for  $w_N < 0.1$
- PP is affected by bias for  $|f_N| > 0.5 - 4 (w_N)^2$
- PP is affected by spectrum asymmetry
- PP is computationally more efficient

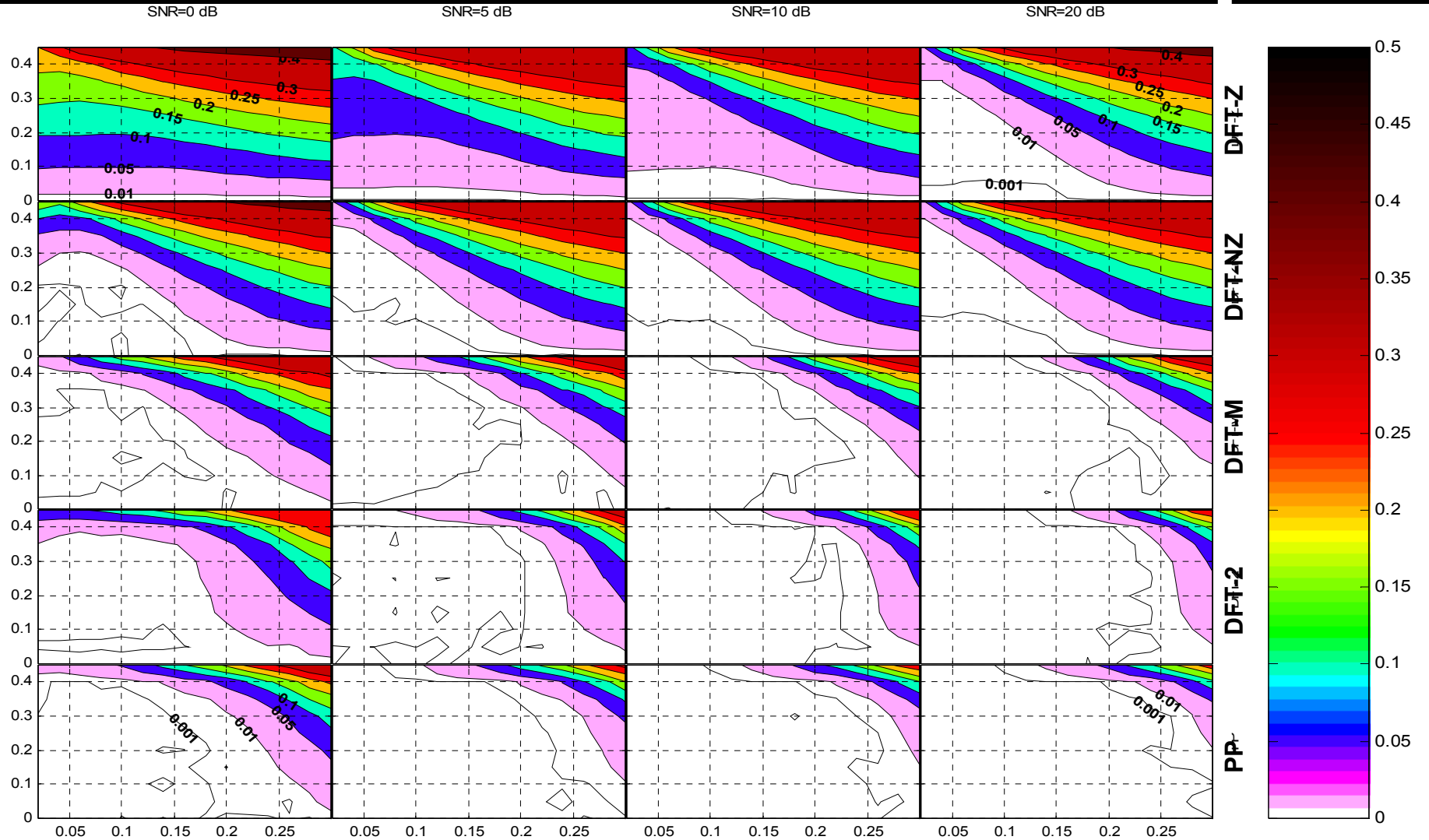
- DFT-2 is best performing for  $0.1 < w_N < 0.2$
- DFT-2 is affected by bias for  $|f_N| > 0.5 - 5 (w_N)^2$
- DFT-2 is more affected by low SNR
- DFT-2 allows to analyze further the spectrum

$$\text{var}(\hat{v}_N) = \frac{PRF^2}{M} \left\{ \left[ \frac{w_N}{4\sqrt{\pi}} + 2w_N^2 \frac{S_N}{S_S} + \frac{1}{12} \left( \frac{S_N}{S_S} \right)^2 \right] + v_N^2 \left[ \frac{(S_N - \hat{S}_N)^2}{\hat{S}_S^2} \left( \frac{1}{2\sqrt{\pi}w_N} + 2 \frac{S_N}{S_S} \right) + \left( \frac{S_N}{\hat{S}_S} \right)^2 \right] \right\}$$



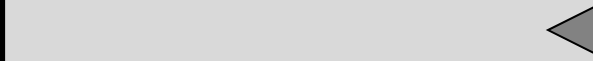
Max Rng (Km)	PRF	Freq		
		13.6 GHz	35 GHz	94 GHz
30.0	5000	27.6	10.7	4.0
25.0	6000	33.1	12.9	4.8
21.4	7000	38.6	15.0	5.6
18.7	8000	44.1	17.1	6.4

# SME Normalized BIAS



Max Rng (Km)	Freq		13.6 GHz	35 GHz	94 GHz
	PRF				
30.0	5000		27.6	10.7	4.0
25.0	6000		33.1	12.9	4.8
21.4	7000		38.6	15.0	5.6
18.7	8000		44.1	17.1	6.4

# SME Normalized Std Dev

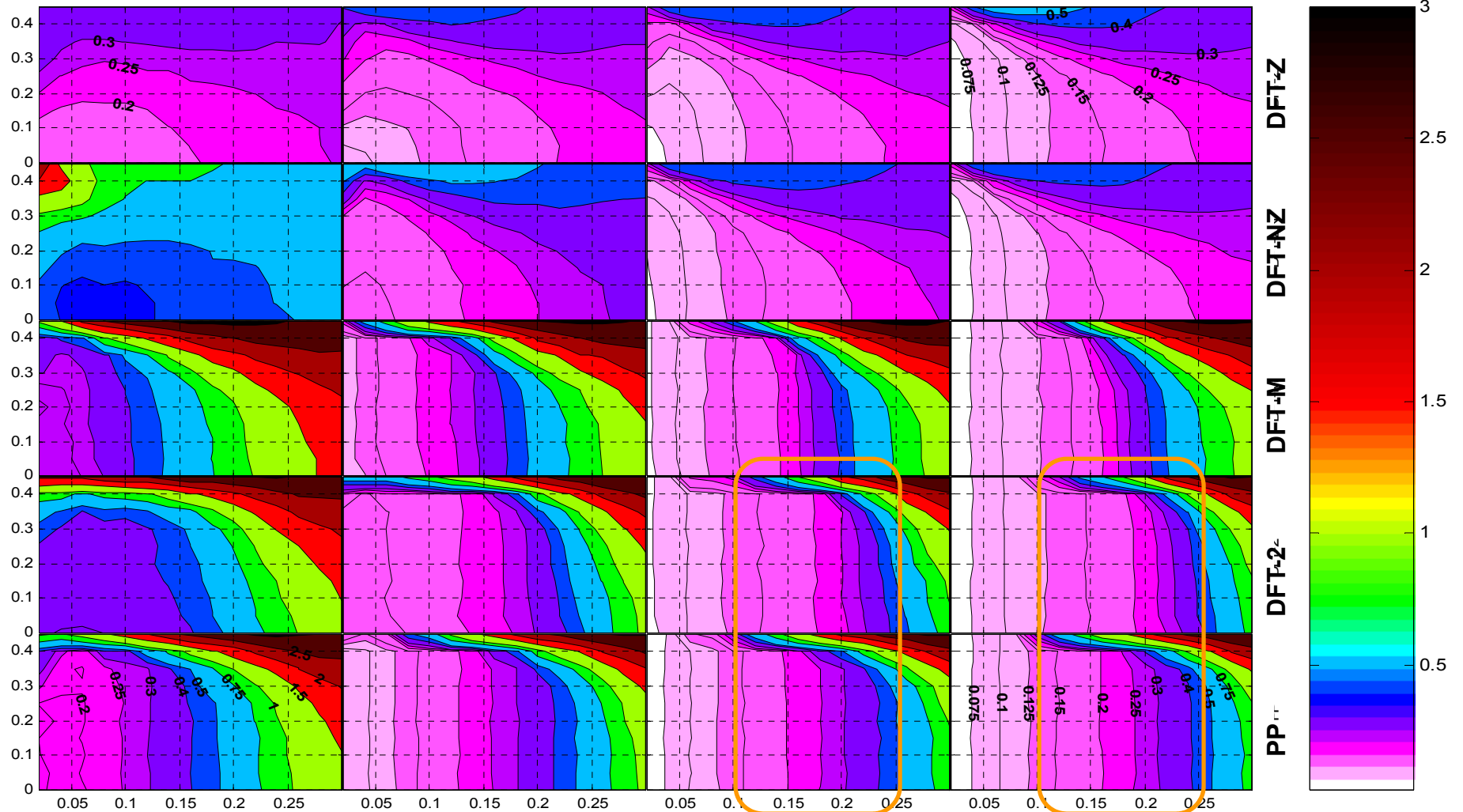


SNR=0 dB

SNR=5 dB

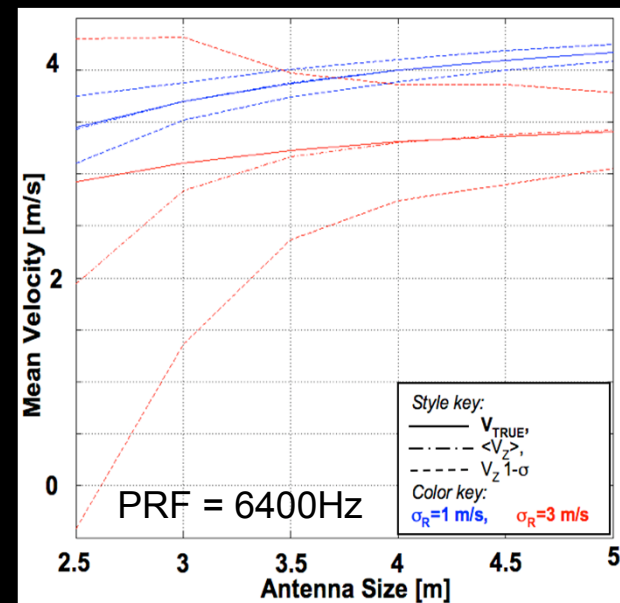
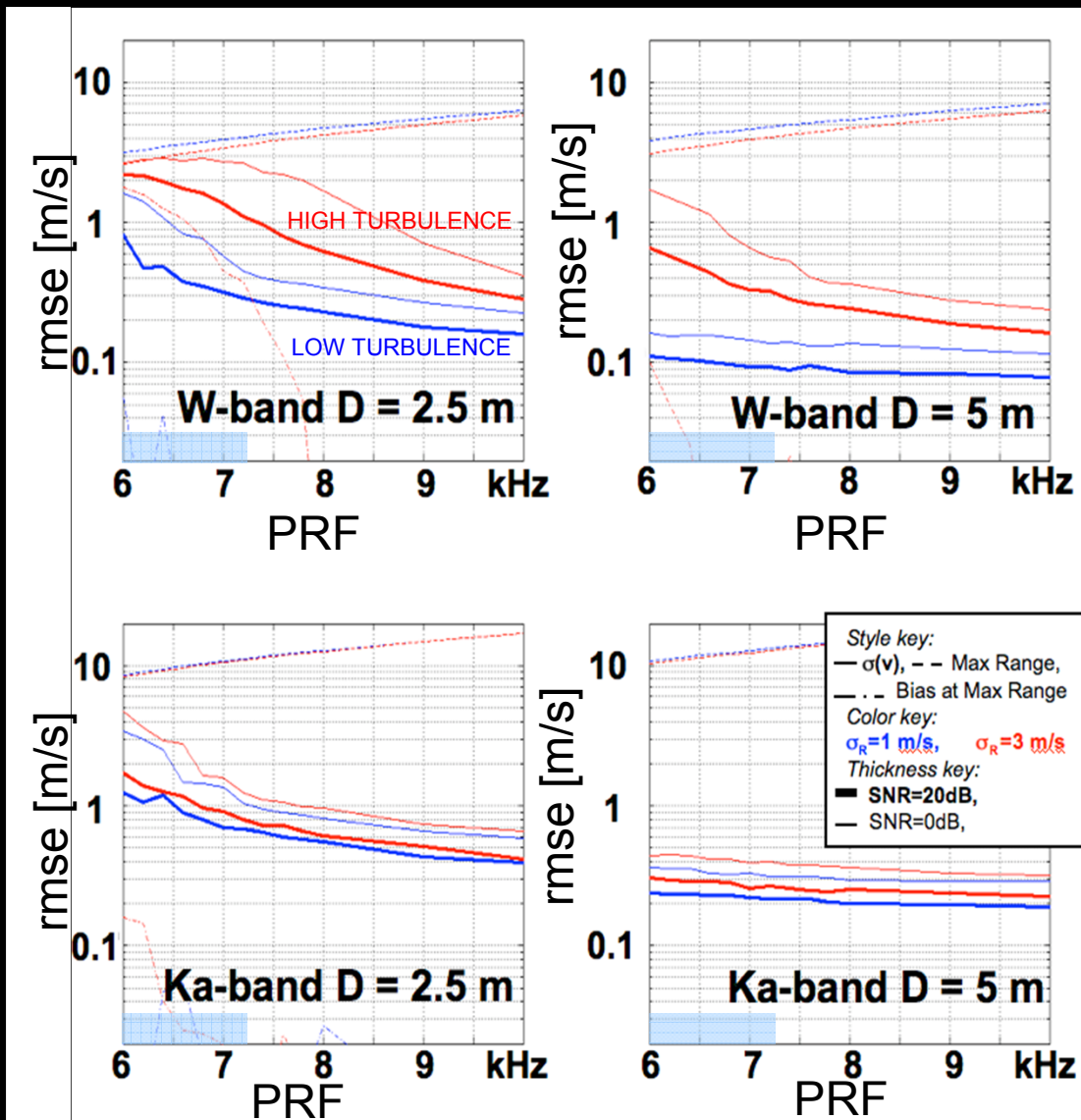
SNR=10 dB

SNR=20 dB





# Effective Maximum unambiguous range



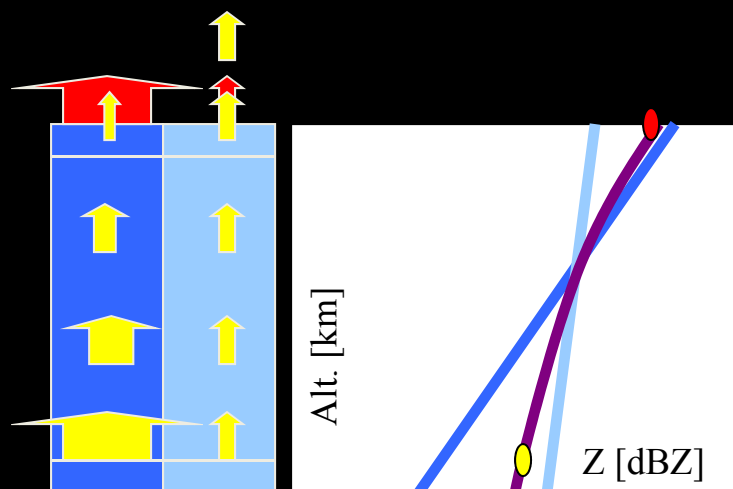
**Range (km)/Doppler (m/s) ambiguity trade-offs**

All Freq.	Freq	13.6 GHz	35 GHz	94 GHz
30.0	5000	27.6	10.7	4.0
25.0	6000	33.1	12.9	4.8
21.4	7000	38.6	15.0	5.6
18.7	8000	44.1	17.1	6.4

1 km integration assumed

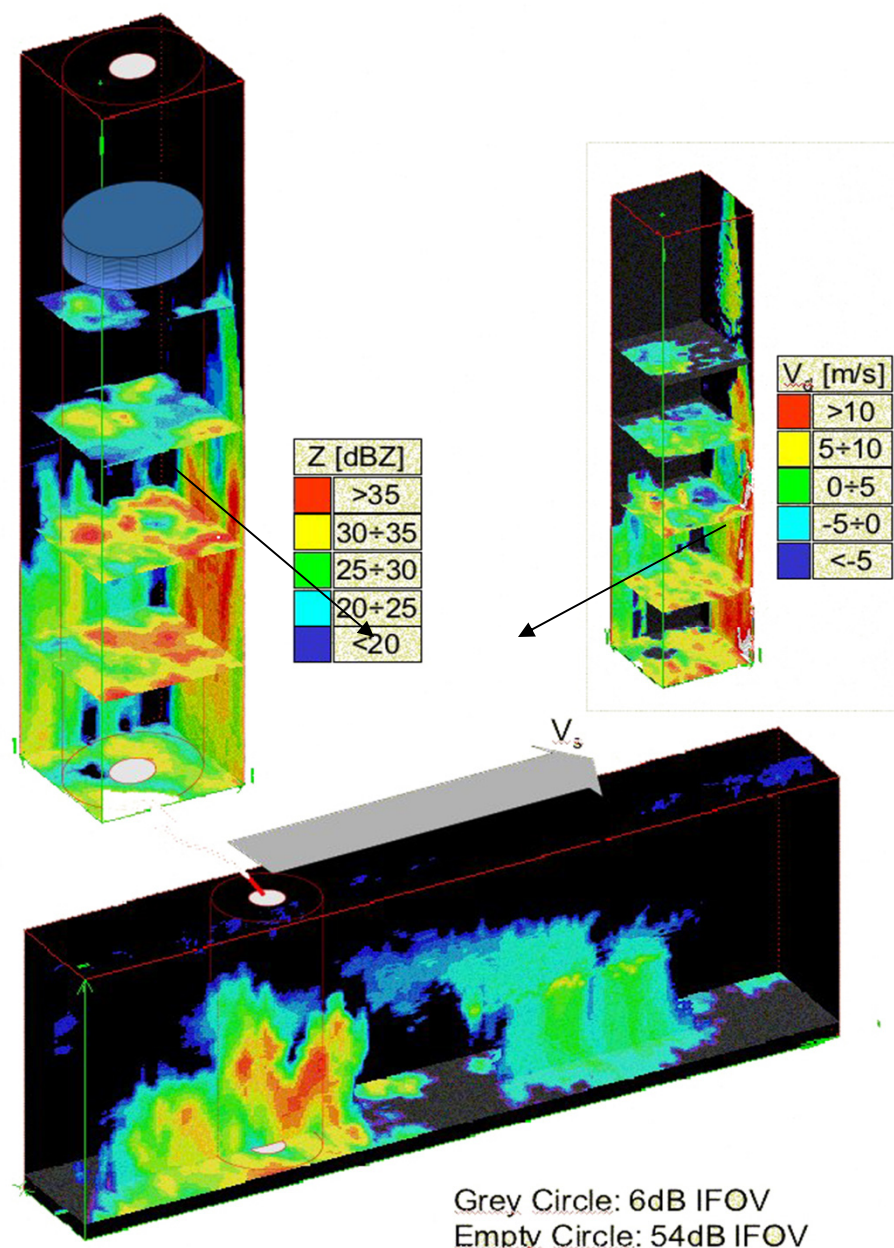


- Vertical features observable in this high resolution ARMAR sample increase the uncertainty due to NUBF at lower radar volumes of resolution. The size of the volume shown is roughly 5x5x10 km.



Measured Reflectivity Factor  $Z_m$  [ $\text{mm}^6 \text{m}^{-3}$ ] when  $R(q,f,r) = R(q,f)$  (horizontal non-homogeneity)

$$Z_m(n) = \frac{1}{\Delta} \int_{(n-1)\Delta}^{n\Delta} \int_0^{\infty} aR^b \left( e^{-q\alpha R^{\beta r}} \right) w(R) dR dr$$



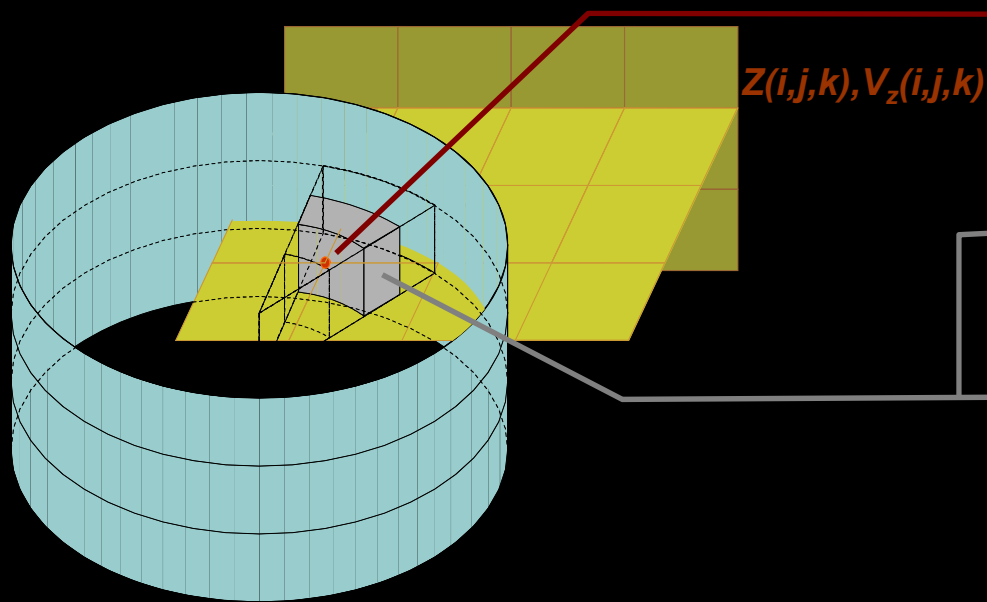


# Single Scattering simulation of Doppler Spectra



## ARMAR - 3D Z & V fields

Cartesian Res - Hor: 200m, Ver:60m



- $R=aZ^b$
- $\Lambda= f(R)$  in the DSD expr.
- $v_t(D)=f(D)$  by Atlas
- Mie Scattering

Radial Spectrum  
 $v_r=f(v,v_s,\theta,\phi)$

$W(r_0,r)$

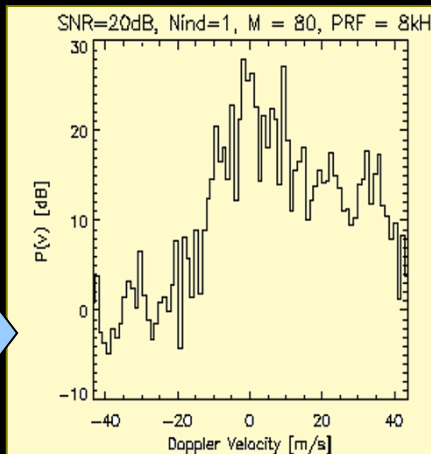
### Broadening

- Turbulence
- Wind Shear
- Satellite Motion

Signal fluct. + thermal noise

Weighted Incoherent Combination

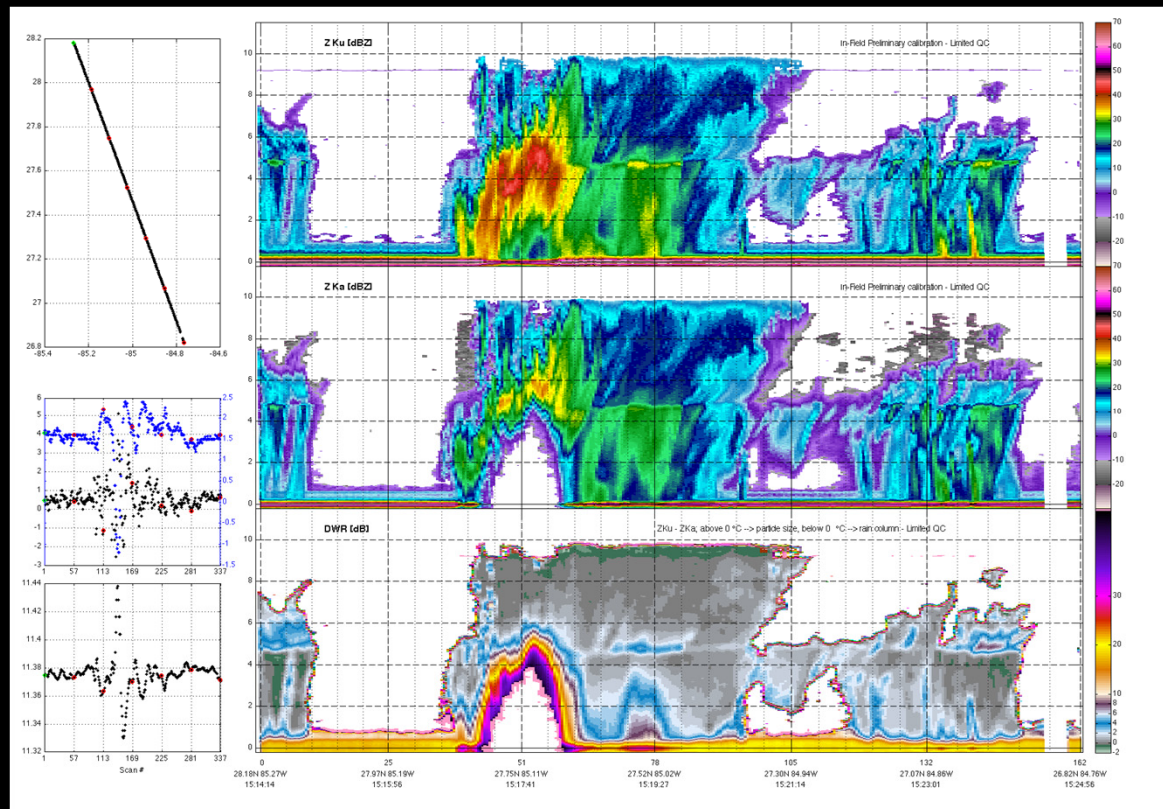
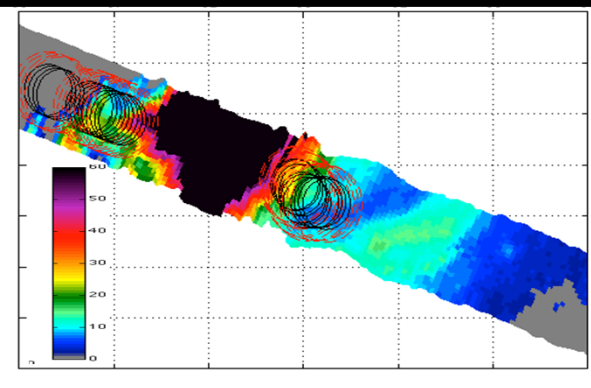
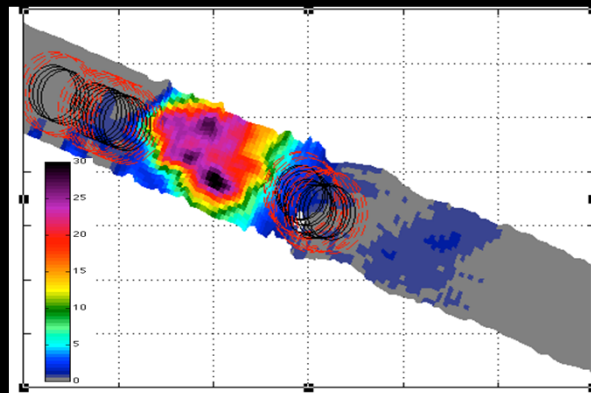
Sampling and DFT



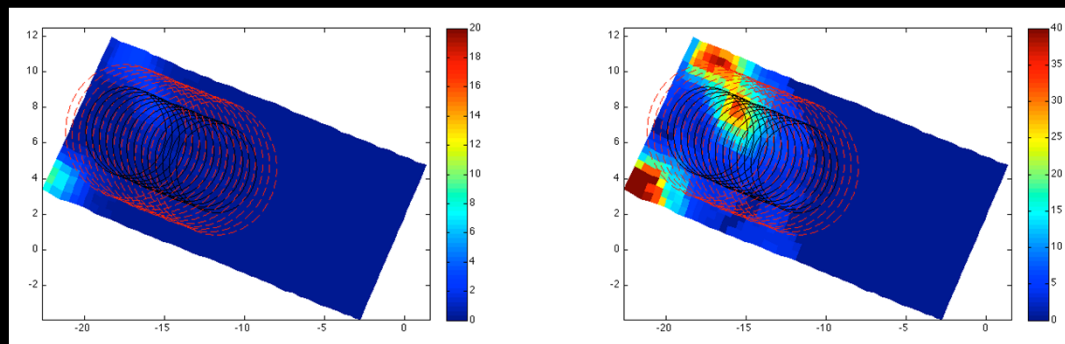
**Resolution Volume**  
 54dB IFOV:  $\varnothing x: \sim 7200m, \Delta r: 250m$



# Impact of NUBF on GPM SRT



The GPM radar footprint was approximated with a Gaussian pattern out to 1.5x 3dB footprint  
Two GPM pattern-weighted quantities were calculated for each frequency: PIA and Zsurf





# GPM simulated PIA from GRIP 2010

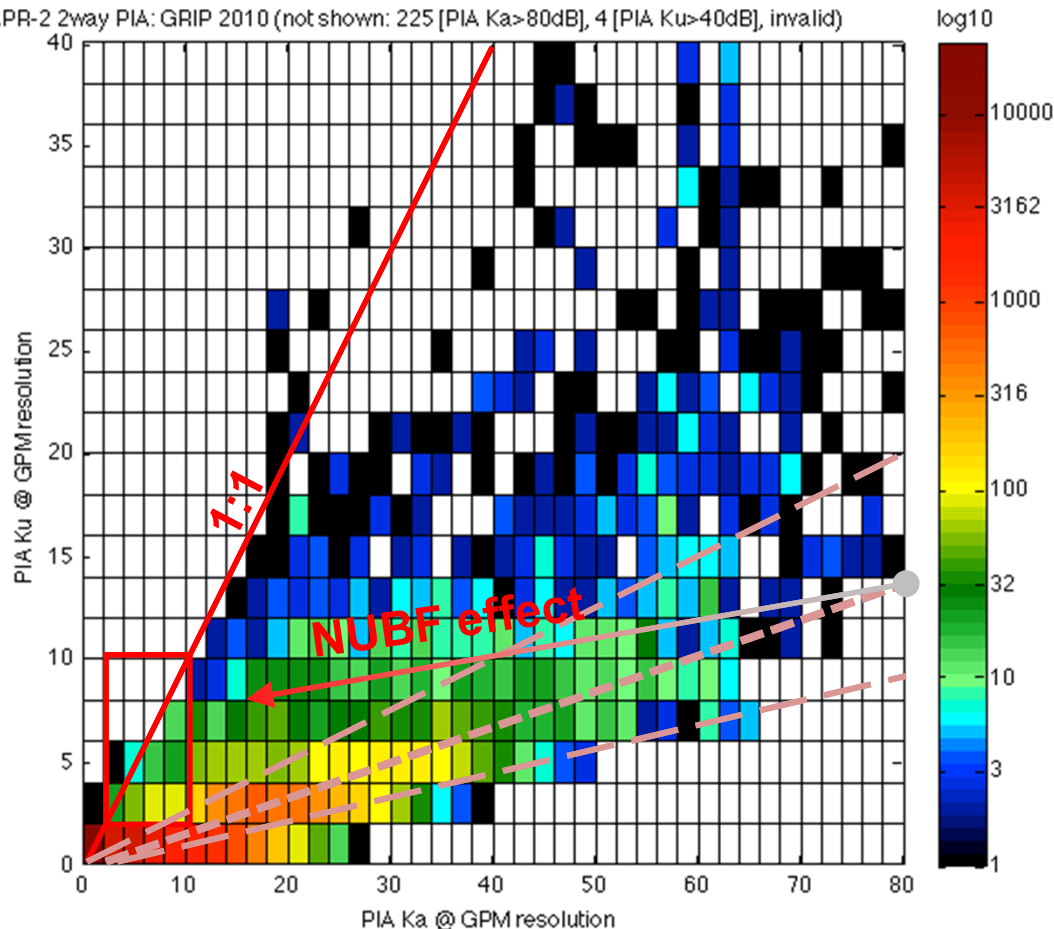


Invalid	32709		
PIA Ku →	< 2dB	<10dB & > 2dB	> 10 dB
Saturated Ka	0	33	225
PIA Ka > 10 dB	4612	6058	559
10dB > PIAKa > 2dB	12524	316	0
PIAKa < 2dB	33882	1	0

SRT useful only for Ka band

Ka-band PIA too low

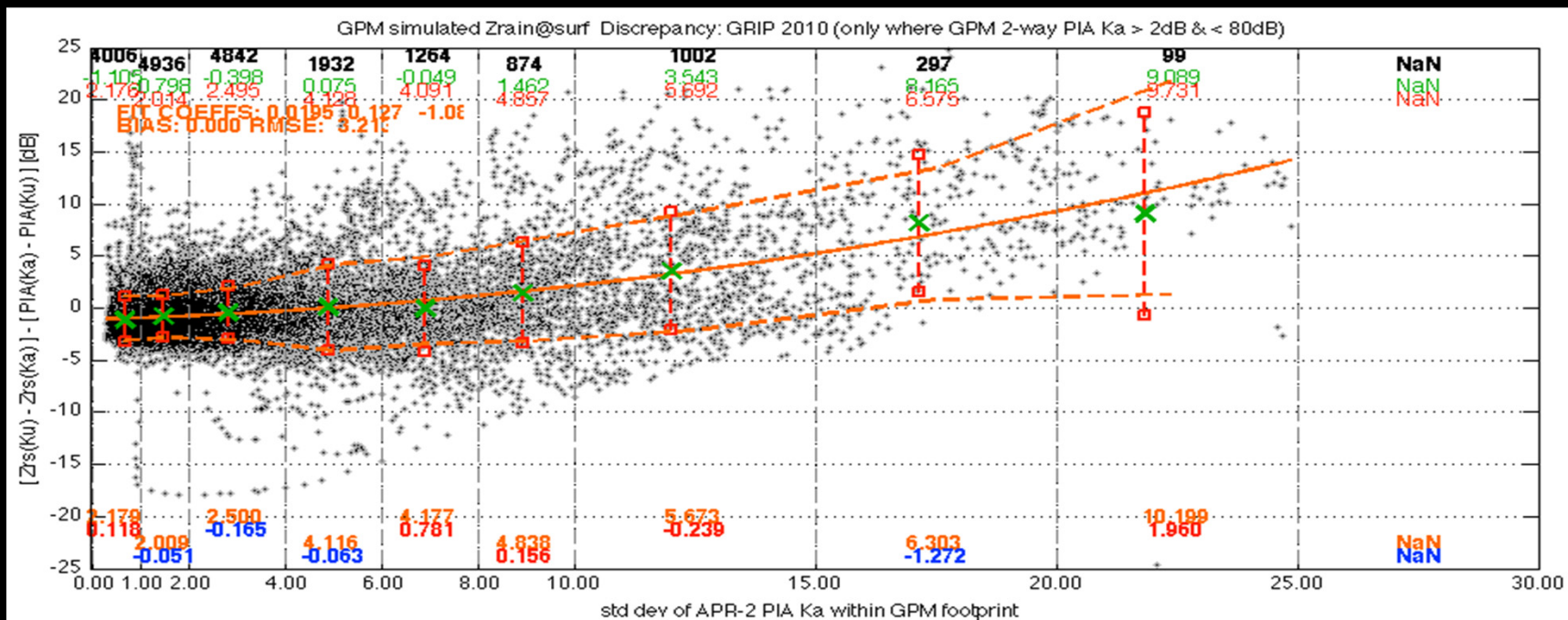
APR-2 2way PIA: GRIP 2010 (not shown: 225 [PIA Ka>80dB], 4 [PIA Ku>40dB], invalid)



- Under UBF conditions:  $PIAKa \approx (6 \pm 2)$
- Approximately 1 in 5 footprints with  $PIAKu > 2dB$  does not fall in this range
- At least 2 in 3 footprints with  $PIA > 10dB$  do not fall in this range
- In these conditions application of PIA from SRT will result in substantial underestimation
- In TRMM we had to live with it and correct statistically
- In GPM we can observe such departure when both PIAs are measurable
- Can we use such departure to correct?

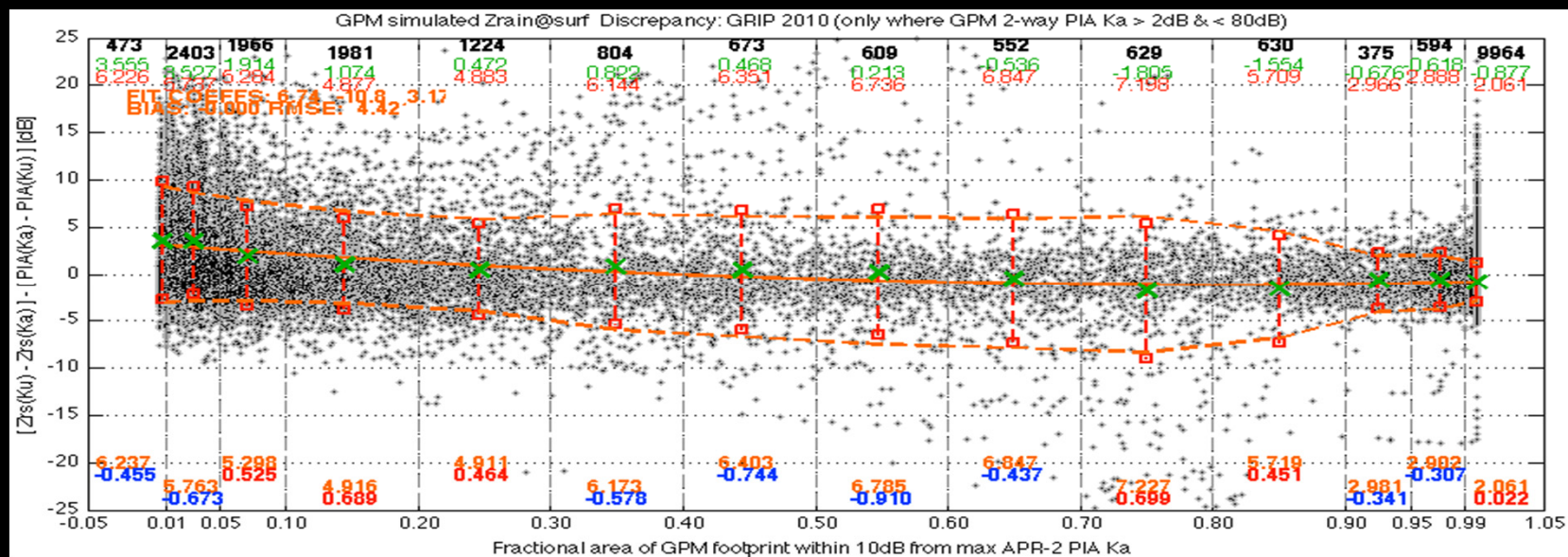
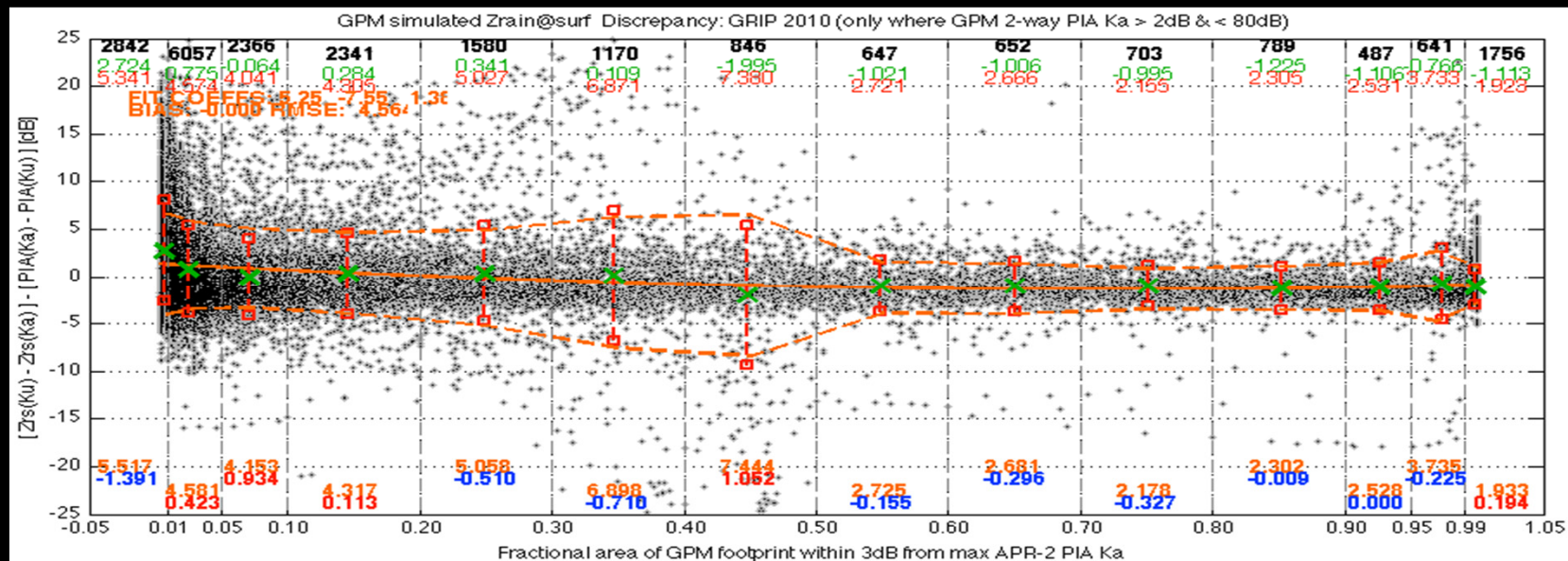


# “Discrepancy”



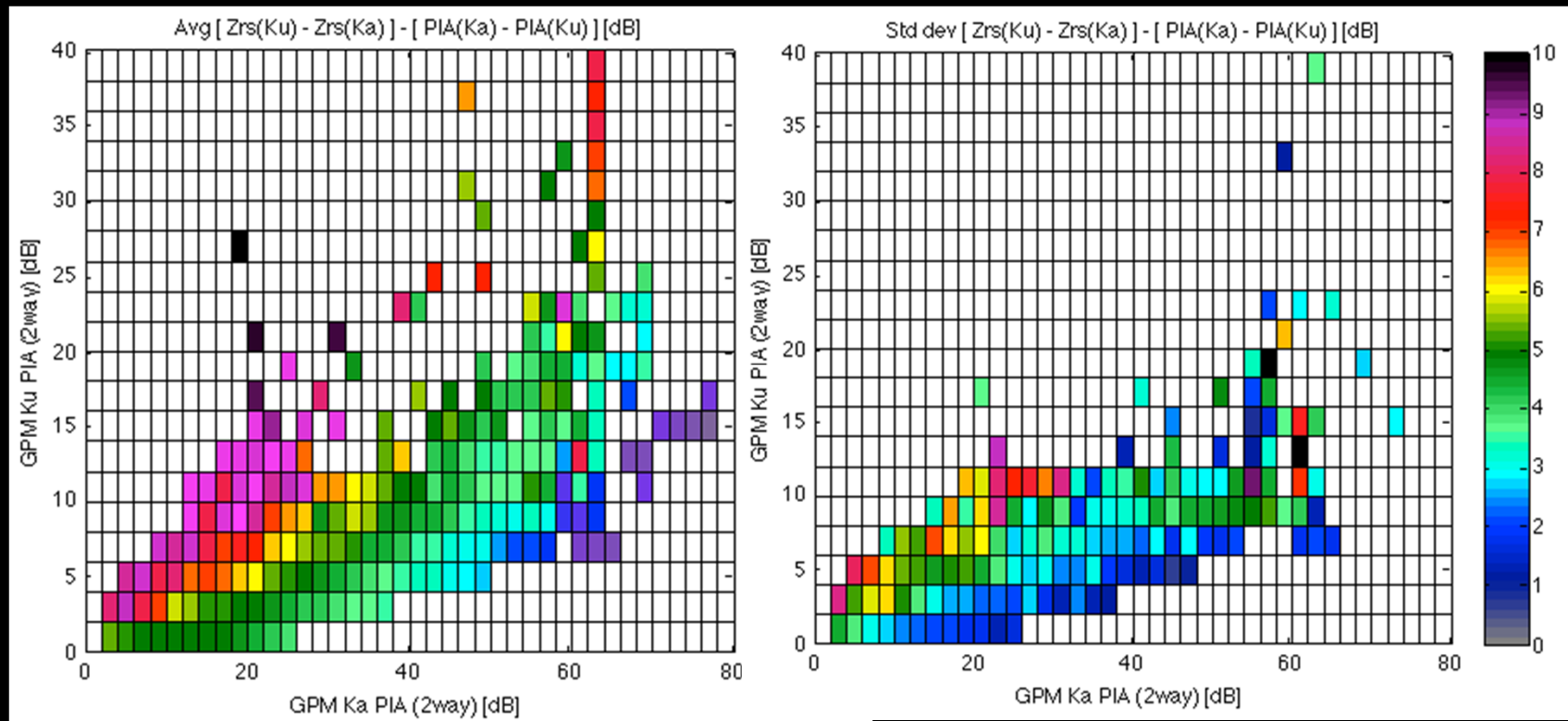


# "Discrepancy"





# Correction & Residual Uncertainty

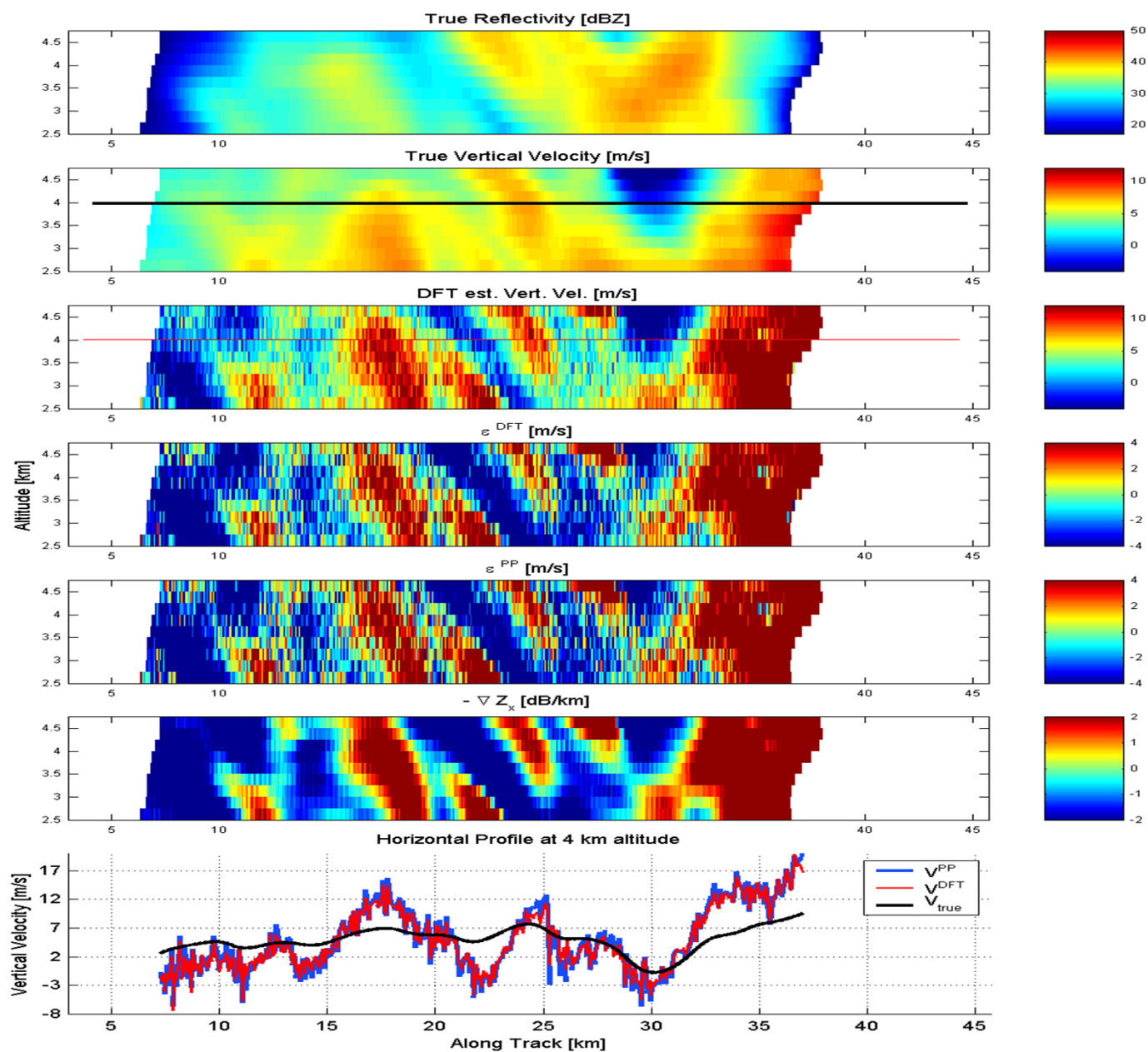




# NUBF-induced bias on velocity estimates



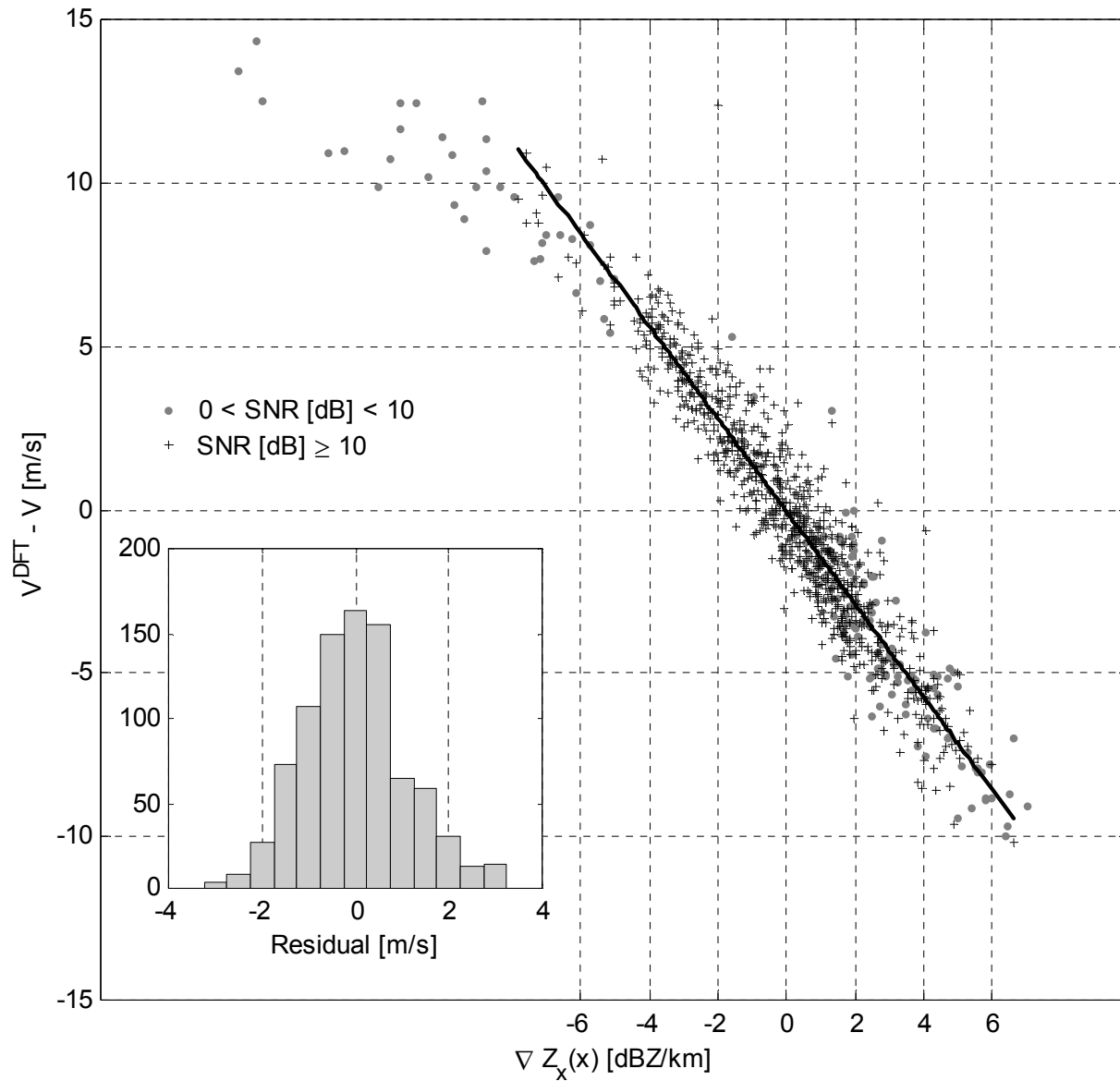
- NUBF (Non Uniform Beam Filling) induces a **bias** on the mean Doppler velocity estimate.
- Using conventional Pair-Pair or FFT techniques, the magnitude of such a bias can be of **several m/s**.
- The bias is highly correlated with the **reflectivity gradient in the along-track direction**. In fact the *isodops* for small  $\theta_{3dB}$  can be approximated by lines in the cross-track direction.





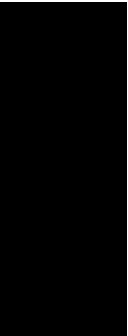
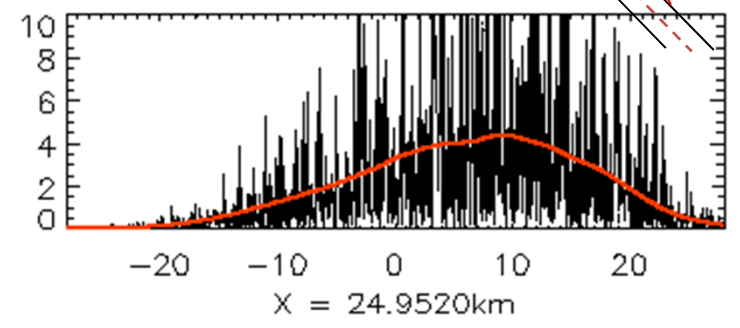
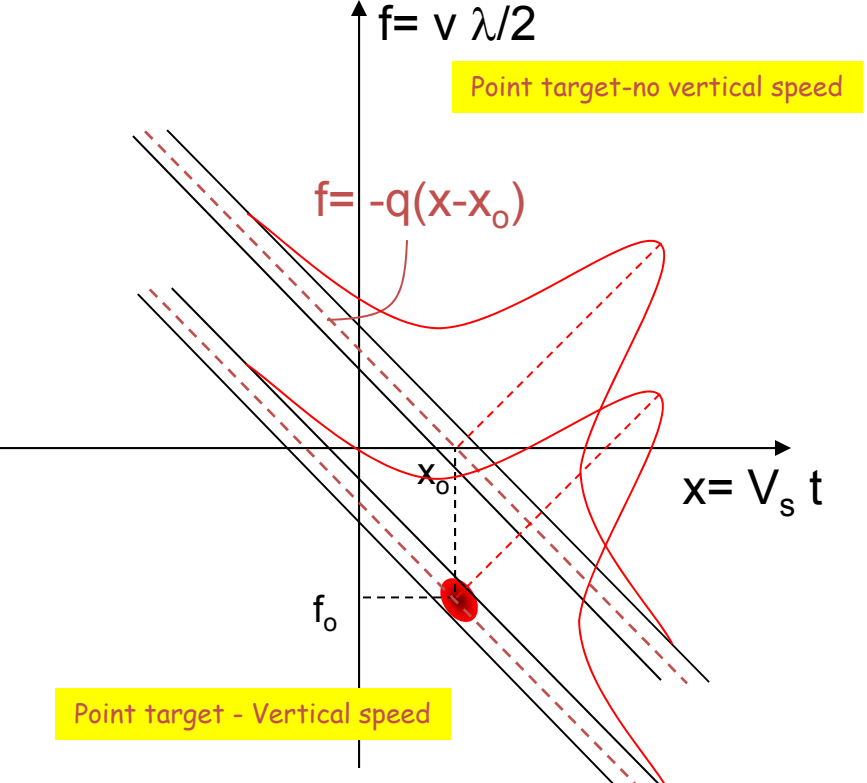
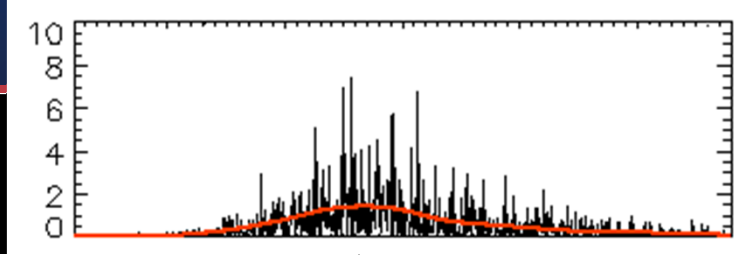
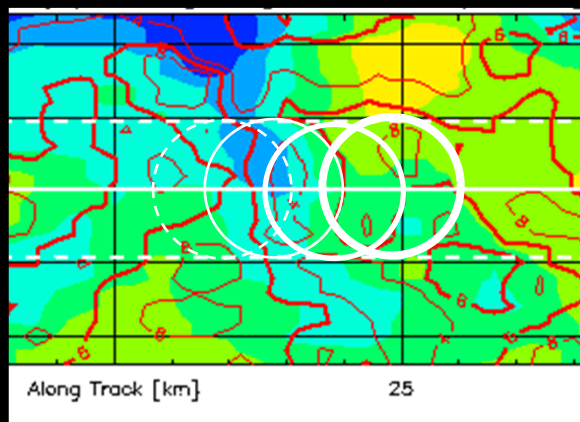
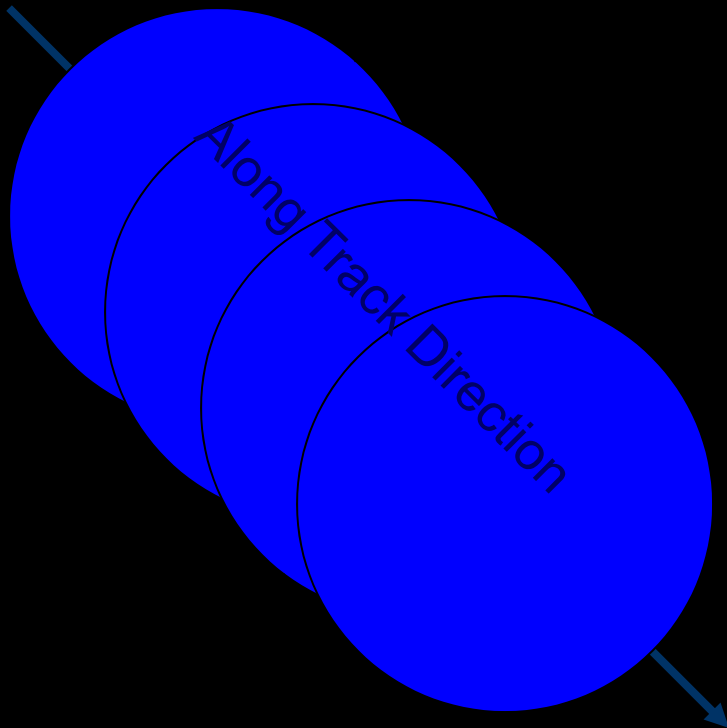
# NUBF induced bias on Velocity Estimates (2)

Correlation NUBF induced BIAS with Reflectivity Gradient in Along-Track direction





# Solution to NUBF: Along-track Oversampling & CFT



## Predicted CFT performance

The results obtained for standard estimators in UBF conditions can be extended to CFT (regardless of UBF or NUBF conditions) by assuming:

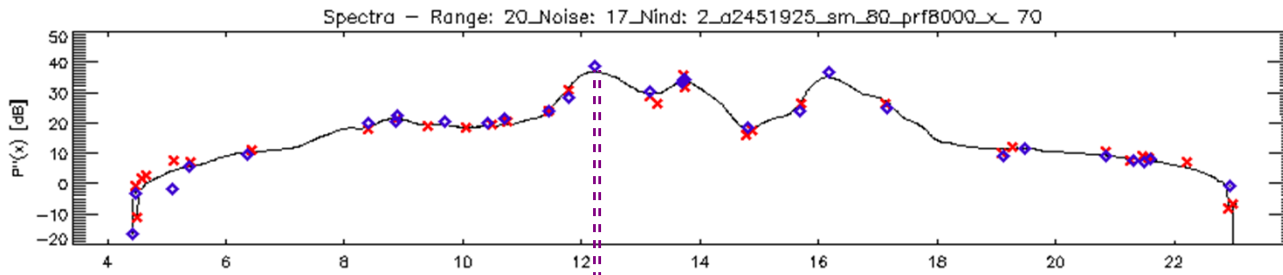
1. Normalized spectral width unaffected by NUBF
2. Equivalent number of samples calculated as:

$$M_{CFT} = \frac{\Delta x}{v_s} \frac{PRF}{N_C}$$

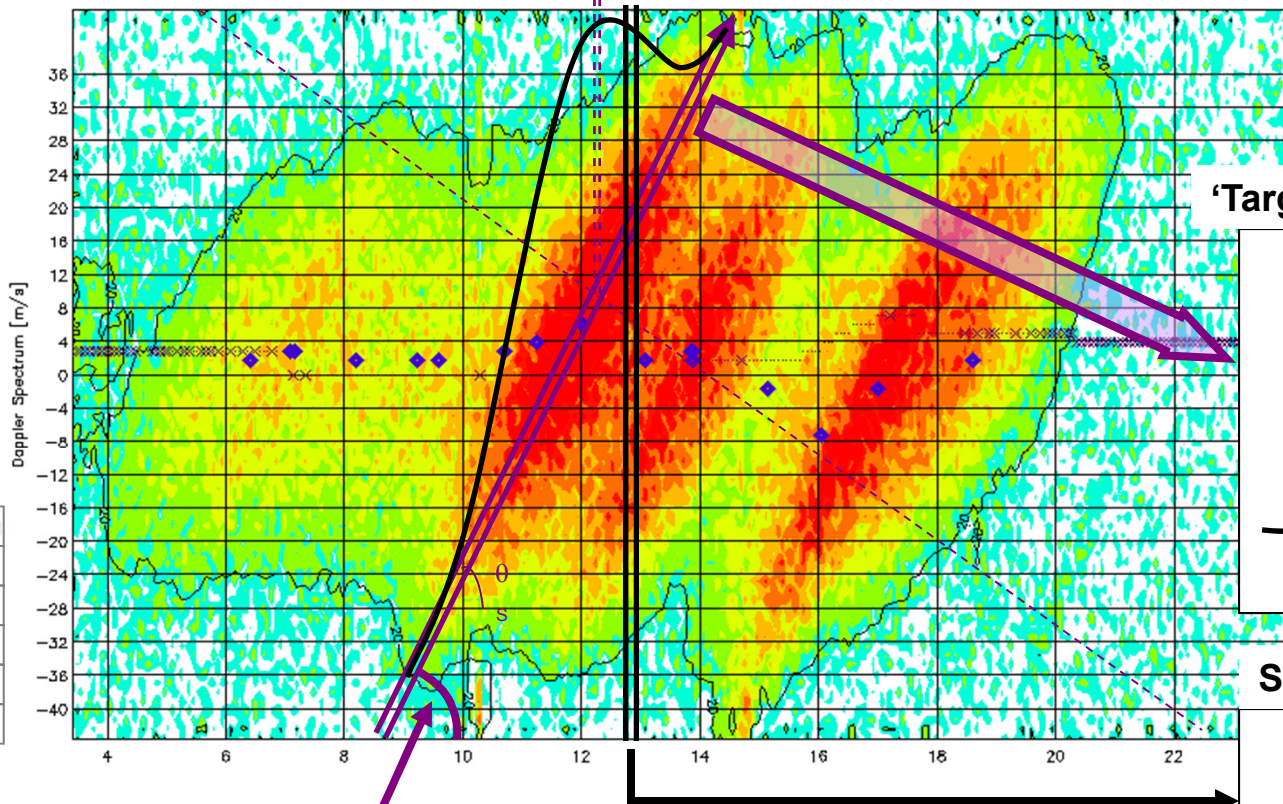
$\Delta x$  = size of along - track averaging window  
 $N_C$  = number of radar beams per cross - track scan

Example: PRF=6000,  $\theta_{3dB} = 0.3^\circ$ ,  $v_s = 7000$  m/s,  $h_s = 432$  km,  
 SNR = > 10 dB,  $\sigma_{\text{std}}$  of mean Doppler estimates (m/s)

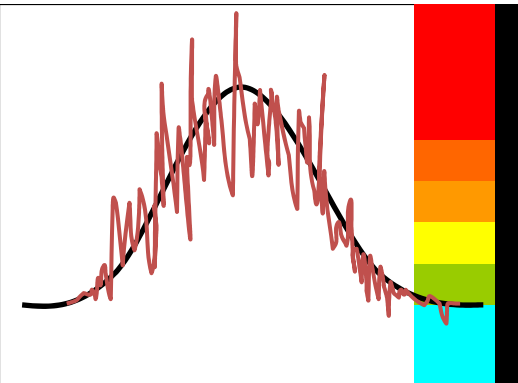
		$\Delta x$		
$M_{\text{TRACK}}$	$N_C$	700 m	2800 m	7000 m
60	1	0.42	0.20	0.13
30	2	0.59	0.29	0.19
20	3	0.72	0.36	0.23
12	5	0.93	0.46	0.29



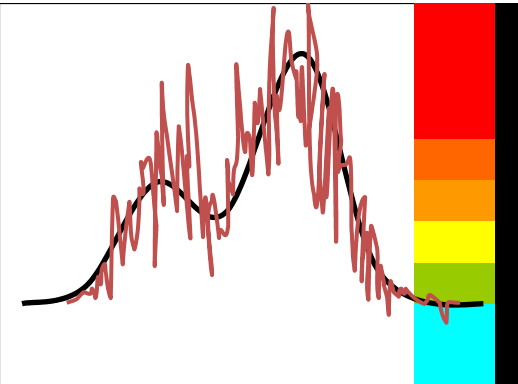
**Combined Frequency-Time (CFT) technique**



**'Target Track' in v-x (f-t) plane**



**Standard Doppler spectrum**



$$v'(\theta, \phi) = \frac{v_s}{h_s} x'$$

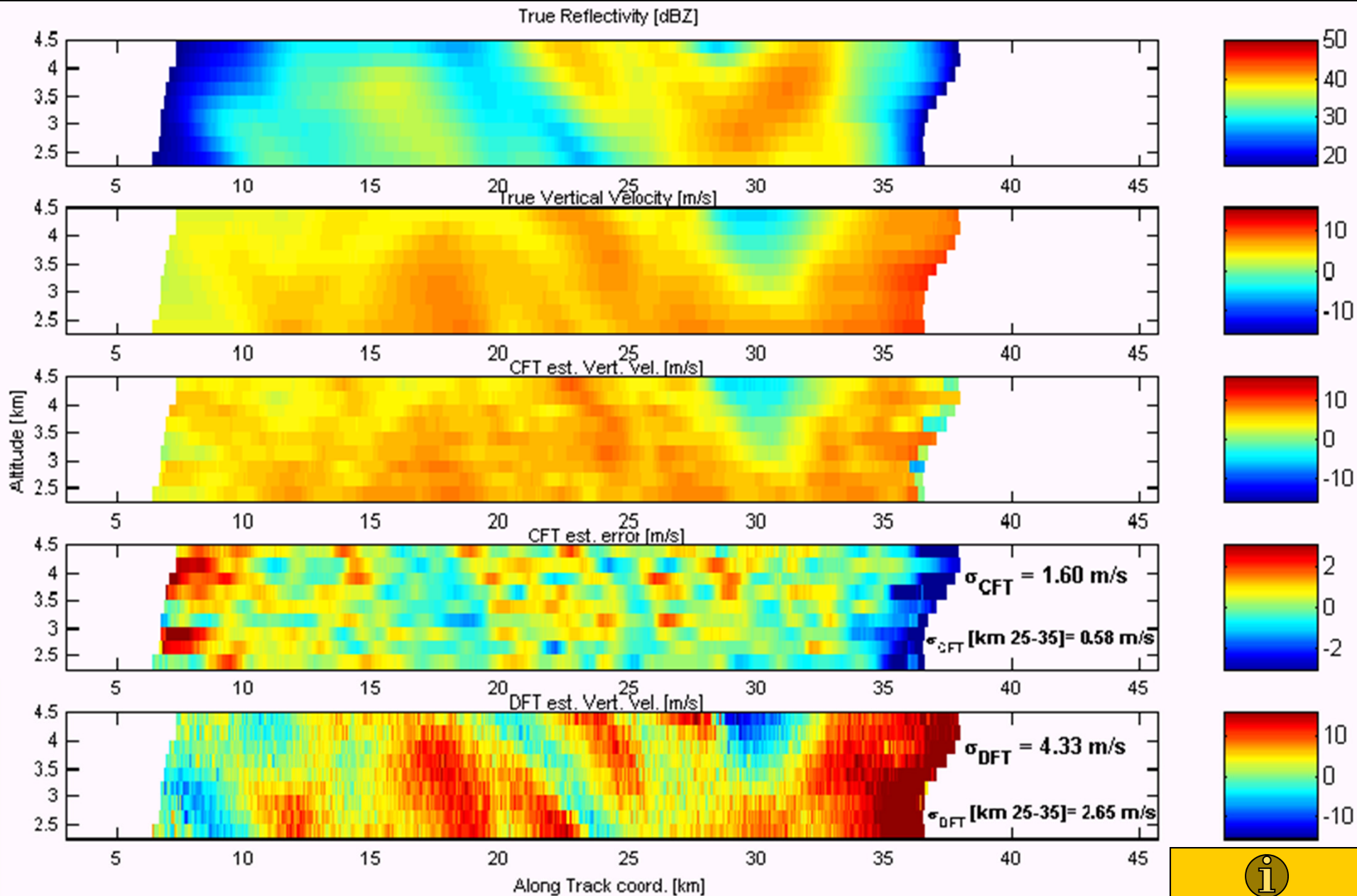
$$\frac{v_s}{h_s} \cong 16.2 \text{ m s}^{-1} \text{ km}^{-1}$$

$v_s$	7 km/s	$\theta_{3\text{dB}}$	$0.3^\circ$
$h_s$	432km	$F_0$	13.45 GHz
PRF	8000	$M$	80
$v_m$	44 m/s	$\sigma_{UN}$	0.13



# (3) NUBF induced error ARMAR-KWAJEX case study

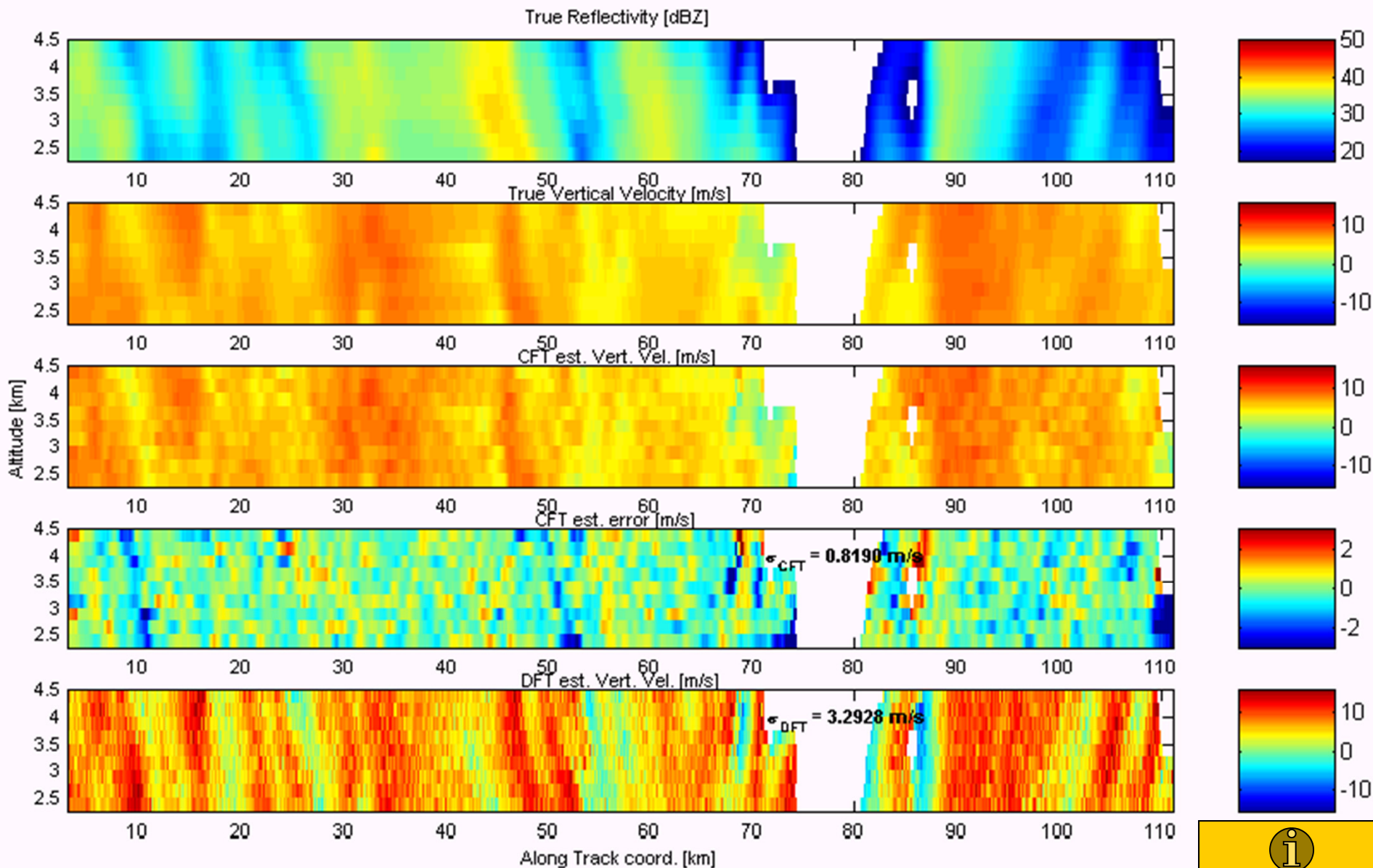
$v_s$	7 km/s	$\theta_{3dB}$	0.3°
$h_s$	432km	$F_0$	13.45 GHz
PRF	6000	$M$	64





# (3) NUBF induced error Hurricane Bonnie

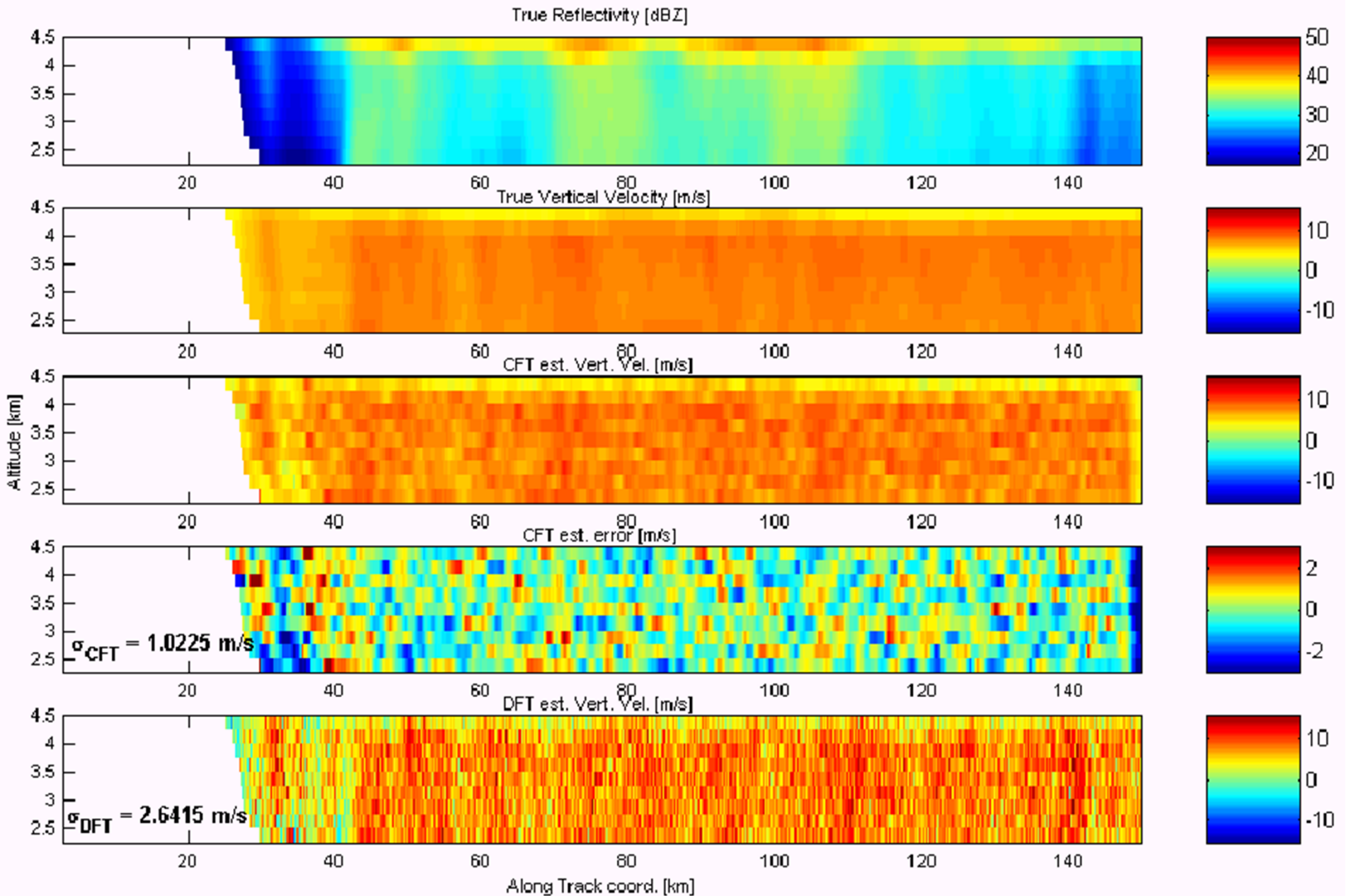
$v_s$	7 km/s	$\theta_{3dB}$	0.3°
$h_s$	432km	$F_0$	13.45 GHz
PRF	6000	$M$	64





### (3) NUBF induced error TOGA/COARE

$v_s$	7 km/s	$\theta_{3dB}$	0.3°
$h_s$	432km	$F_0$	13.45 GHz
PRF	6000	$M$	64





(4) Pointing induced error  
**Effects of Pointing Error**

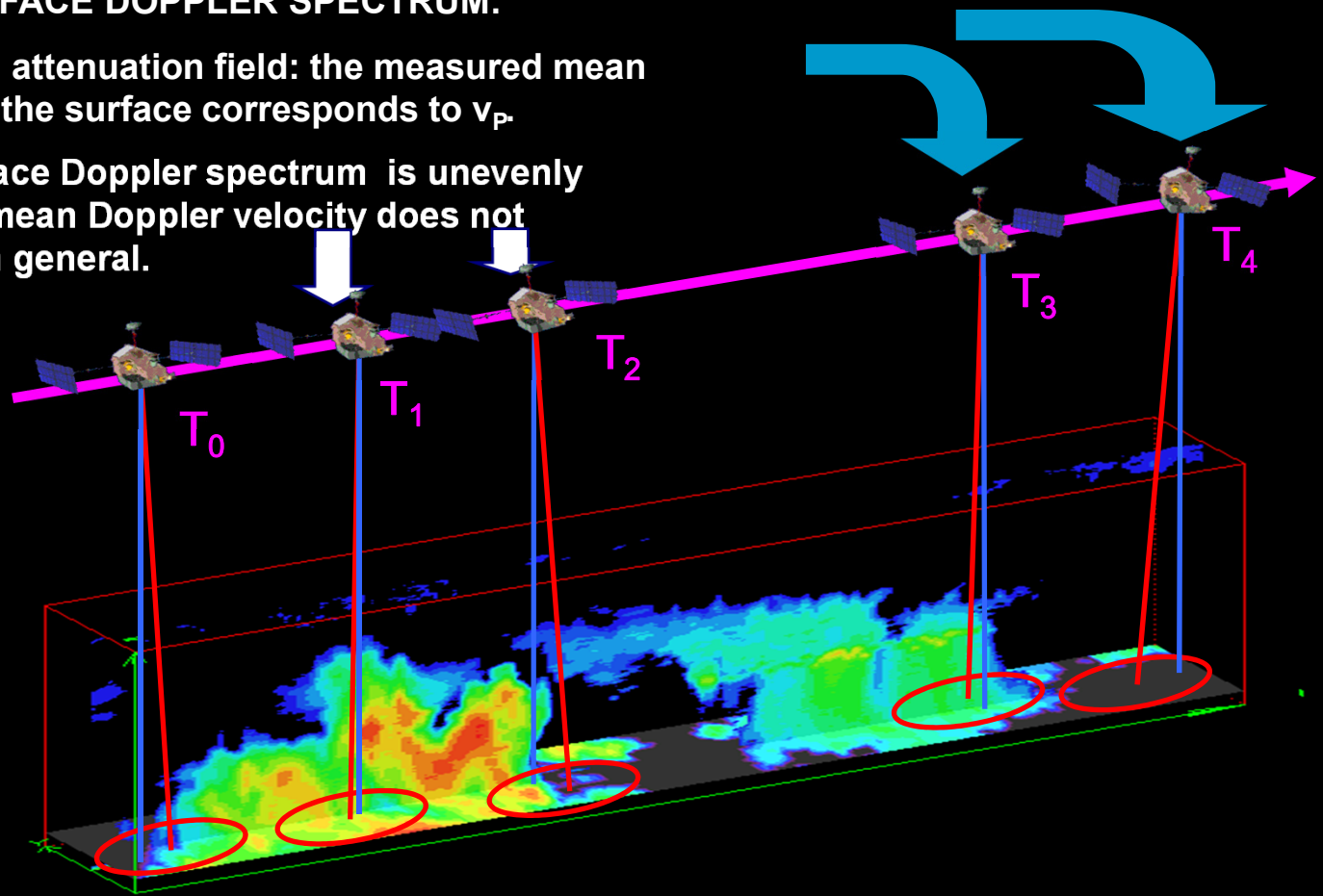
Options to satisfy the scientific requirement of 1 m/s accuracy in vertical rainfall velocity estimates:

1. VERY TIGHT POINTING ACCURACY BUDGET:  
 $\text{rms}(\theta_v) = 4 \text{ arcsec}$  is challenging for LEO satellites
2. ANALYSIS OF SEA SURFACE DOPPLER SPECTRUM:

- Clear air or uniform attenuation field: the measured mean Doppler velocity of the surface corresponds to  $v_p$ .
- NUBF: the sea surface Doppler spectrum is unevenly attenuated and its mean Doppler velocity does not correspond to  $v_p$ , in general.

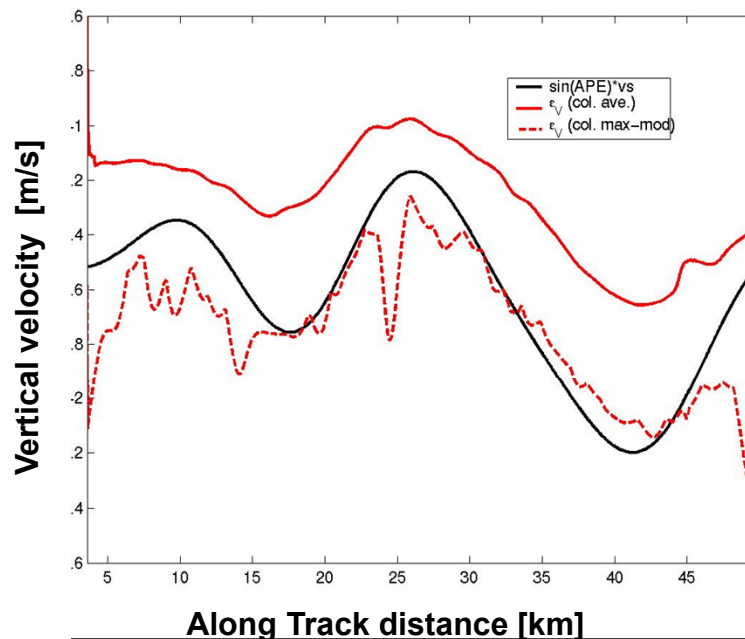
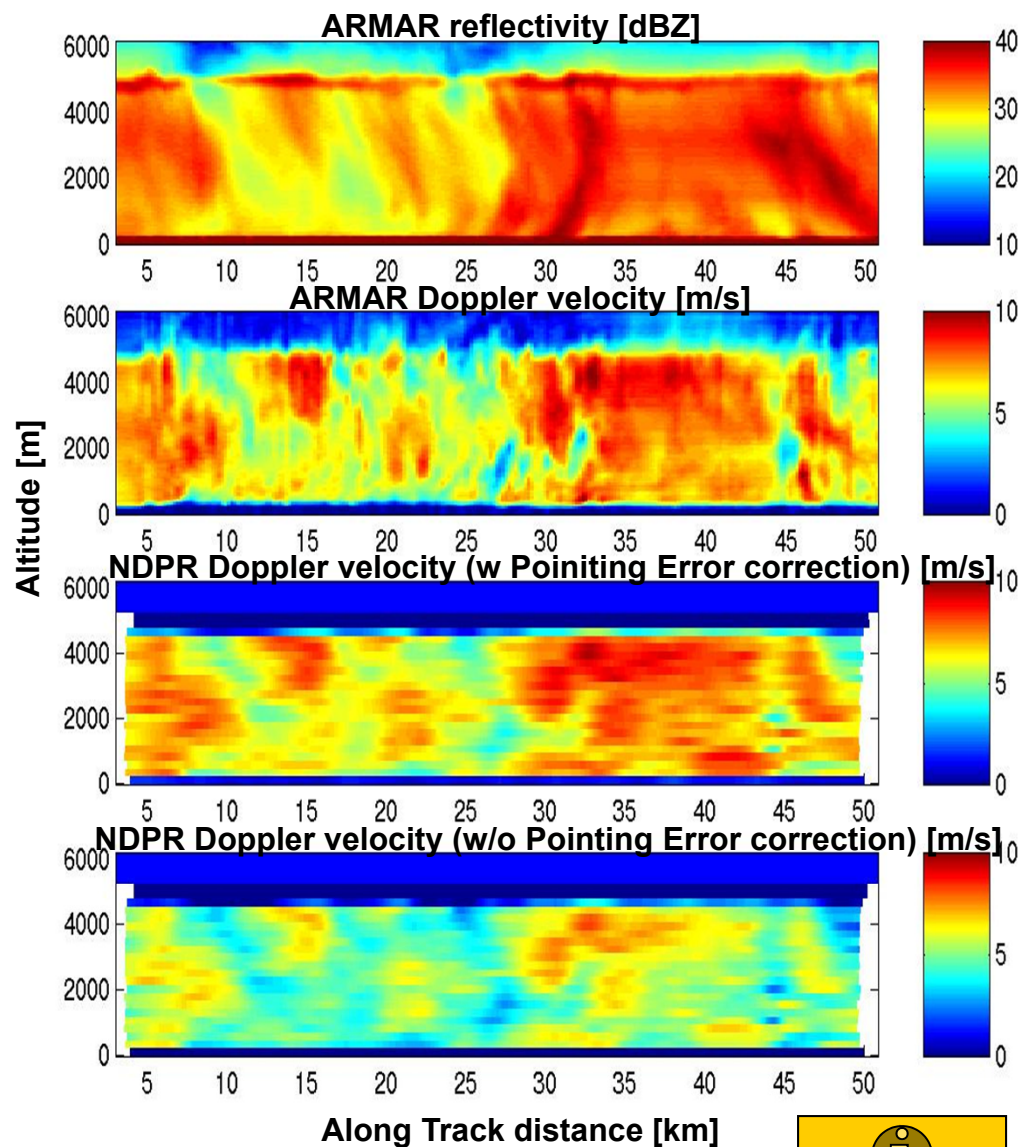
**Challenging pointing error budgets**

Pointing error (max. $\theta_v$ )	Vertical velocity offset (max. $ v_p $ )
4 arcsec	$(\theta_3/270) \Rightarrow 0.135 \text{ m/s}$
$0.01^\circ$	$(\theta_3/30) \Rightarrow 1.22 \text{ m/s}$
$0.05^\circ$	$(\theta_3/6) \Rightarrow 6.1 \text{ m/s}$





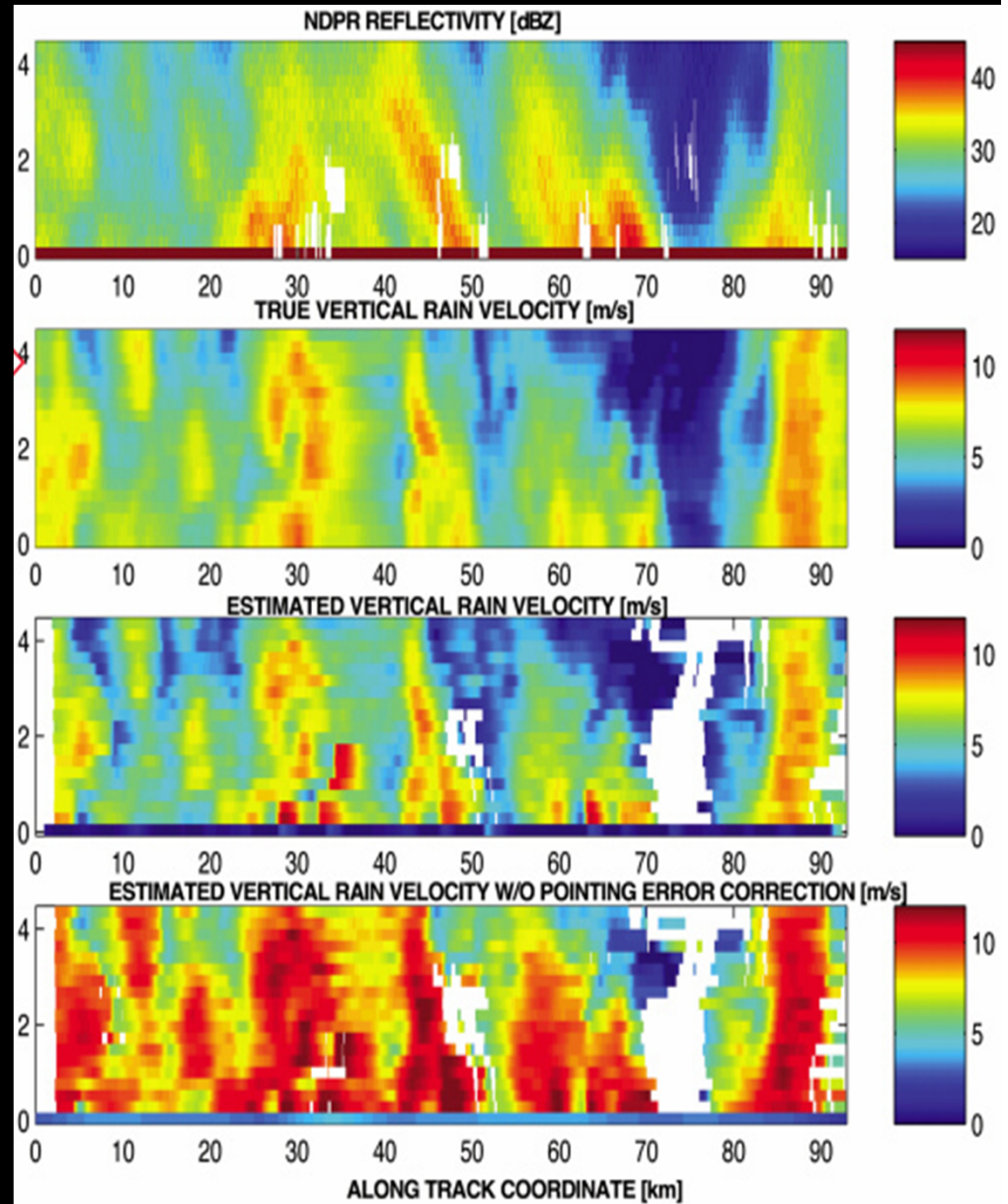
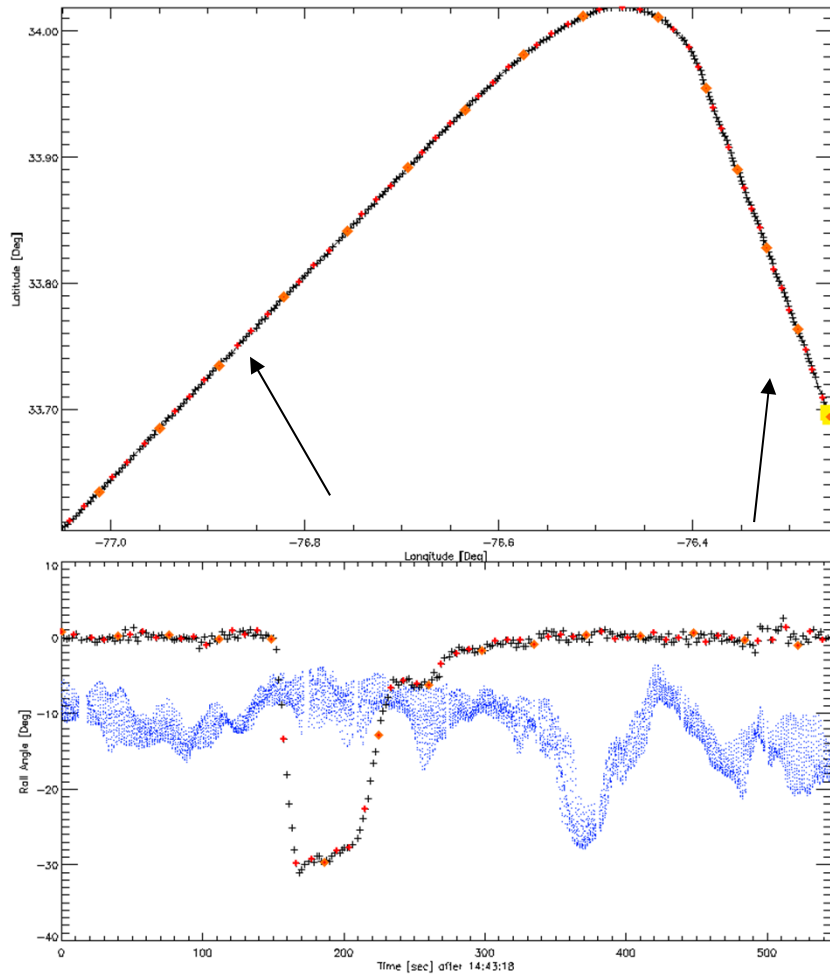
# Correction of Pointing induced Error





# Correction of Pointing Error - Hurricane Bonnie

(4) Pointing induced error





# Simulated Example from Spaceborne Doppler Radar



- Reflectivity and Doppler measurements of a CRM-generated storm

Mass content  
Black = Rain  
Blue = Ice

True Vert.  
Vel. [m/s]

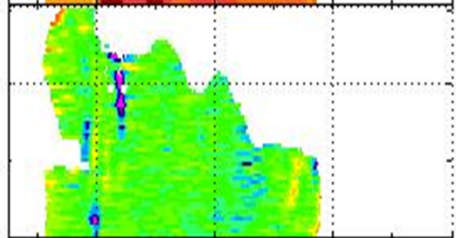
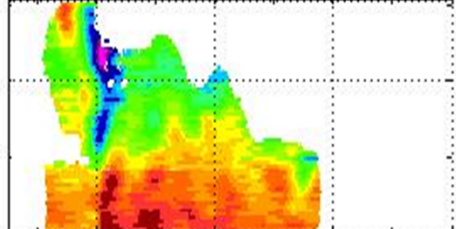
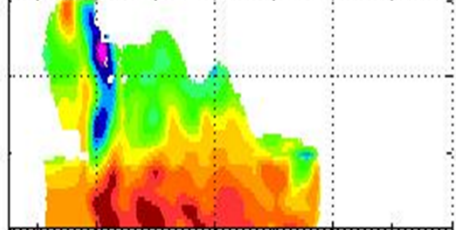
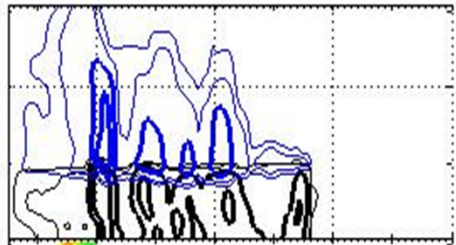
$V_{true}$

Estimated [m/s]

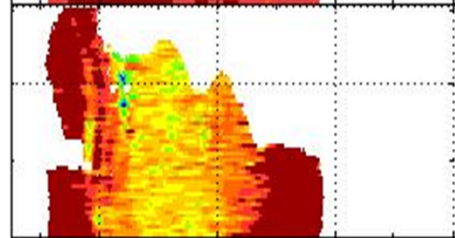
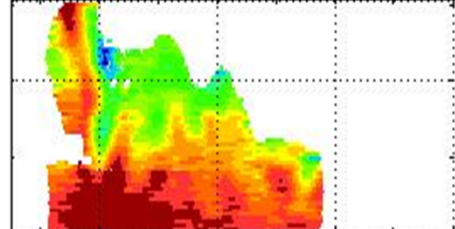
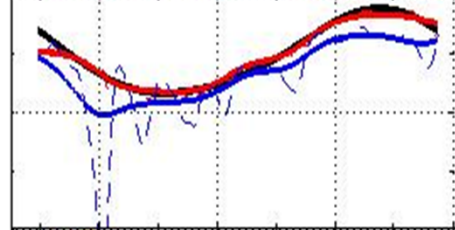
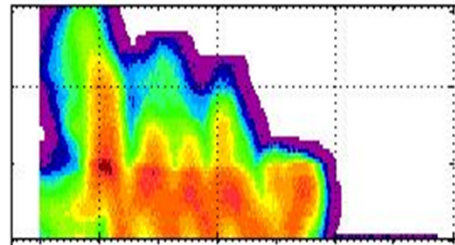
$V_{CFT/CFT}$

Error [m/s]

$V_{CFT/CFT} - V_{true}$



Along Track distance [km]



Along Track distance [km]

Reflectivity 14 GHz  
[dBZ]

Apparent surface vel.  
[m/s]: black=true, blue:  
DFT, red:CFT

Error [m/s]

$V_{DFT/CFT} - V_{true}$

Error [m/s]

$V_{NO/CFT} - V_{true}$



# Solution to Pointing Errors



- CFT can be applied to the Doppler spectrum of the sea surface

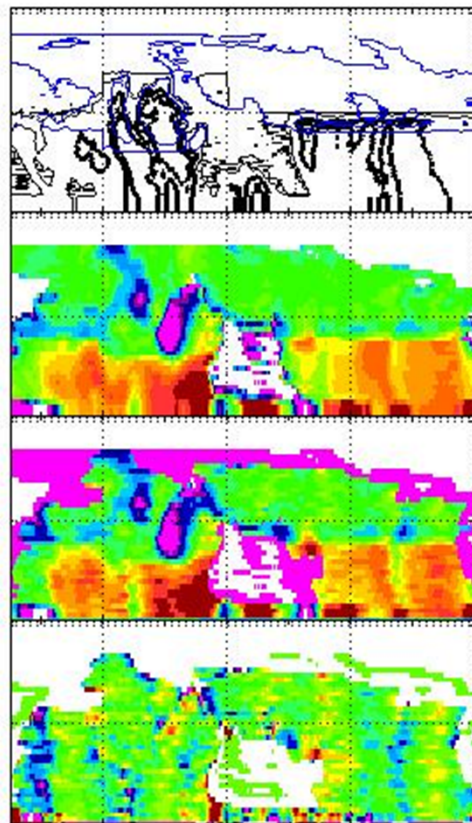
ARMAR Kwajex

Mass content  
 Black = Rain  
 Blue = Ice

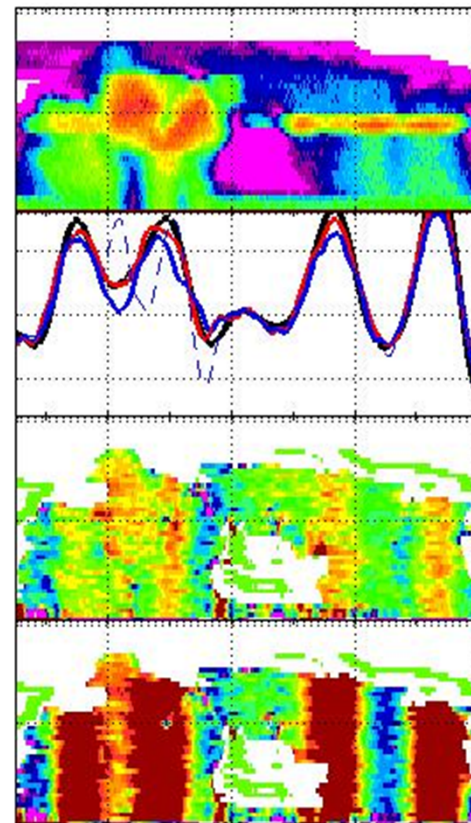
True Vert. Vel.  
 [m/s]  $V_{true}$

Estimated [m/s]  
 $V_{CFT/CFT}$

Error [m/s]  
 $V_{CFT/CFT} - V_{true}$



20 40 60  
 Along Track distance [km]



20 40 60  
 Along Track distance [km]

50 Reflectivity  
 14 GHz [dBZ]  
 0  
 +5 Apparent surface vel.  
 [m/s]: black=true, blue  
 DFT, red:CFT  
 0  
 -5  
 +2 Error [m/s]  
 0  $V_{DFT/CFT} - V_{true}$   
 -2  
 +2 Error [m/s]  
 0  $V_{NO/CFT} - V_{true}$   
 -2

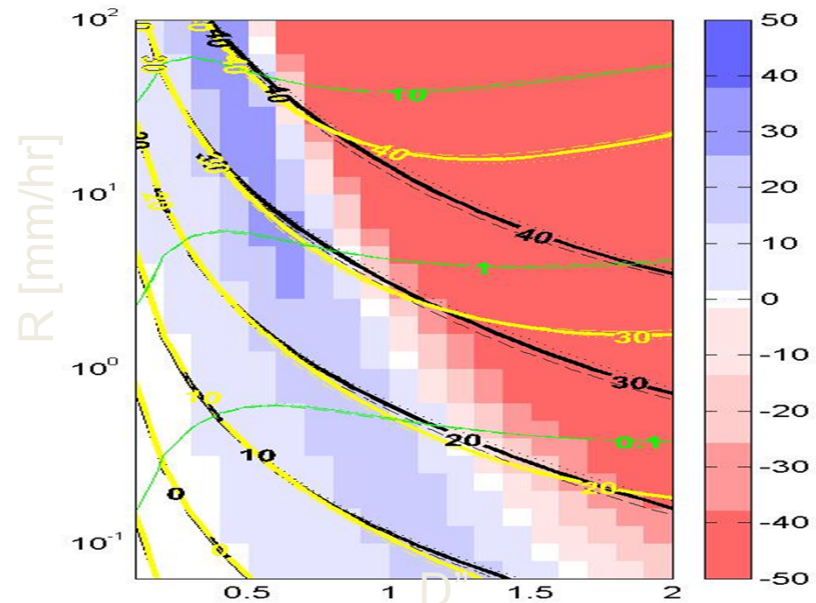
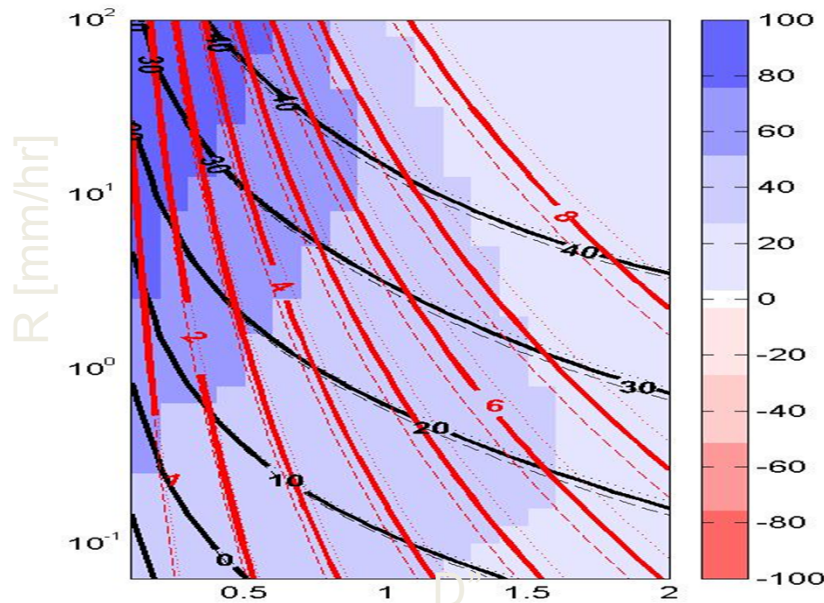


# Estimation of Precipitation Intensity and Mean Hydrometeor Size



Jacobian Determinant  $J_{Z14/V-R/D''}$

Jacobian Determinant  $J_{Z14/Z35-R/D''}$

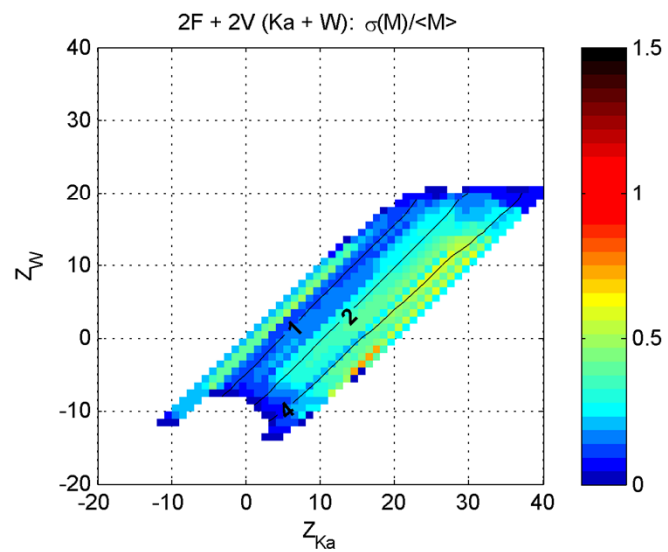
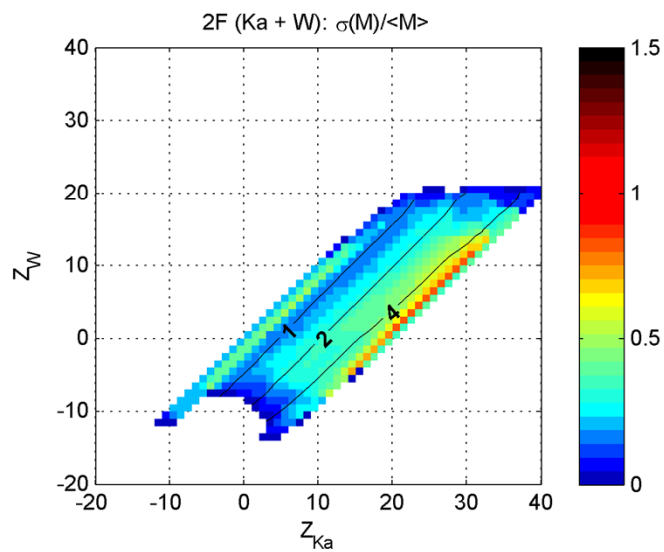
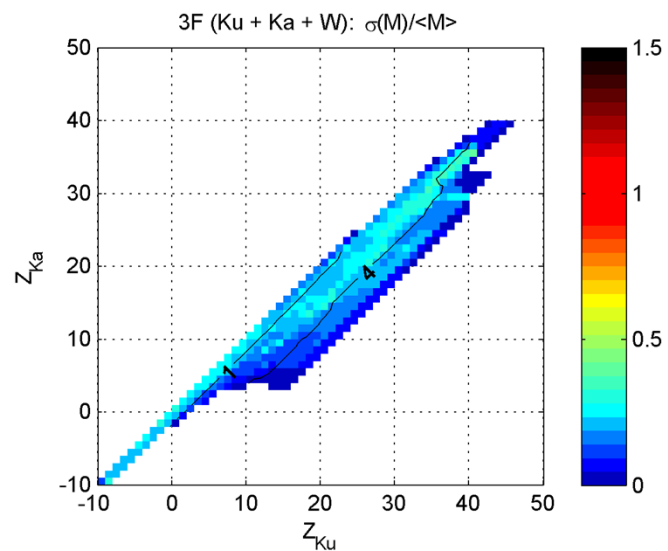
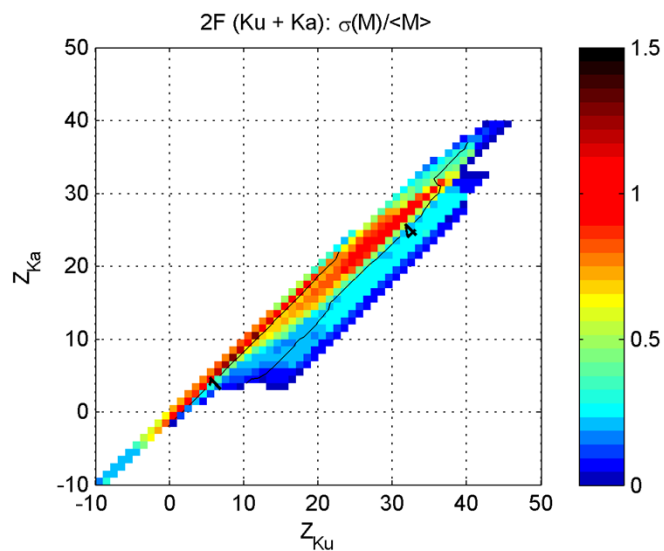


- Color
- Reflectivity 14 GHz [dBZ]
- Mean Doppler velocity [m/s]
- Reflectivity 35 GHz [dBZ]
- Specific Attenuation 35 GHz [dB/km]
- Linestyle
- $s'' = 0.38$
- $s'' = 0.34$
- $s'' = 0.42$

- DSD parameter estimation

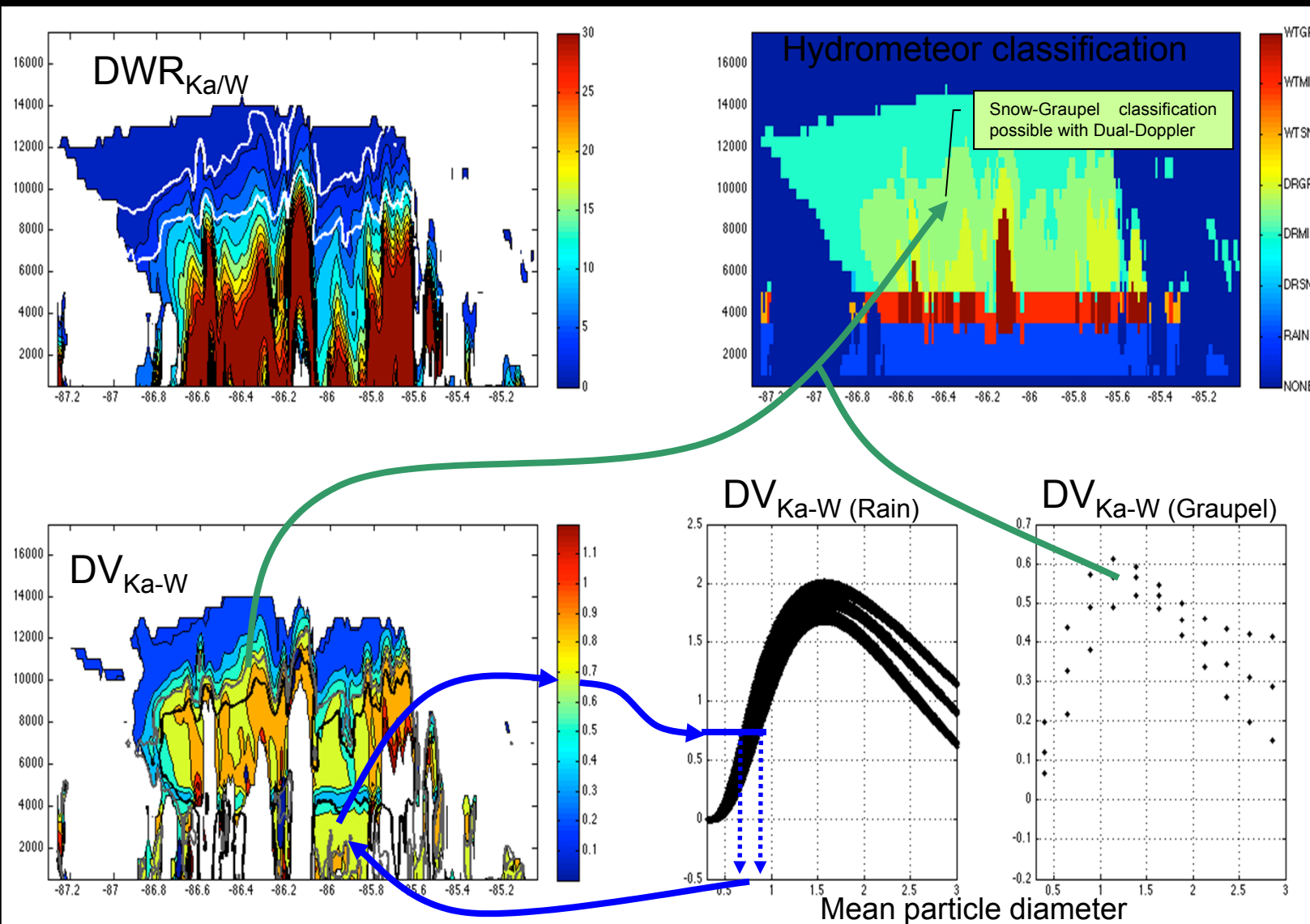


# Residual uncertainties in frozen hydrometeor estimation





# Dual-Doppler (Ka-W) measurement





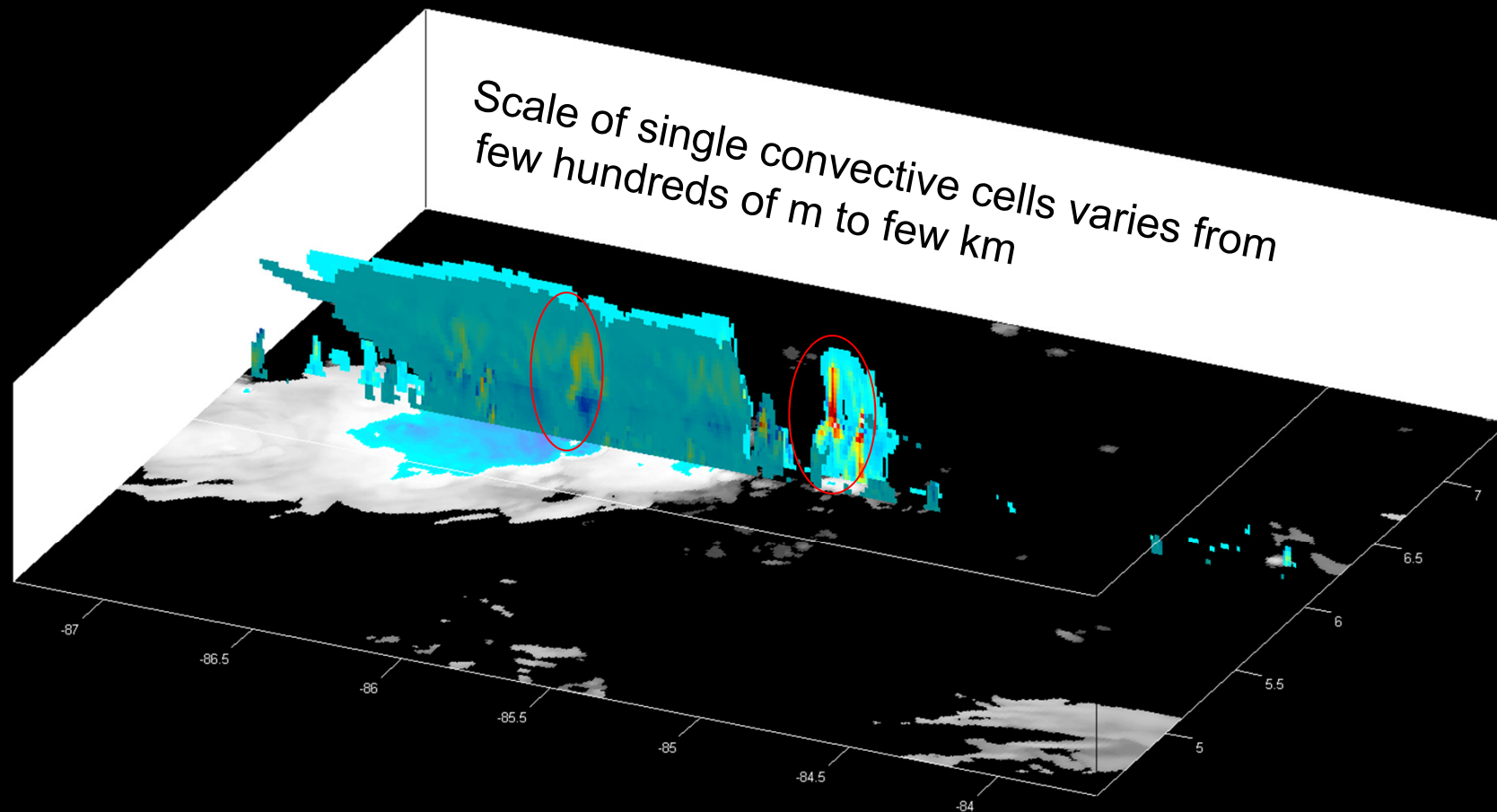
# Why Doppler? (again)



Goal	Potential of Doppler	Alternative spaceborne observing systems & methods	Contribution to Weather and Climate knowledge
<i>Measurement of Vertical Air Motion and Characterization of Convection</i>	Essential	None in precipitation – Potential use of lidar in clear air	<ul style="list-style-type: none"> <li>- Improvement in GCM's skills by assimilating vertical velocity</li> <li>- Understanding of precipitation processes and dynamics on a global scale</li> <li>- Improvement in the characterization of convection (vertical profiling and temporal evolution)</li> <li>- Improvement of global databases for characterizing convection in models</li> </ul>
<i>Hydrometeor Classification</i>	Moderate	Radiometers - <i>limited vertical resolution.</i> Non-Doppler multi-frequency radars - <i>performances to be verified.</i>	<ul style="list-style-type: none"> <li>- Cloud microphysics</li> </ul>
<i>Estimation of Precipitation and DSD parameters</i>	High in stratiform Low in convection	Multiparametric approaches (multifrequency, combined radar/radiometer) - <i>limited accuracy and/or vertical resolution</i>	<ul style="list-style-type: none"> <li>- Improvement in rainfall rate estimates for assimilation in GCM's</li> </ul>
<i>Convective/Stratiform Classification</i>	Moderate	Non-Doppler Radar - <i>acceptable performances over the tropics (TRMM) - to be verified on a global scale (GPM)</i>	<ul style="list-style-type: none"> <li>- Improvement in Latent Heating global maps</li> <li>- Improvement in radiation budget studies</li> <li>- Improvement in rainfall rate estimates</li> </ul>
<i>Latent Heat</i>	High	Multiparametric approaches (multifrequency, radar/radiometer) - <i>good in estimating maximum, unreliable performances in vertical profiling (especially in convection)</i>	<ul style="list-style-type: none"> <li>- Improvement in Latent Heating vertical profiling for assimilation in atmospheric models</li> </ul>



## Characterization of convection and vertical transport



- Model generated scenarios are used to create the database for microphysics and dynamic retrievals. High resolution model outputs (in this example WRF 1km) have been compared to observations only for a limited set of field campaigns.



# Heating and dynamics



Apparent Heat Source  $Q_1 = \frac{\partial \bar{s}}{\partial t} + \nabla \cdot \bar{s} \bar{V} + \frac{\partial \bar{s} \bar{w}}{\partial p} = Q_R + L_v(\bar{c} - \bar{s}) + (L_v + L_f)(\bar{d} - \bar{s}_w) + L_f(\bar{f} - \bar{m}) - \nabla \cdot \bar{s}' \bar{V}' - \frac{\partial \bar{s}' \bar{w}'}{\partial p}$

**Hydrometeor Phase Change Rate**

$$P_{1,2} = \left| \frac{\partial F_1(z)}{\partial z} - \frac{\partial F_2(z)}{\partial z} \right|$$

**Hydrometeor Vertical Mass Flux**

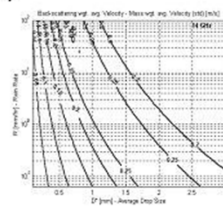
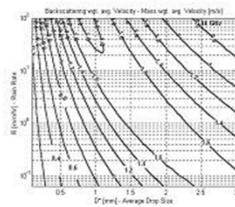
$$F(z) = M(z)[v_T(z) - w(z)]$$

**Mean (mass-weighted) Terminal Velocity**

$$v_T = \frac{\pi \rho}{6M} \int v_t(D) D^3 N(D) dD$$

**Mean (reflectivity-weighted) Particle Velocity**

$$v_P = \frac{1}{\eta} \int [v_t(D) - w] \sigma_b(D) N(D) dD$$



SHIGE ET AL.

*GCE-simulated  $Q_1 R_p$  Profiles*  
 == Convective Regions ==

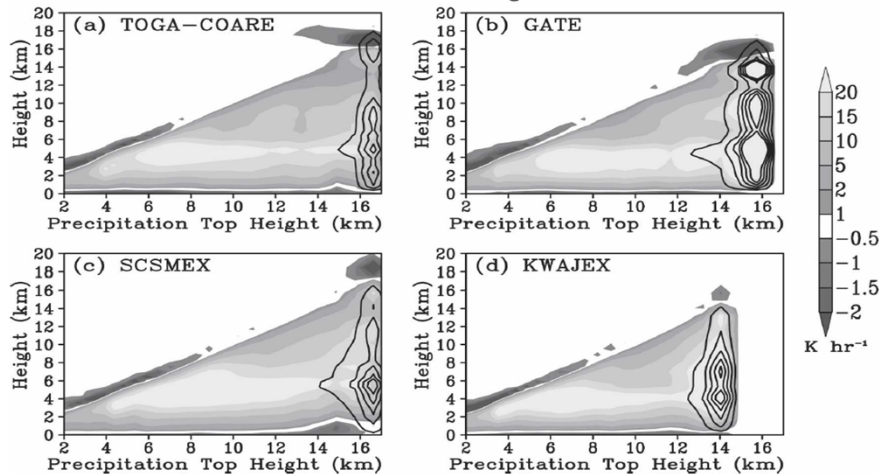


FIG. 5. Ensemble-mean GCE-simulated  $Q_1 R_p$  profiles plotted as a function of PTH from the convective regions of the (a) COARE, (b) GATE, (c) SCSMEX, and (d) KWAJEX cases. Contours indicate confidence intervals for a mean at the 95% level using the Student's  $t$  test. The contour interval (CI) is  $2.0 \text{ K h}^{-1}$ .

- Three main quantities must be estimated either directly or indirectly:
  - Mass
  - Phase
  - Vertical Motion
- Non-Doppler measurements carry information on Mass and Phase but vertical motion must be inferred entirely from pre-constructed Databases.
  - At a scale large enough not- to resolve convection the residual variability is small, though not negligible (Shige et al. 2007).
  - At a convection-resolving scale the residual variability is large enough to include sign reversals (next slide)
  - In general, extension of TRMM algorithms to extratropical observations will require a large effort to characterize variability on a global scale
- Doppler measurements at nadir are close proxies to the Mass weighted mean vertical velocity of hydrometeors



## Apparent Heat Source

$$Q_1 = \frac{\partial \bar{s}}{\partial t} + \nabla \cdot \bar{s} \bar{V} + \frac{\partial \bar{s} \bar{\omega}}{\partial p} = Q_R + L_v (\bar{c} - \bar{e}) + (L_v + L_f)(\bar{d} - \bar{s}^*) + L_f (\bar{f} - \bar{m}) - \nabla \cdot \bar{s}' \bar{V}' - \frac{\partial \bar{s}' \bar{\omega}'}{\partial p}$$

- **Latent Heat Absorption/Release** due to the water phase changes is one of major contributors to the overall heating.
- **Stratiform Precipitation:** heating in the upper troposphere (deposition and freezing) and cooling in the lower troposphere (evaporation). Vertical profiles are quite consistent over the globe (aside from the altitude of the 'sign' change which is dependent on the altitude of the melting layer).
- **Convective Cells:** Heating and cooling are determined by the presence and magnitude of updrafts and downdrafts. Vertical profiles of latent heating differ significantly from stratiform precipitation and are also quite different for different regions, seasons and even within the diurnal cycle.
- **Surface Rainfall Rate:** assuming no horizontal advection, the surface rainfall rate corresponds to the integral (column) amount of condensed liquid water and can therefore be used to estimate the integral latent heat released.
- **Refer to:** Yanai et al. 1973, Houze 1982, Houze 1989, Tao et al. 2001

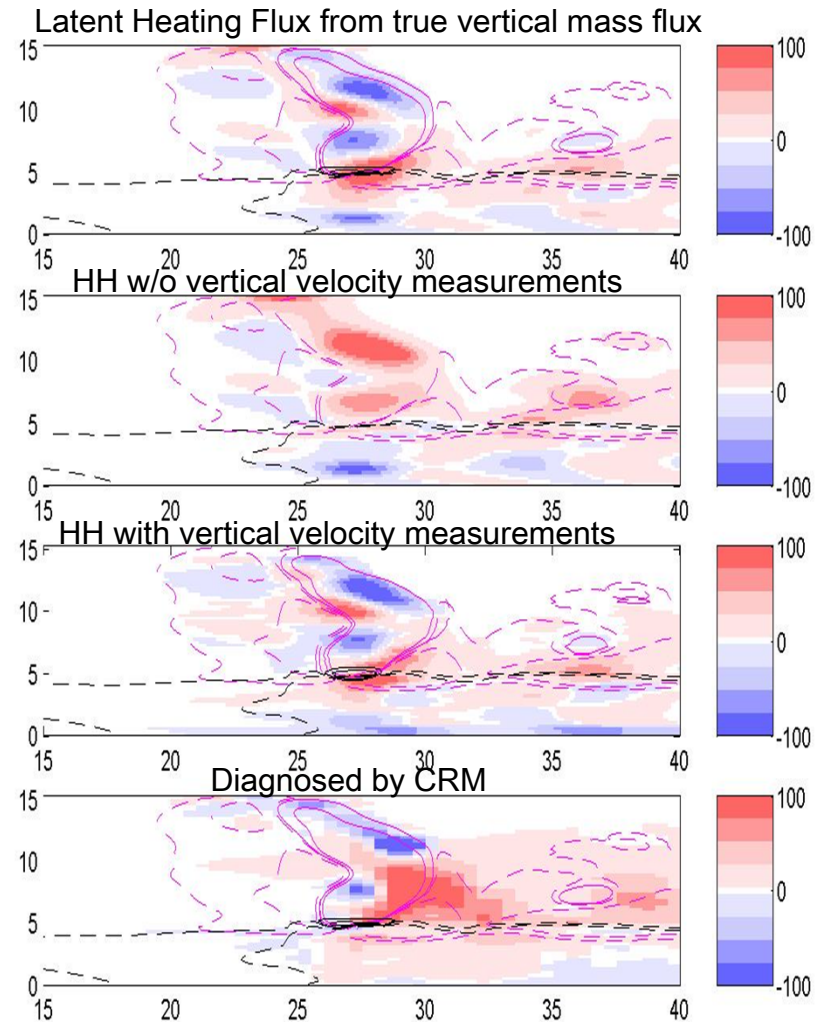
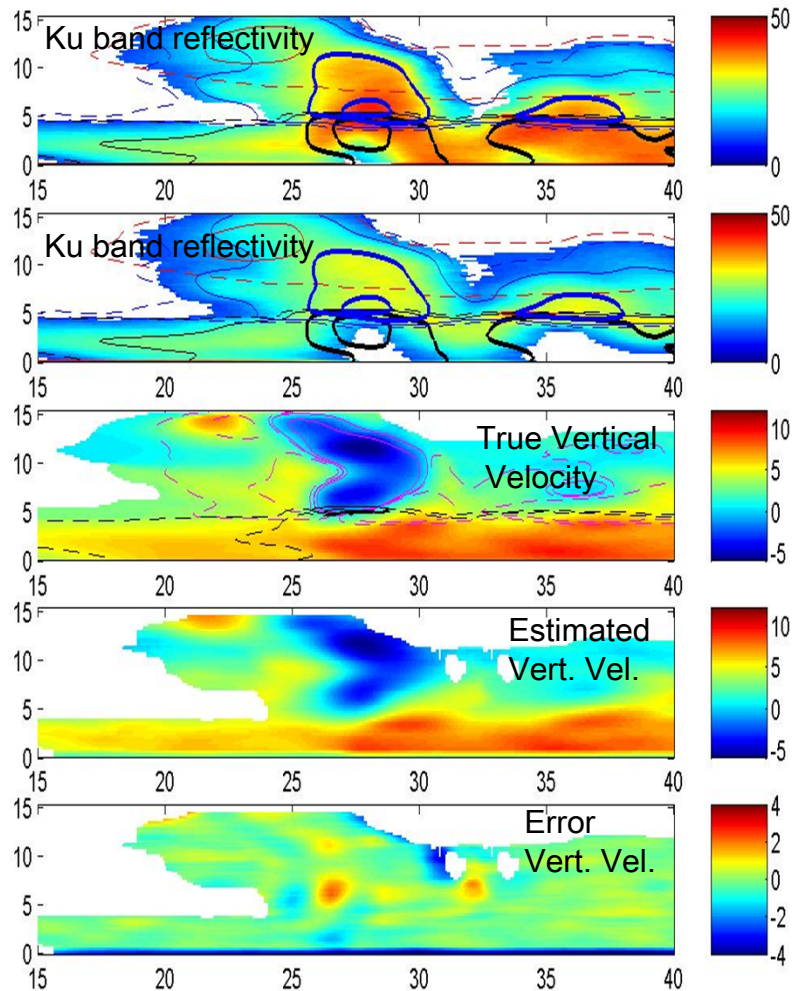


# Estimation of Latent Heat Flux



- Hydrometeor-heating algorithm + vertical motion measurement

CRM simulated storm (Dr. S. Hristova-Veleva)

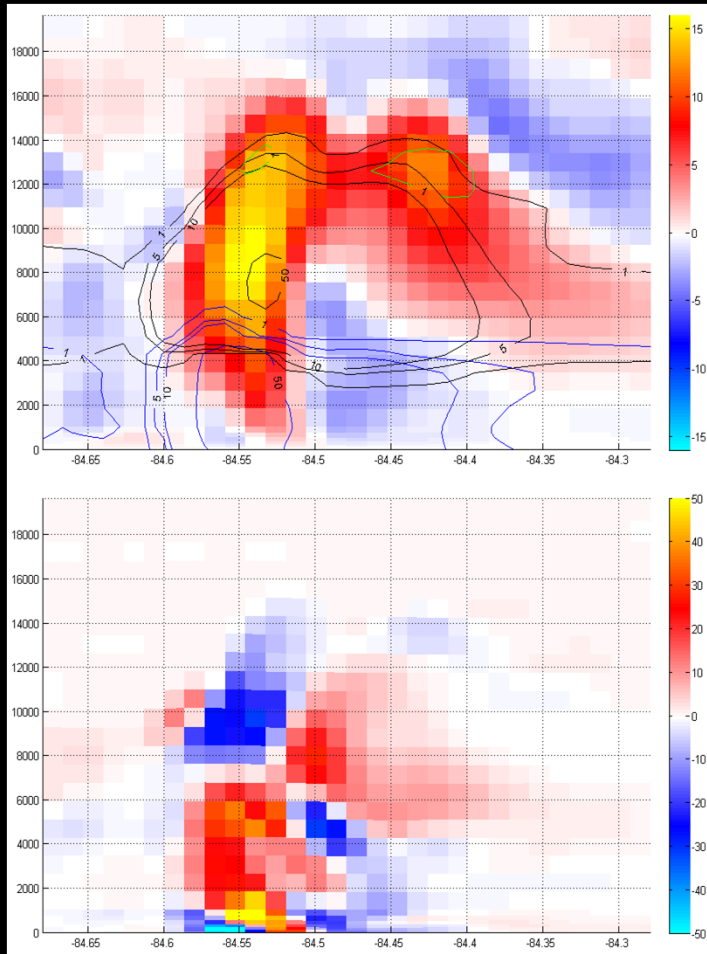




# Latent Heat Profiling with Doppler: vertical mass fluxes and horizontal advection

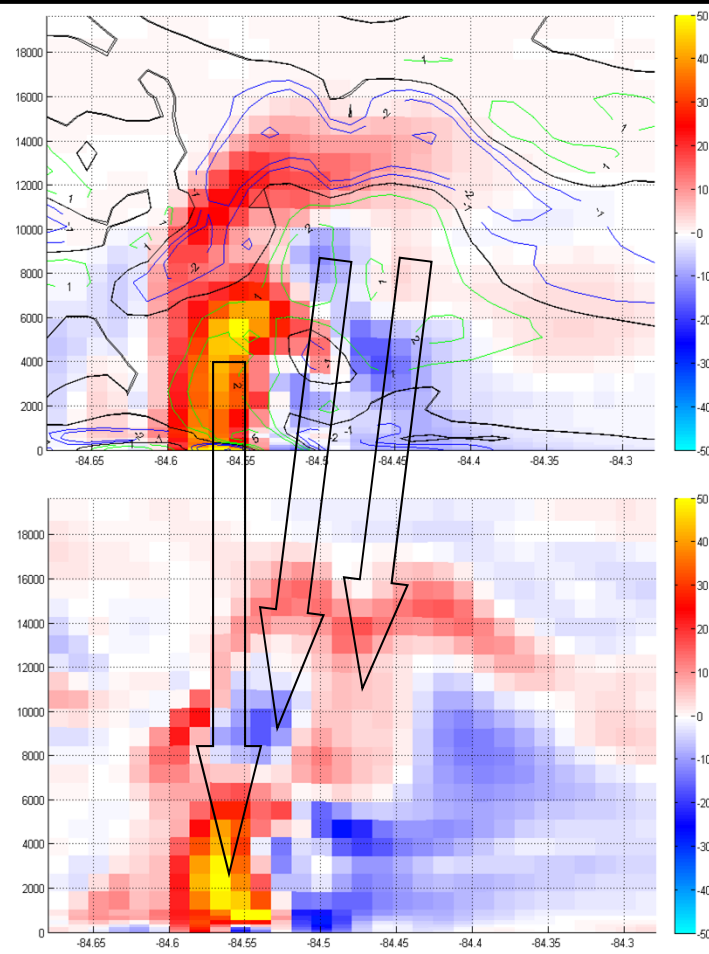


**Vertical velocity (color), rain (blue),  
graupel (black), snow (green)**

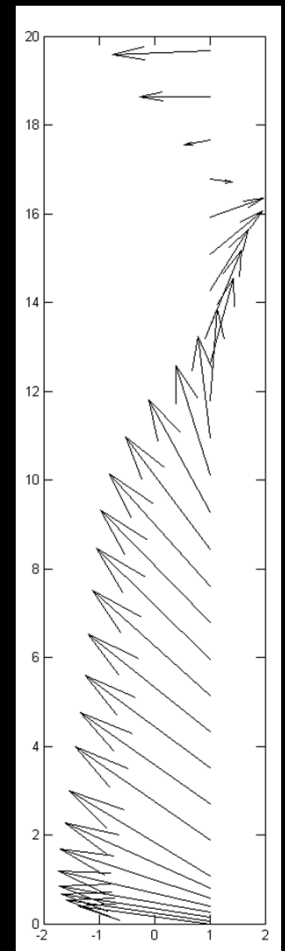


**HH-LH without horizontal advection**

**Latent Heat (color)  
and divergence**



**HH-LH with estimated advection**



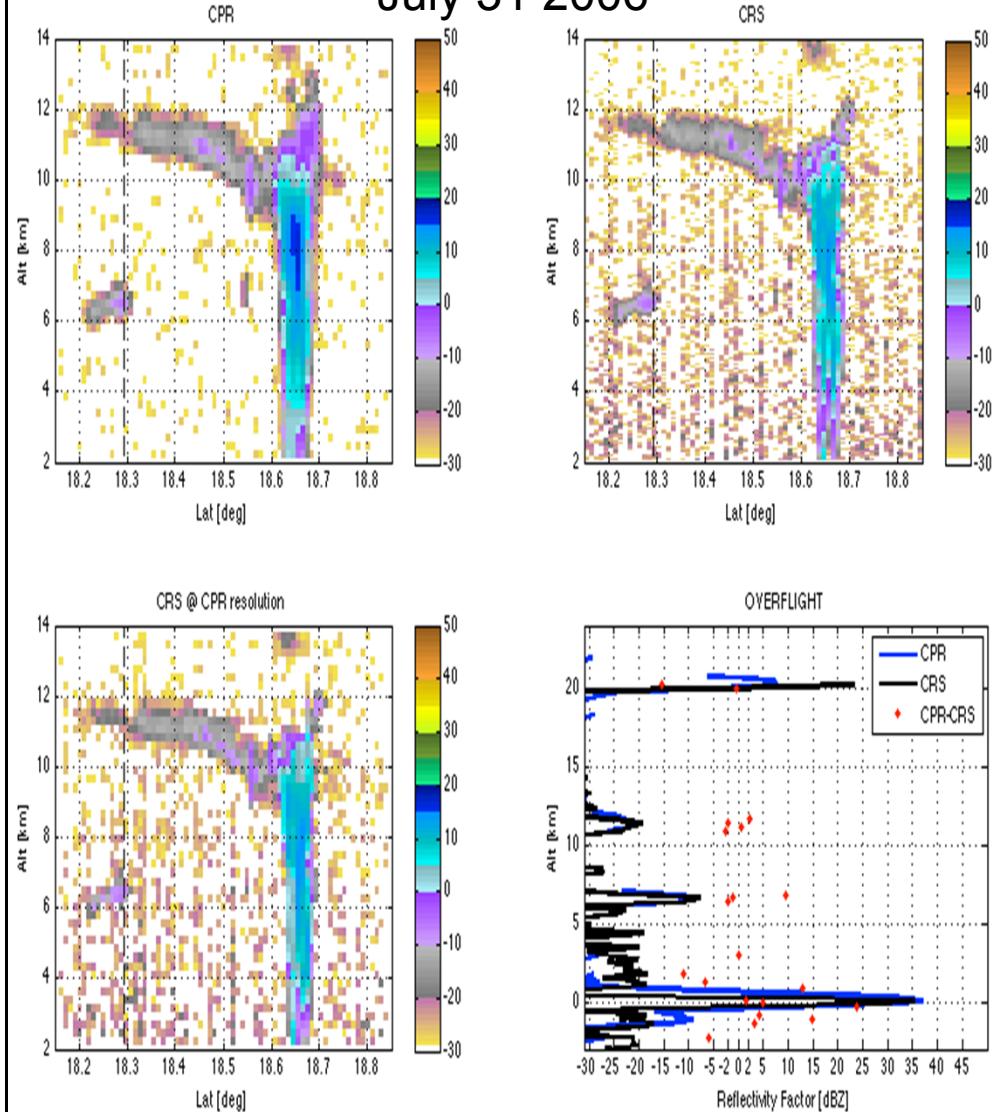
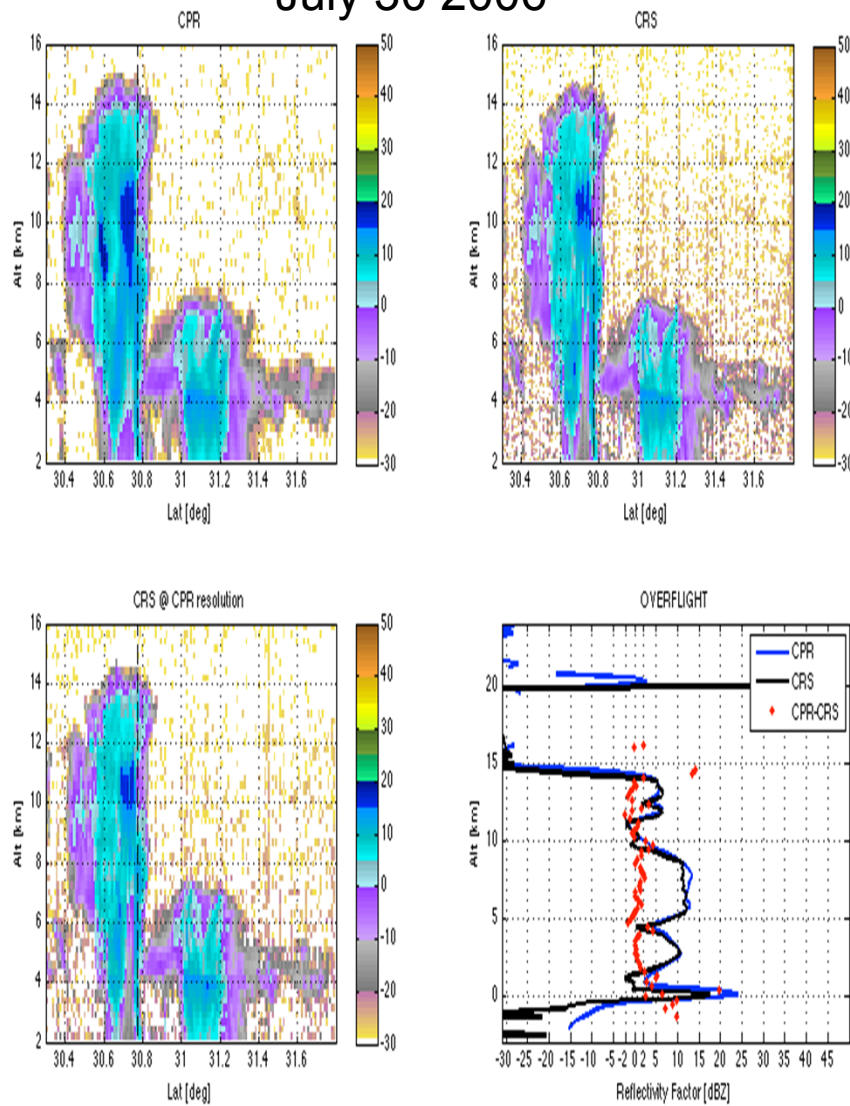


# Multiple Scattering: Airborne Validations: CRS



July 30 2006

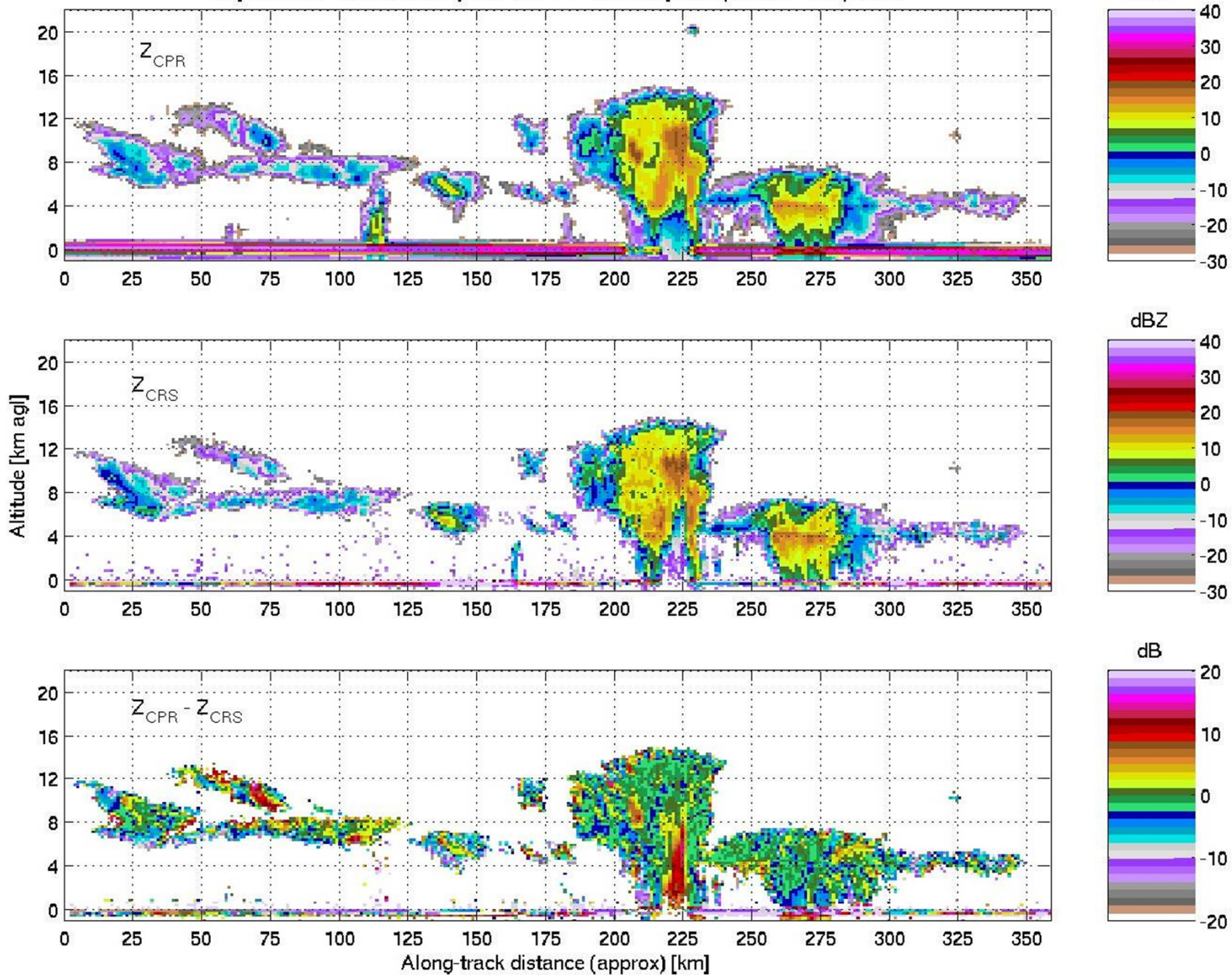
July 31 2006



Multiple scattering effects are visible in CPR images because of the larger footprint.

# CPR vs. CRS

July 30 2006 - CRS underflight of CPR - Preliminary Comparison - Snapshots

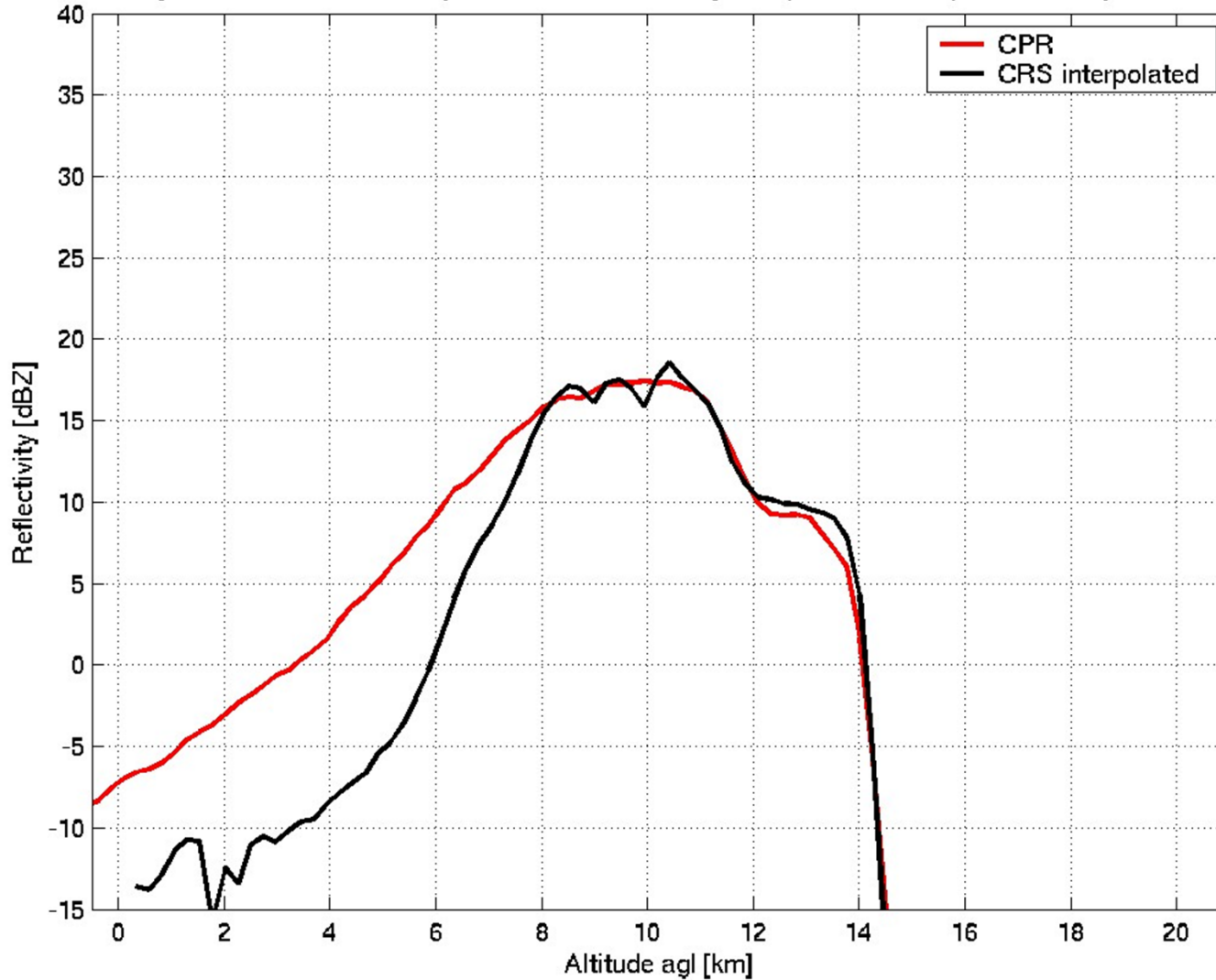




# CPR/CRS Altitude Profiles - Multiple Scattering

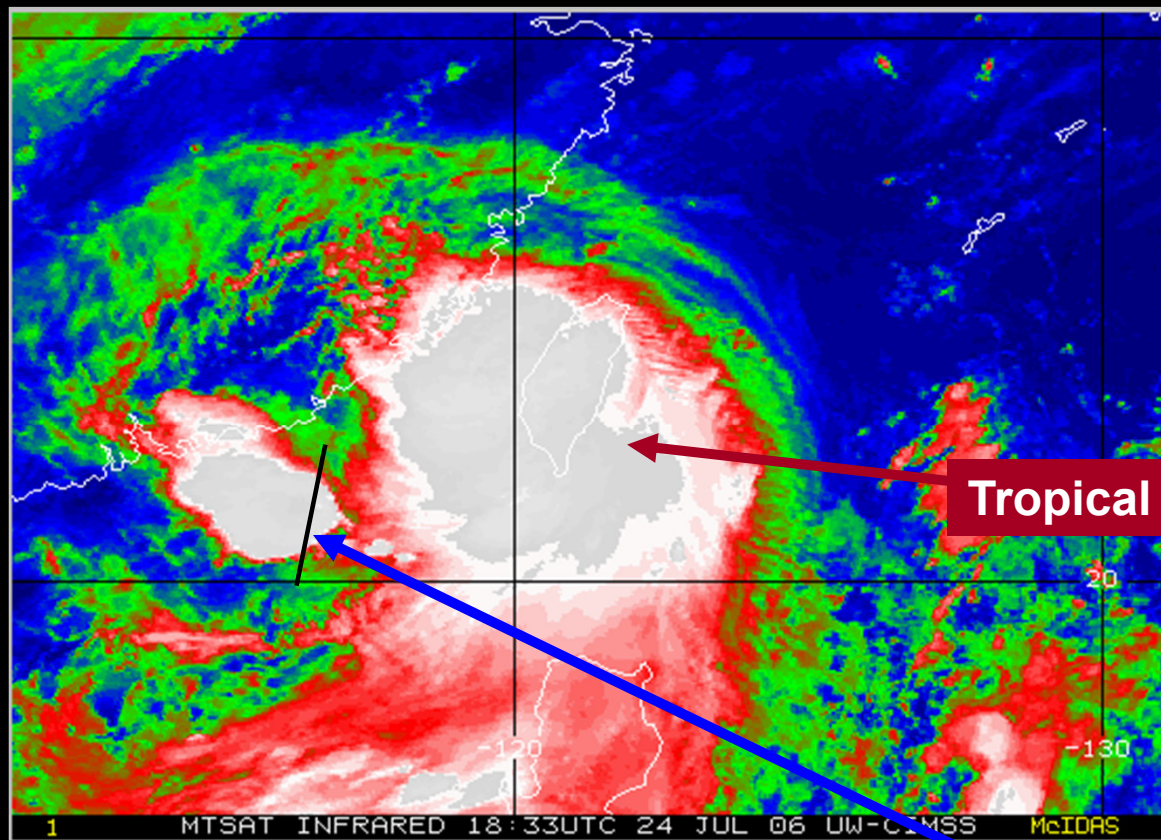


July 30 2006 - CRS underflight of CPR - Preliminary Comparison - Multiple Scattering Profile

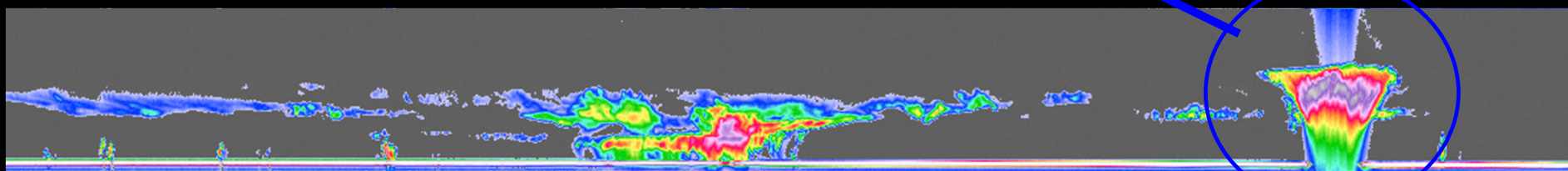




# CPR Observation of Mushroom Cloud in Storm 06W, July 24, 2006



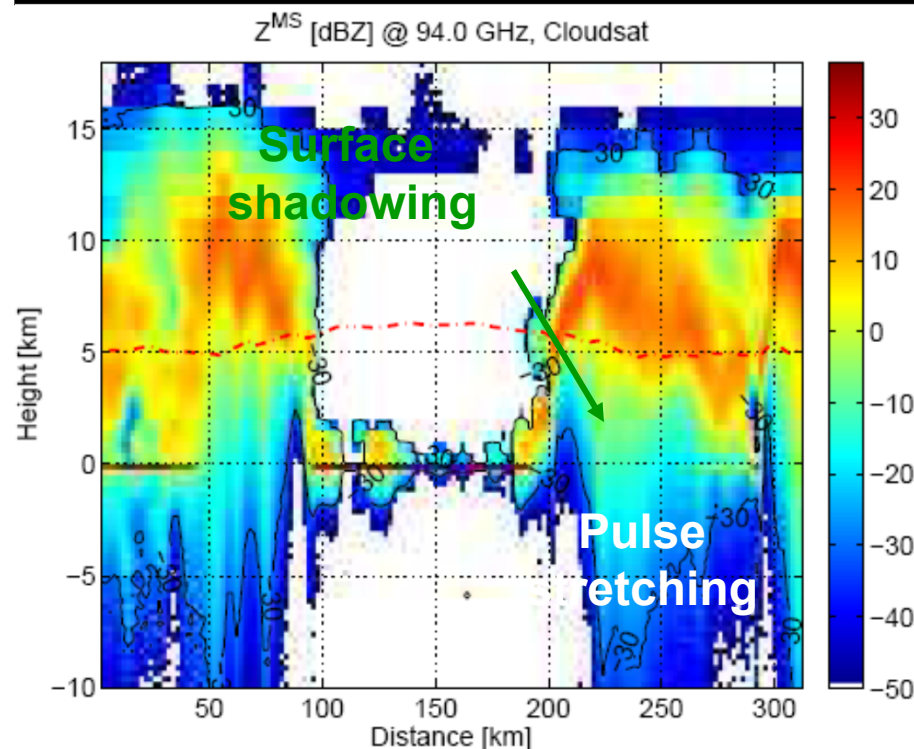
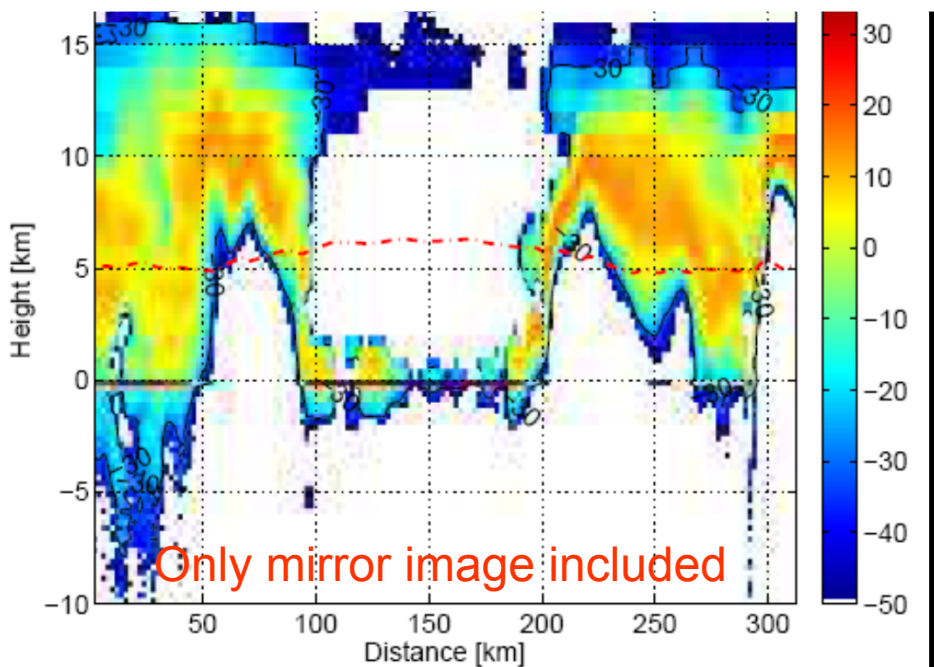
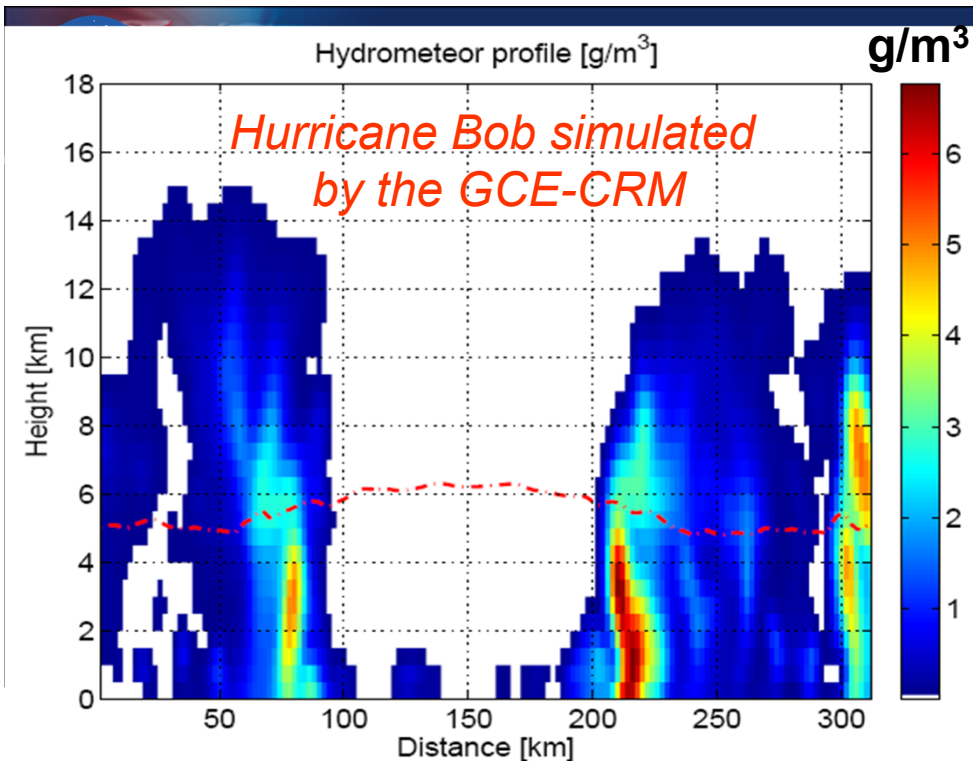
Tropical Storm 06W



Reflectivity: Low High

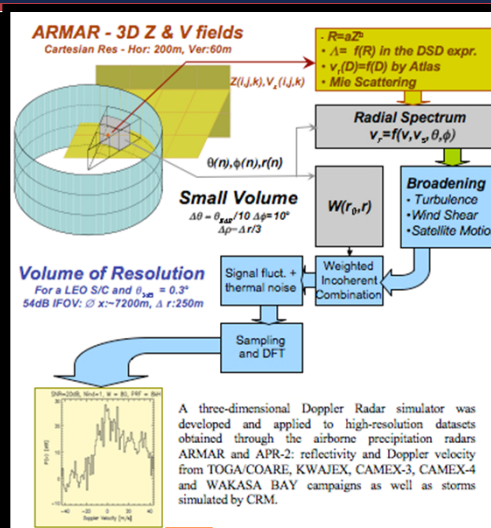
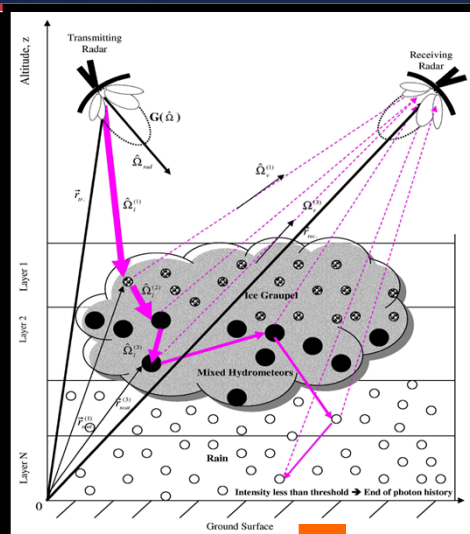


# CPR flight over Hurricane Bob

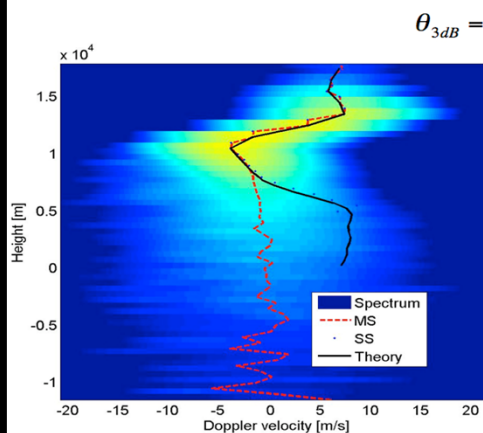




# Multiple Scattering & Doppler

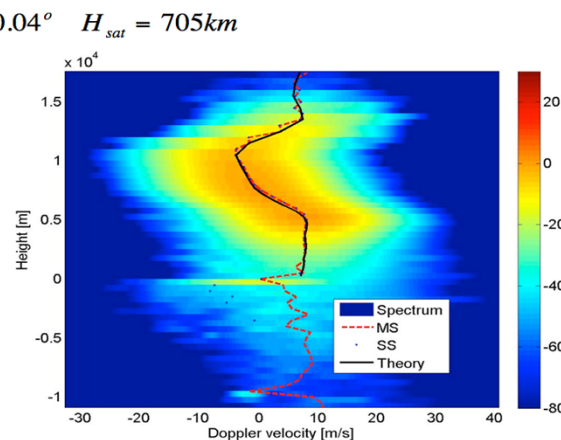


## ACE705km W+K<sub>a</sub> band



W band

$\theta_{3dB} = 0.04^\circ$   $H_{sat} = 705km$

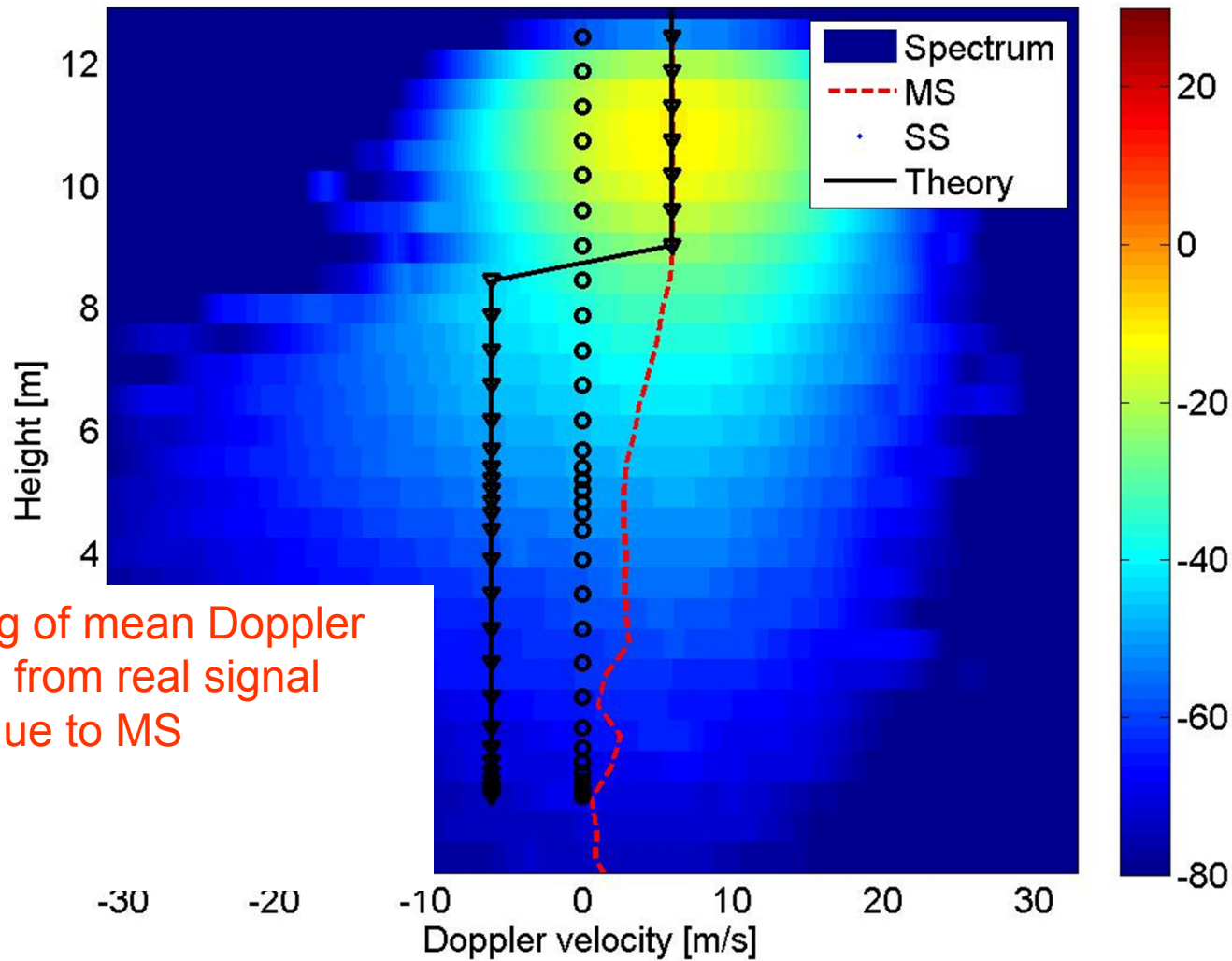


K<sub>a</sub> band

$\theta_{3dB} = 0.1^\circ$   $H_{sat} = 705km$



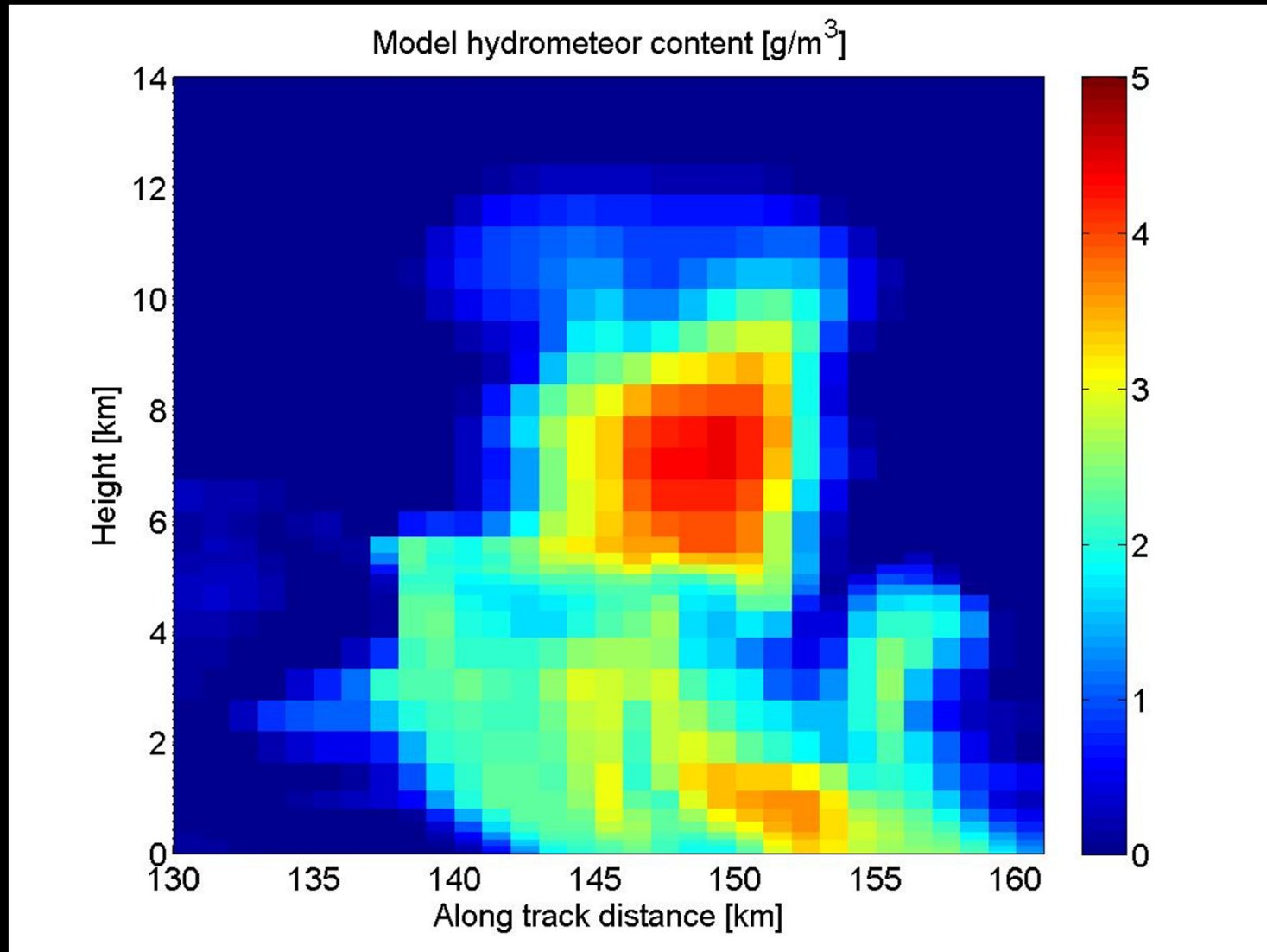
# Multiple Scattering & Doppler



Decoupling of mean Doppler velocity from real signal due to MS



# Multiple Scattering & Doppler



DOMUS can now account for the full 3D geometry as well

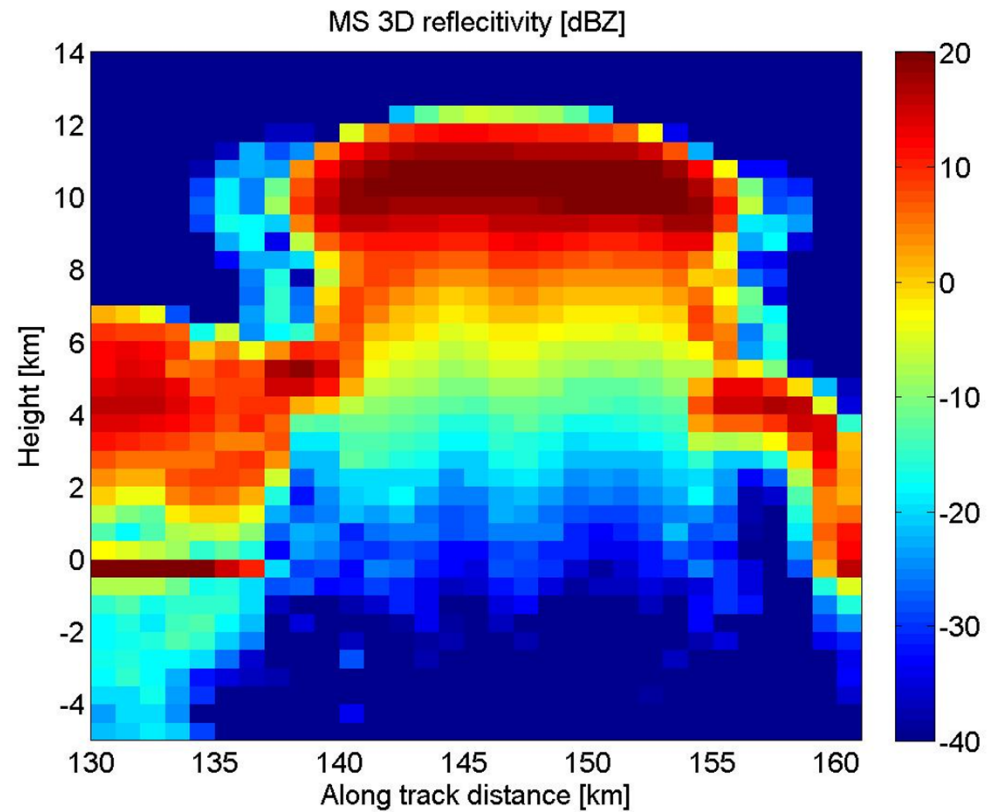
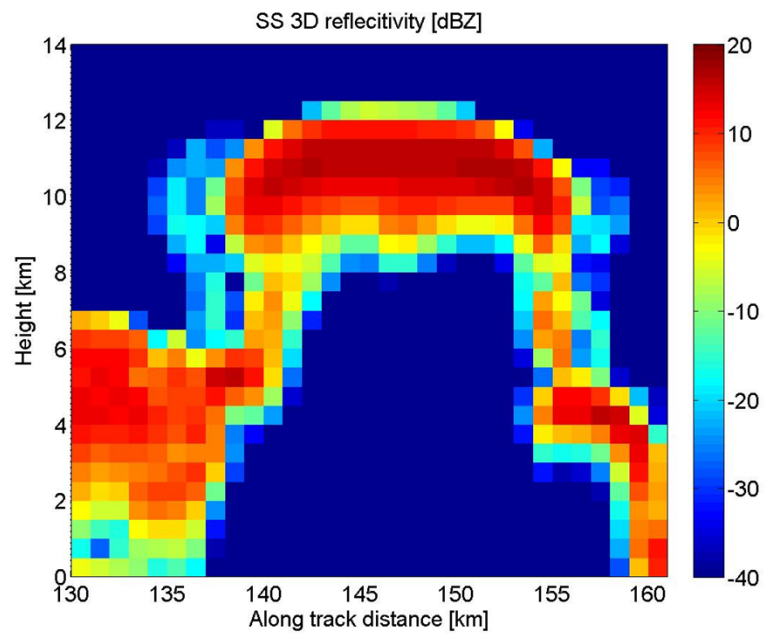


# Multiple Scattering & Doppler



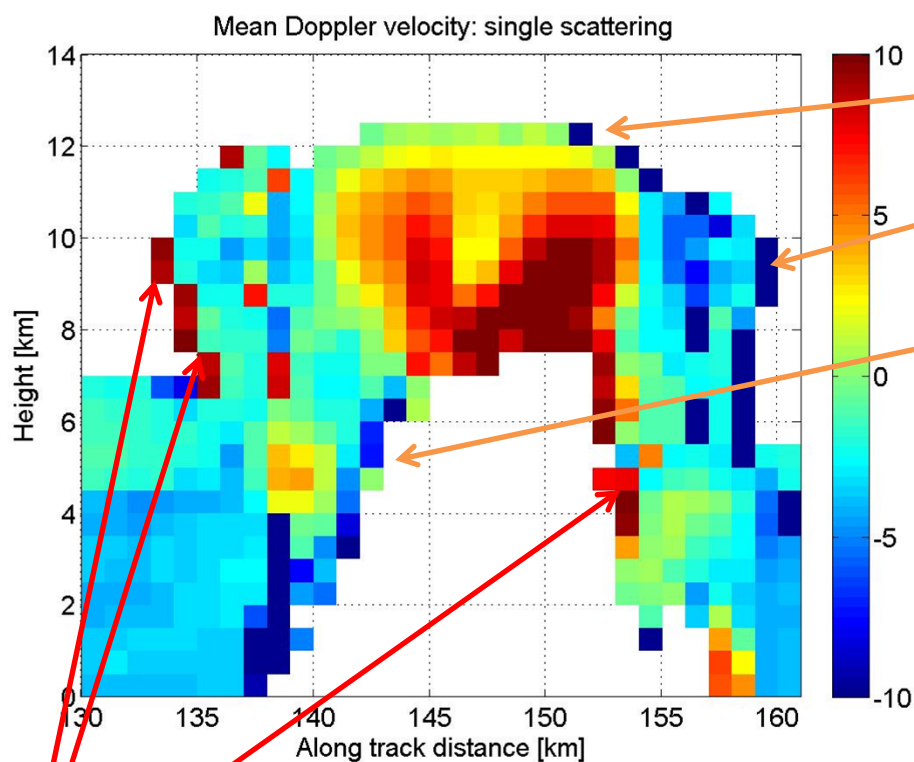
## DOMUS single scattering

## DOMUS multiple scattering



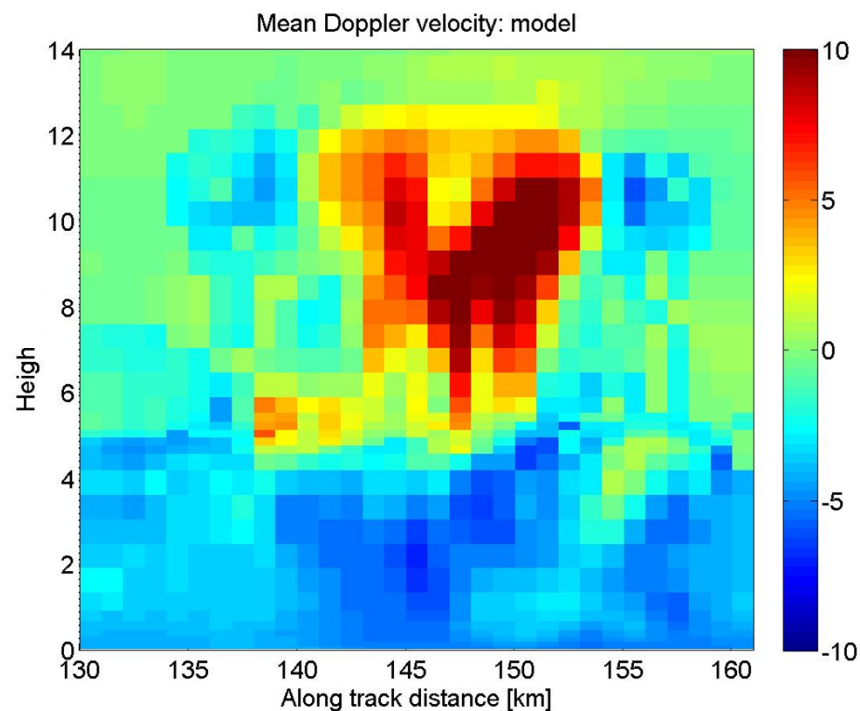


# Multiple Scattering & Doppler



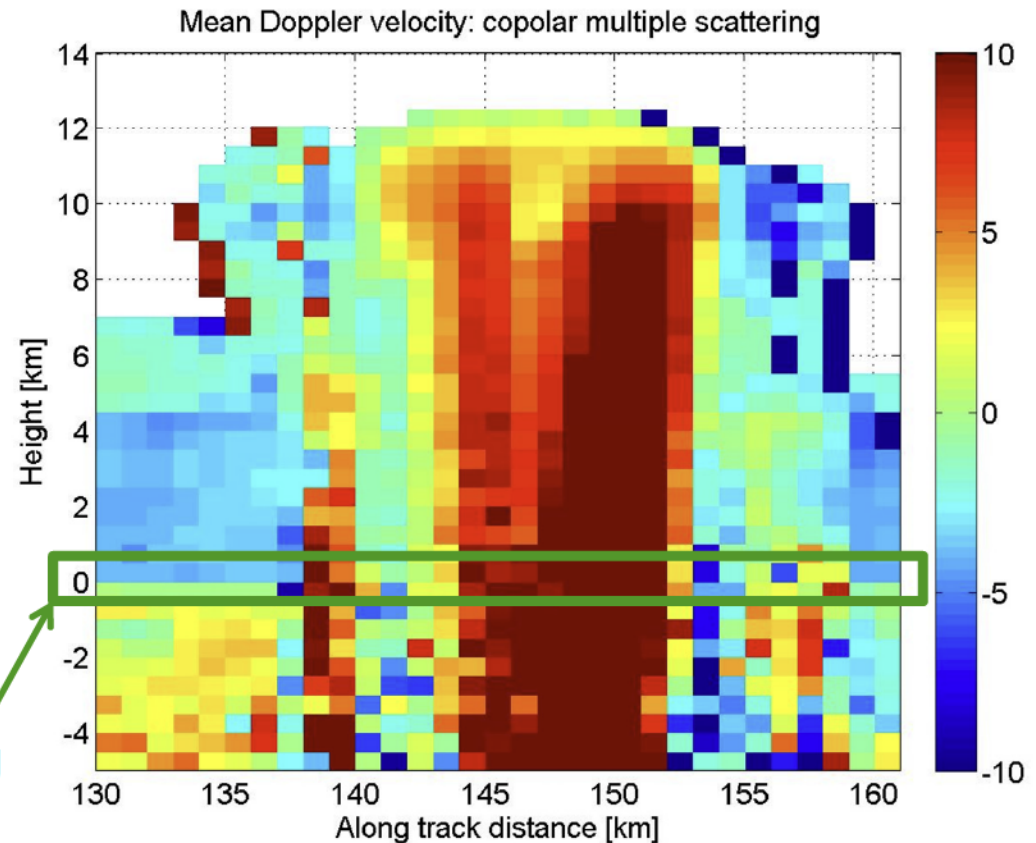
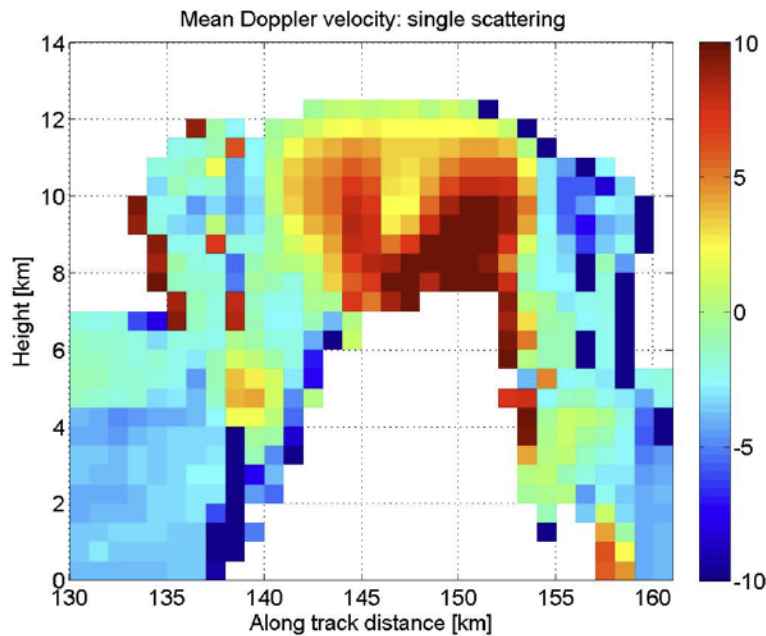
Negative (downward vel) bias when going out from high reflectivity region

Positive (upward vel) bias when going in high reflectivity region





# Multiple Scattering & Doppler



Surface velocity simulated as well< key features for overcoming pointing uncertainties

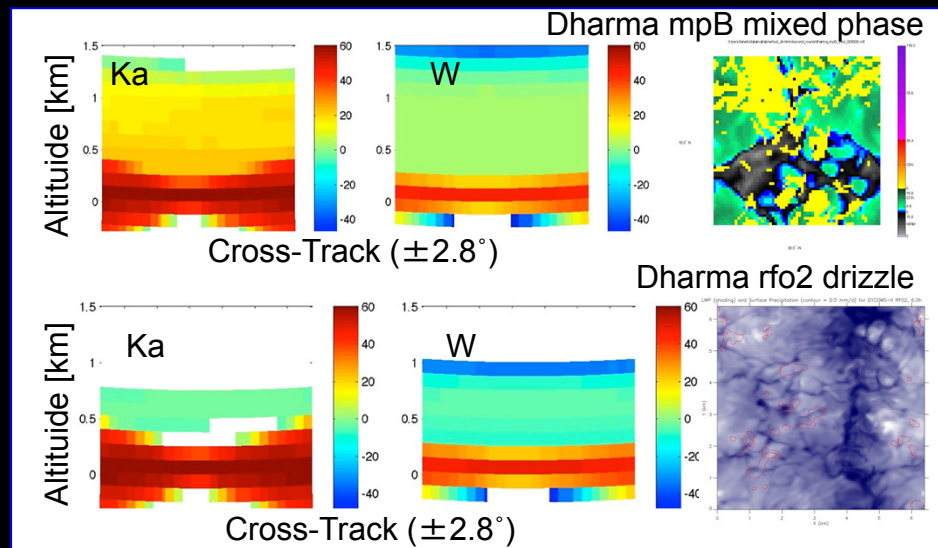
In the belly of the jelly the Doppler velocities are uncorrelated to the true signal: instead of a strong downward we actually see strong upward velocities



# Challenges in Spatial/Temporal Coverage



- CloudSat and EarthCARE are nadir-looking radars: do not reconstruct 3-D context.
- TRMM/PR and GPM/DPR are cross-track scanning radars: near-surface measurements are suffered from ground clutter contamination
- The planned ACE W/Ka-band radar approach (dual requirement):
  - Nadir beam: allow sufficient dwell time for meet detection requirement
  - Limited (30-km) cross-track scan: to obtain wider spatial coverage

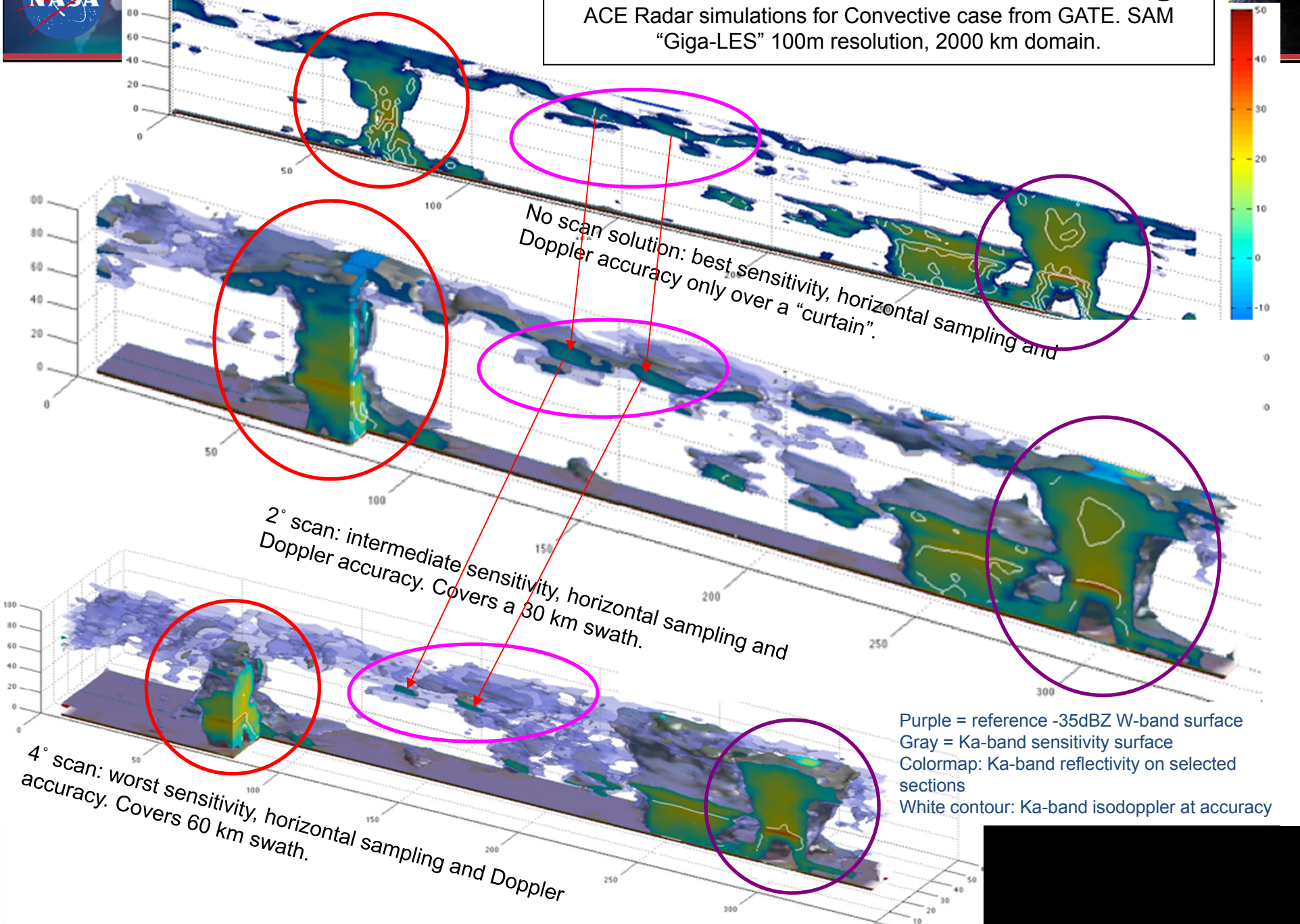


- These radars are for LEO operations. Temporal coverage and revisit time can be improved only by LEO constellation, or by moving to MEO or GEO orbits.



# Performance trades with Scanning

ACE Radar simulations for Convective case from GATE. SAM  
"Giga-LES" 100m resolution, 2000 km domain.

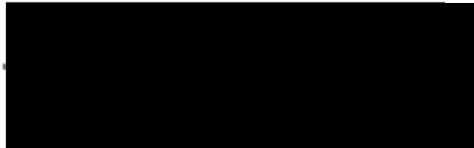


No scan solution: best sensitivity, horizontal sampling and Doppler accuracy only over a "curtain".

2° scan: intermediate sensitivity, horizontal sampling and Doppler accuracy. Covers a 30 km swath.

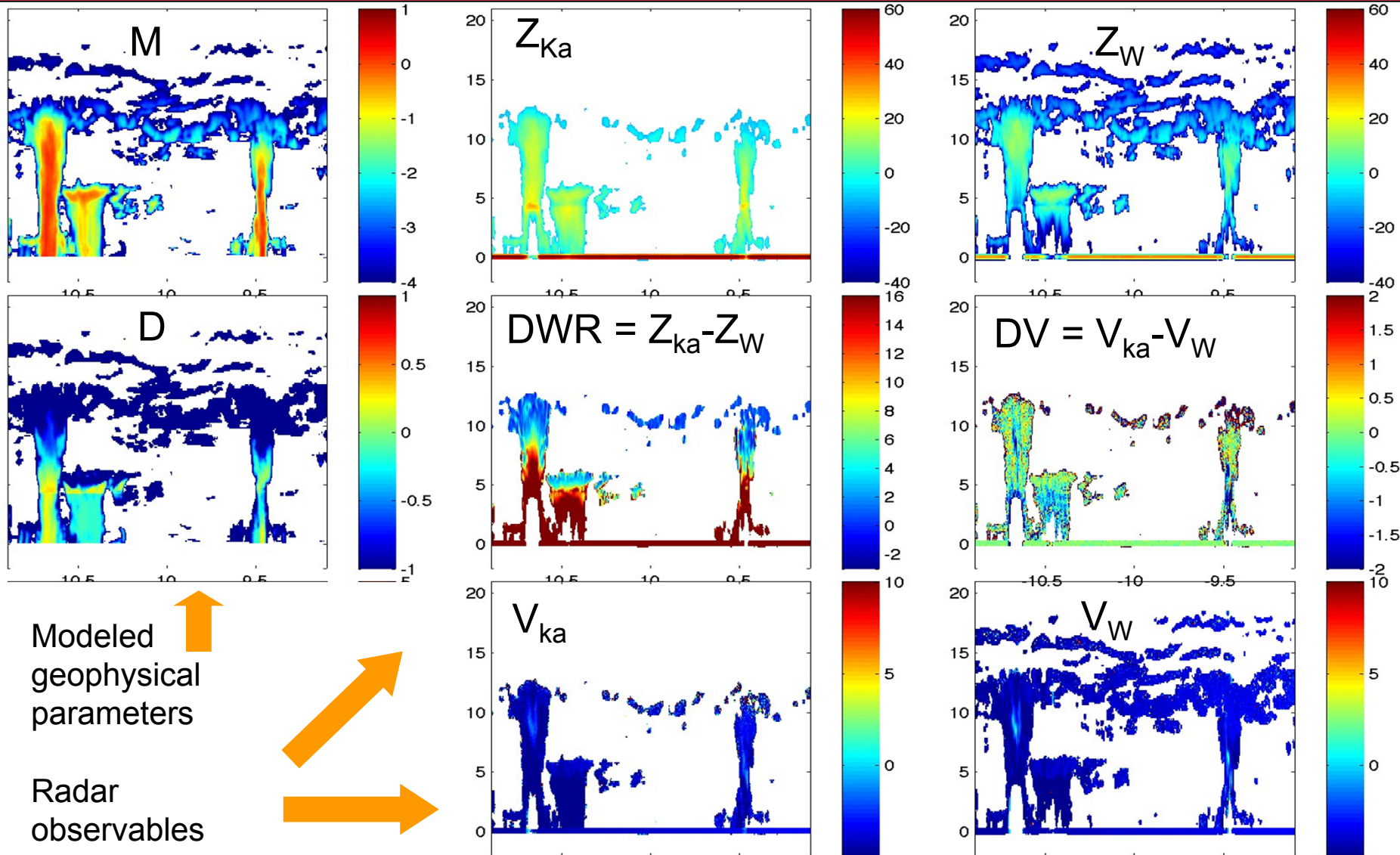
4° scan: worst sensitivity, horizontal sampling and Doppler accuracy. Covers 60 km swath.

Purple = reference -35dBZ W-band surface  
Gray = Ka-band sensitivity surface  
Colormap: Ka-band reflectivity on selected sections  
White contour: Ka-band isodoppler at accuracy





# Example of Products





# One possible solution (notional)

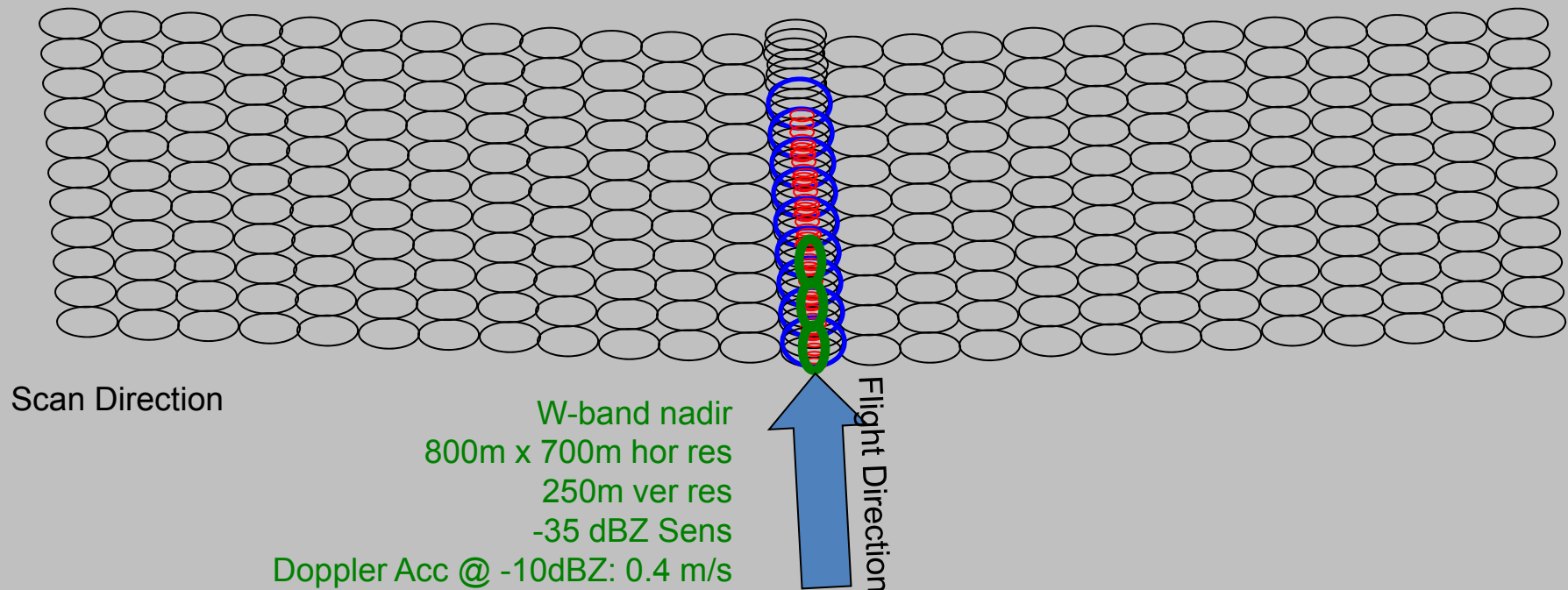


Meet Science Requirements

Ka-nadir  
1000m x 1800m hor res  
250m ver res  
-13 dBZ Sens  
Doppler Acc @ +5dBZ: 0.7 m/s

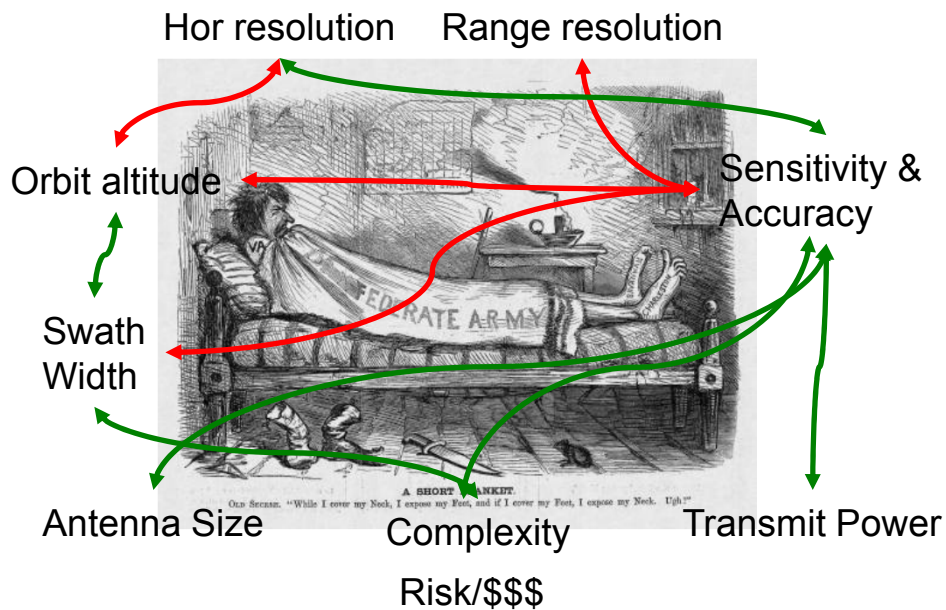
Provide additional information on 3D structure

Ka-scan  
>25 km swath width  
900m x 1800m hor res  
250m ver res  
-6 dBZ Sens  
Doppler Acc @ +5dBZ: 1.9 m/s



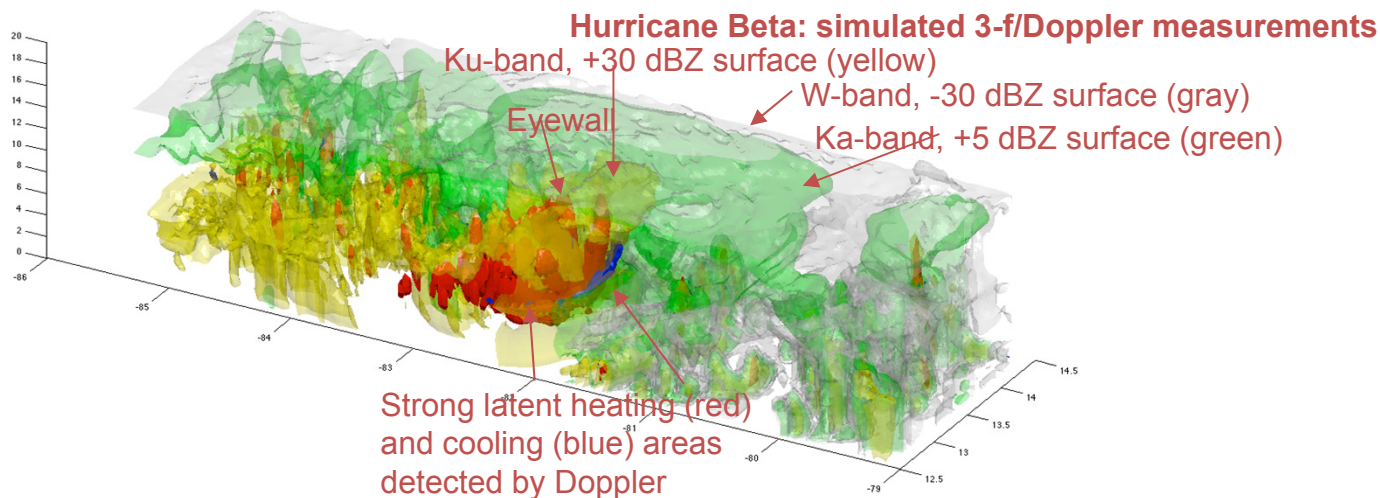


# Main Trade-Offs



$$Z_{sens} \propto \frac{L_{atm} L_{sys}}{f^4 A_{eff}} \cdot \frac{B_{noise}}{(P_t \tau)} \cdot \frac{1}{\sqrt{N_{ind}}} \cdot r^2$$

	Reference (EarthCARE)	Modified	Delta dBZ Sensitivity
Distance (km)	450	<b>715</b>	4.02
Number of beams	1	<b>64</b>	9.03
Range Res. (m)	500	<b>250</b>	6.02
Diversity	1	<b>8</b>	-4.52
Antenna Surf (m2)	4.91	<b>100</b>	-13.09
			1.47





# Instrument requirements & goals



	PARAMETER	UNIT	REQUIREMENT	GOAL (#Priority)	ACERAD	Science Mnemonic
W-band, nadir	Min Det Sens	dBZ	-35	-40 (#3)	-35	EarthCARE level of detection.
	Doppler Acc	m/s	0.4	<b>0.2(#2)</b>	0.2	Precipitating/non-precipitating, sedimentation, cloud scale entrainment.
	Vert Res	m	250	<b>100 (#1)</b>	250	Melting layer, geometrically thin clouds, in-bin attenuation
	Sfc Cltr max hgt	m	500	<b>250 (#1)</b>	400	Cloud base vs surface precipitation.
	Hor Res	km	1 x 1	--	0.7 x 1	CRM scale.
	Polarimetry (LDR)		--	YES (#5)	YES	Mixed phase and multiple scattering.
W-band, off-nadir	Swath Width	km	--	≥2 (#4)	--	Convective cell resolution (10km), radiometer footprint (25km). Ka-radar footprint (2km)
	Min Det Sens	dBZ	--	-20	--	All light precipitation, most large particle clouds.
	Doppler Acc	m/s	--	1	--	
	Vert Res	m	--	250	--	
Ka-band, nadir	Hor Res	km	--	1 x 1	--	
	Min Det Sens	dBZ	-10	<b>-20 (#2)</b>	-12	Most (all) light precipitation, some (all) large particle clouds.
	Doppler Acc	m/s	1	0.5 (#3)	0.5	Rain/no rain, convection.
	Vert Res	m	250	100 (#4)	250	
	Sfc Cltr max hgt	m	500	250 (#4)	400	
	Hor Res	km	2 x 2	1 x 1	1.8 x 1	CRM scale / matched beam.
Ka-band, off-nadir	Polarimetry (LDR)		--	YES (#5)	YES	
	Swath Width		--	<b>&gt;25 (#1)</b>	33	Convective cell resolution, radiometer footprint. 100km would achieve meso-scale features.
	Min Det Sens	dBZ	--	-10	-10	
	Doppler Acc	m/s	--	1	1	
	Vert Res	m	--	250	250	
	Hor Res	km	--	2 x 2	1.8 x 1	



# Concepts for future atmospheric radars



- **Diversity techniques**

- Polarization, Frequency, PRT: in all cases increased hardware complexity, and/or increased power demands, and/or decreased performance
  - Their application is in principle governed by the same considerations that resulted in the many ground and airborne Cloud radars currently employing them.

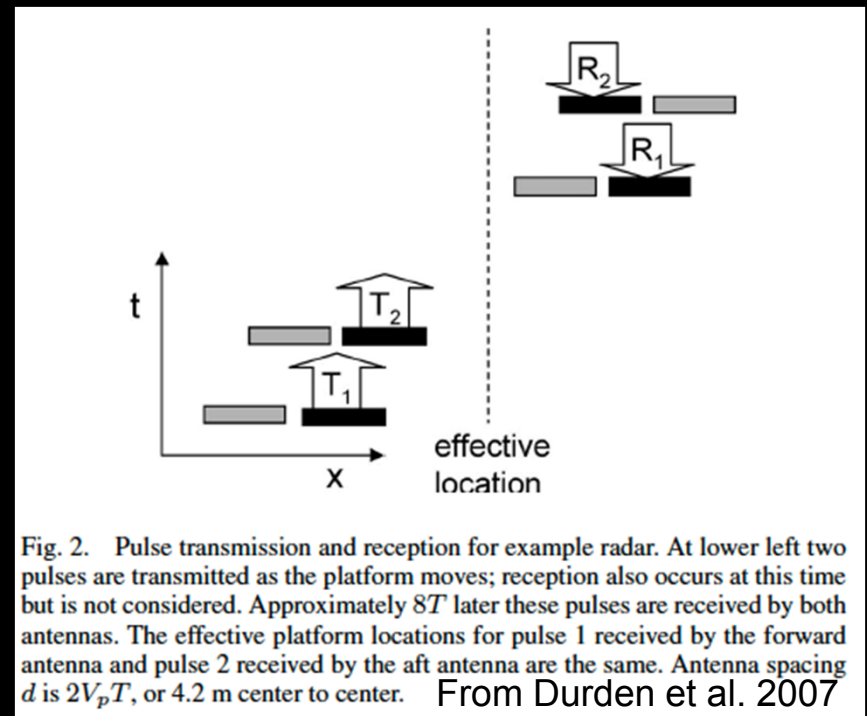
- **Multi Antenna**

- **Geostationarity**

# Dual Phase Center Antenna



- One alternative approach to measure accurate Doppler velocities from space, alternative to the use of large L / T is, is given by use of two (or more) antennas displaced in the along-track direction.
- With the appropriate timing solutions between the transmit and receive events, the effective phase center of the antenna pair can be kept stationary between two consecutive pulses: this effectively cancels the effects of the spacecraft velocity.



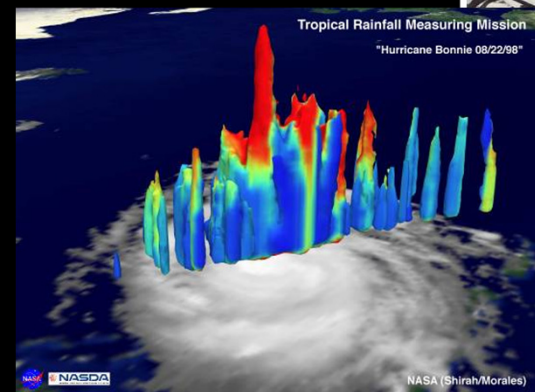
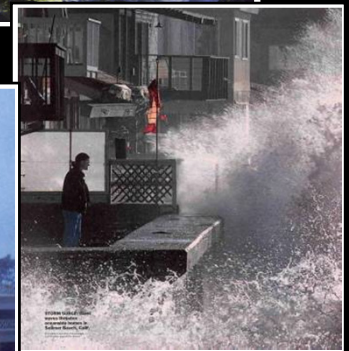
- The main advantage of this approach is that if Doppler accuracy is the primary scientific requirement of a mission, it can be achieved with a LEO platform without requiring large antenna sizes or operating power.
- The main drawbacks of this approach are that the antenna Gain is effectively reduced to less than half, with respect to that of an antenna of size equal to the pair, and the system complexity to achieve the required phase accuracy among the antennas is greater than that for a single antenna system.



# GEO Atmospheric Radars: Benefits and Challenges



- Extension of LEO radar technology:
  - Ka/W-band instrument electronics technologies can be applied for GEO radar to monitor hurricanes and severe weather
  - Lower frequency radars will have difficulty achieving adequate spatial resolution
- GEO advantages:
  - GEO allows frequent time sampling and revisit: excellent for hurricane and severe weather monitoring
  - With scanning and Doppler capability, a GEO radar is analogous to a spaceborne “weather radar network” to provide accurate “weather report at sea” in a timely fashion
    - Hurricane prediction, aviation safety, etc.
- GEO disadvantage:
  - Long ranging distance to earth would require extremely large aperture in order to obtain reasonable horizontal resolution and detection sensitivity

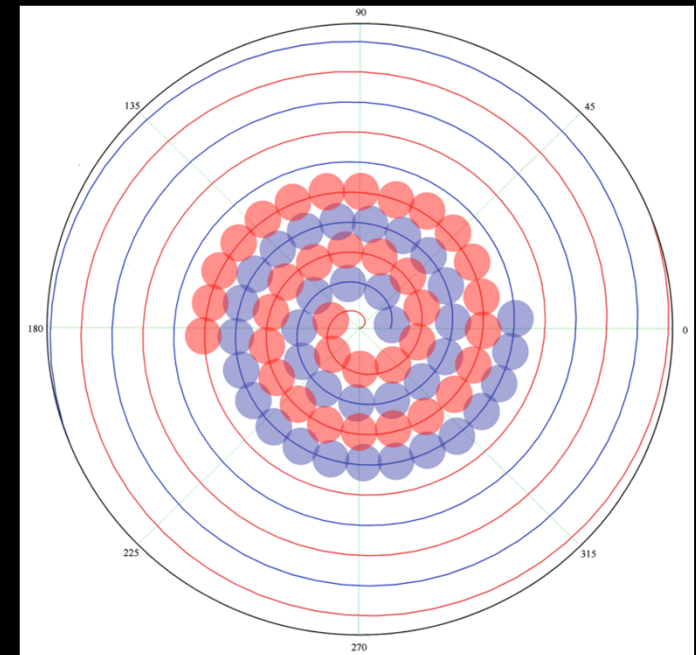
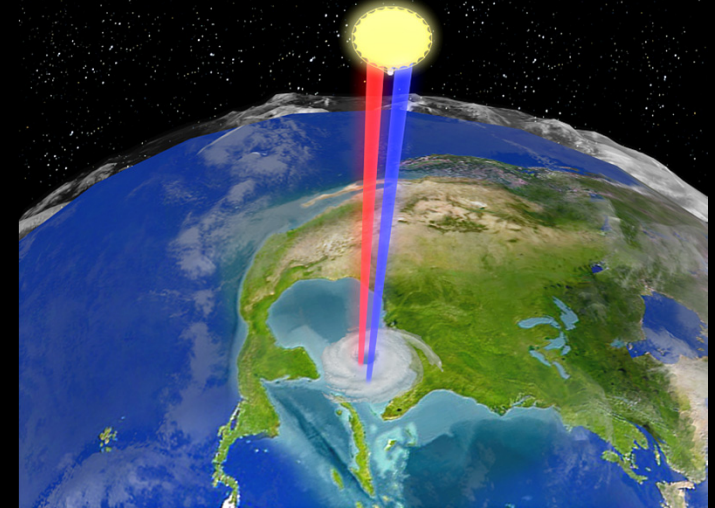




# A GEO Atmospheric Radar Concept studied by NASA ESTO



- Operating in geostationary orbit (alt.  $\sim 36,000$  km)
- Using a lightweight, deployable, 35-m spherical antenna to achieve good horizontal resolution and detection sensitivity
  - Illuminating 28-m sub-apertures of the antenna to obtain 12-14 km horizontal resolution
  - Extra antenna reflector surface is needed for scanning
- Using a combination of spherical antenna reflector and spirally scanning antenna feeds to cover 5300 km diameter of earth surface disk area
  - Equivalent to a coverage of  $48^\circ$  latitude  $\times$   $48^\circ$  longitude
  - Additional coverage can be achieved by small articulation of spacecraft (e.g., a fixed  $2^\circ$  satellite pointing will extend coverage to  $38^\circ$  N)
- Spiral scan achieved by linear motion of 2 sets of transmit/receive feed pairs along a rotating track
  - 1 transmit feed and 1 receive feed with fixed spacing to compensate for pulse delay
- Vertical resolution of 250 m using pulse compression
- Rain detection sensitivity:  $\sim 5$  dBZ
  - $\sim 12$  dB more sensitive than the TRMM radar
- Line-of-sight Doppler velocity: 0.3 m/s (rms) accuracy
- One 3-D full-scan image once per hour
- Real-time processing to reduce downlink data volume/rate



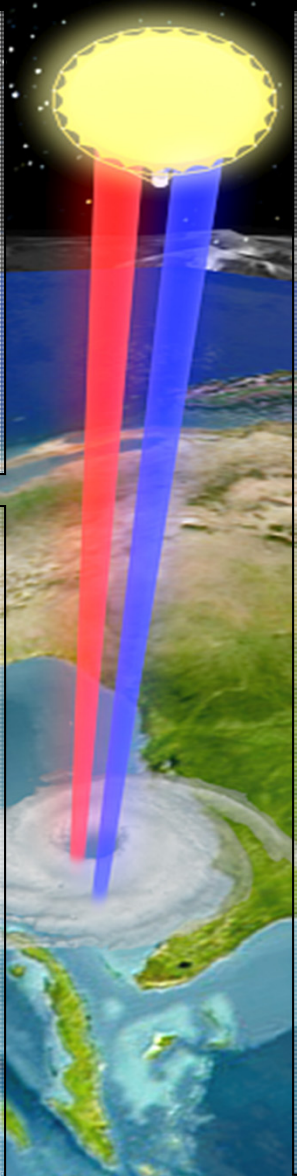
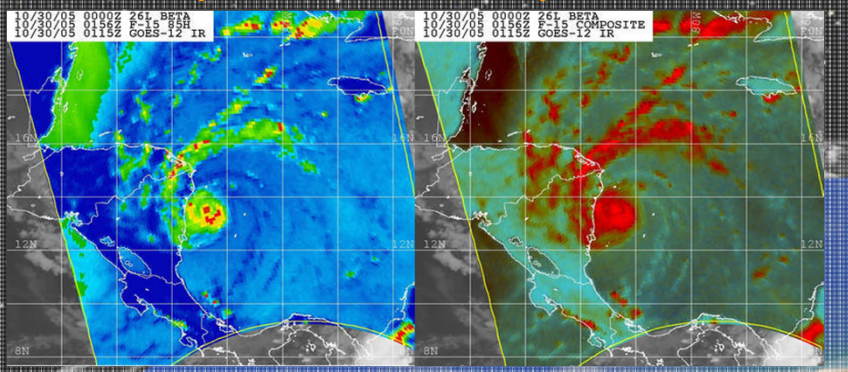


# NEXRAD In Space (NIS)

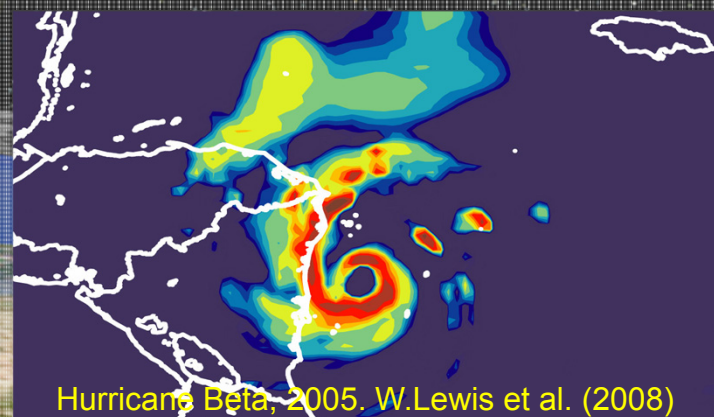
## Impact of geostationary Doppler Weather Radar for Hurricane Studies



Geostationary sensors grant shortest revisit time, but currently lack 3D and velocity information.



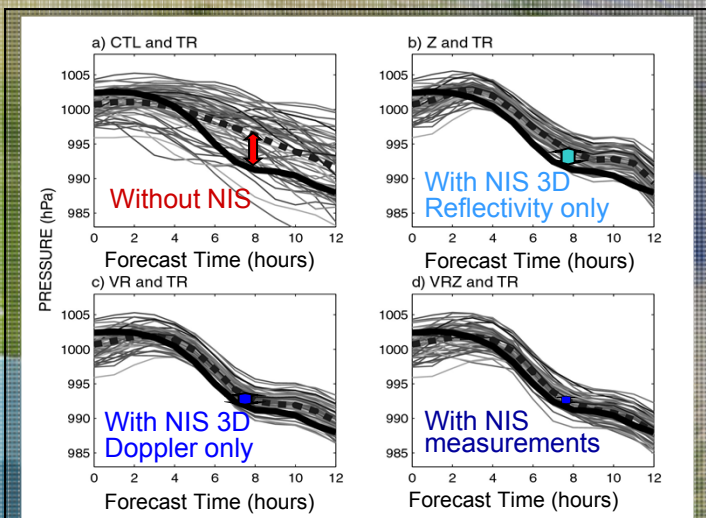
OSSE shows predicted impact on Hurricane intensity forecast skill



NIS is a Ka-band geostationary Doppler radar: it would fill this gap



E.Im et. al, Radar Meteorology Conference 2007



G. Tripoli et al. American Meteorological Society 88<sup>th</sup> Annual Meeting, 2008

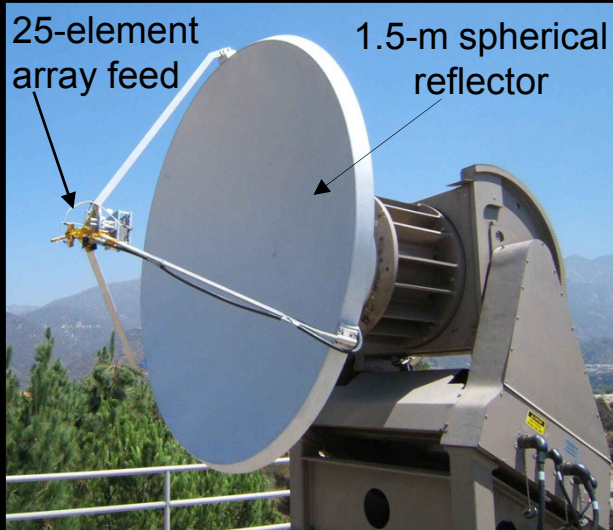


# A GEO Atmospheric Radar Space Operation Concept: An Illustration





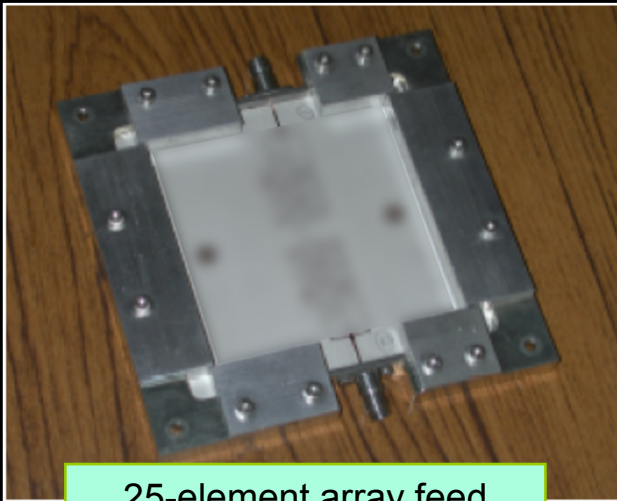
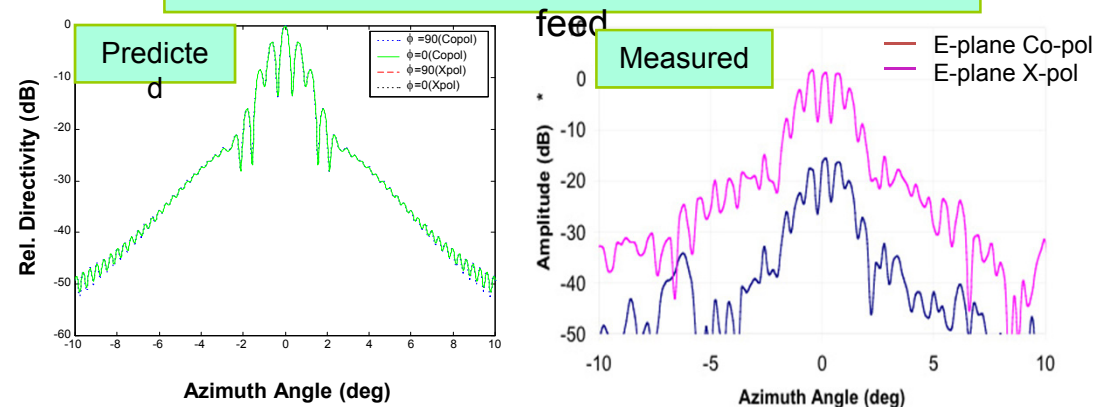
# Spherical Reflector Antenna Technology Prototype



Objectives: Demonstrate feasibility of spherical antenna approach

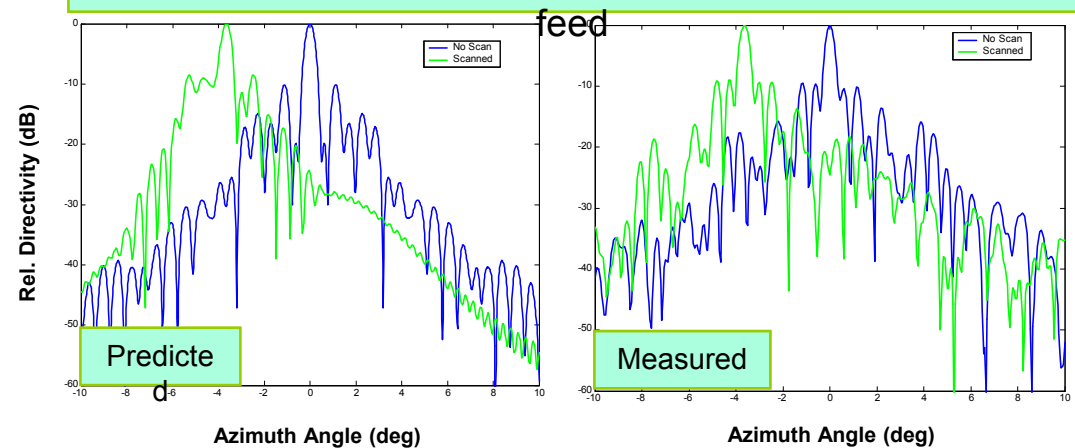
- Correction for spherical aberration
- Pointing up to  $4^\circ$  from boresight

## Far-field patterns of 1.5-m reflector with horn



25-element array feed

## Far-field patterns of 1.5-m reflector with 25-element array





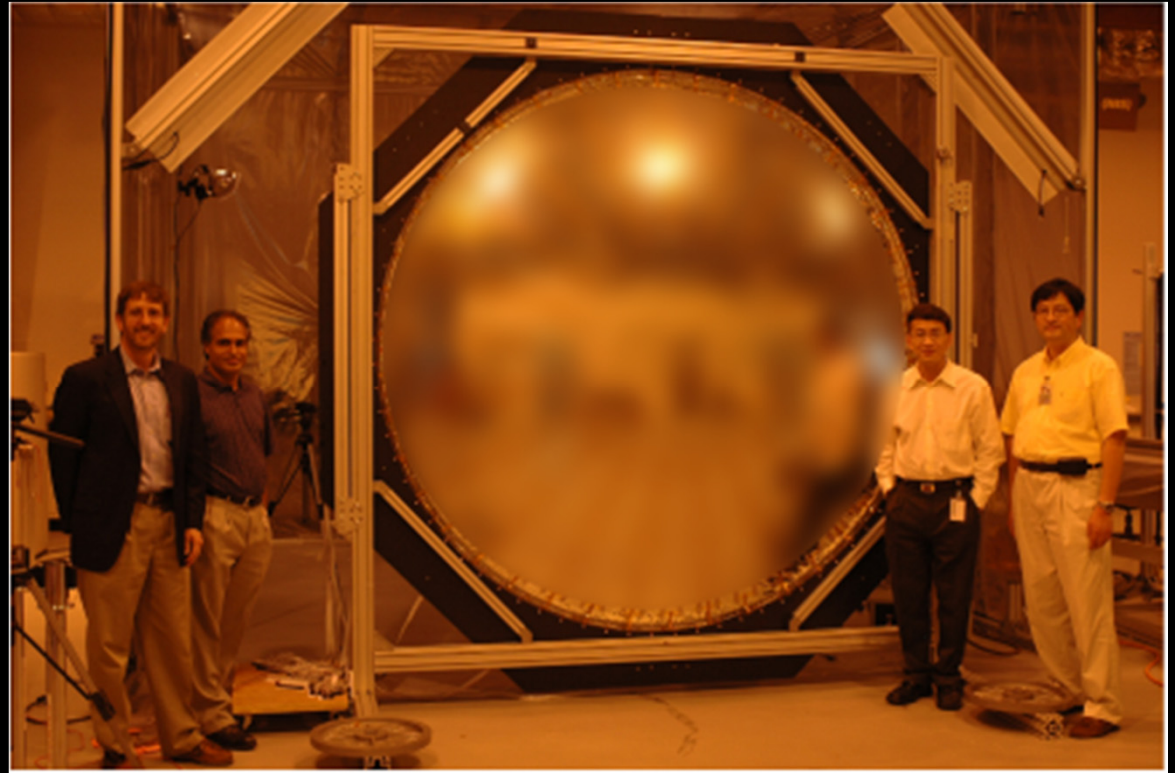
# 2.4-m Spherical Inflatable Membrane Antenna Prototype



Front view



Back view



The 2.4-m diameter prototype model consisting of:

- inflatable membrane reflector,
- 168 pizo-electrical actuators with embedded flexible voltage supply circuits for voltage supply
- 735 photogrammetry targets for surface accuracy measurements
  - Measured accuracy: 0.19 mm RMS (meet the  $\lambda/30=0.3$ -mm requirement)



## Further Works on GEO Atmospheric Radars are Required!!



- So far, the framework for the GEO atmospheric radar concept has been established. But this is just the beginning. A lot more work are required before such sensor can be realized.....
- Quote from 2007 US Earth Science Decadal Survey Report (p. 318):  
***“Frequent measurements of precipitation profiles require an active microwave (radar) sensor. The LEO based TRMM precipitation radar was the first such space-borne instrument. A MEO or GEO version of the TRMM radar would be needed to meet the 15- to 30-min temporal sampling requirement. The technology readiness level of such a sensor is still too low. The panel encourages continued development of the technology necessary to mount precipitation radars on MEO or GEO platforms.”***
- From the instrument technology prospective, the following are examples of some critical areas that need further development:
  - Science requirements
  - Design trade and optimization
  - Lightweight, deployable antenna reflector
  - Antenna feed design trade and optimization
  - Antenna deployment
  - In-flight antenna surface shape control



# Summary and Remarks



- Radar technologies have continued to advance to support next-generation of spaceborne atmospheric measurements of clouds and precipitation
  - Focus on improved measurement accuracy, multi-parameter observations, mass/size/data reduction
  - Technologies can be infused incrementally
- Atmospheric radar technology advances must be accompanied by advances in:
  - Science
    - Cloud model
    - weather forecast model
    - climate model
    - hydrological models and applications
  - Algorithms
    - DSD parameterization
    - Multi-frequency rain rate retrieval
    - Radar/radiometer rain retrieval
    - Doppler
    - Multi-polarization
    - Ice/rain/graupel/snow retrieval



# Bibliography



- R.J. Doviak and Zrníc D.S., "Doppler radar and weather observations", *Academic Press*, 1984.
- Amayenc, P, 1993: Proposal for a spaceborne dual-beam rain radar with Doppler capability. *J. Atmos. Oceanic Technol.*, 10, 262-276.
- Battaglia A. and S. Tanelli, 2011: Doppler Multiple Scattering Simulator (DOMUS), *IEEE Trans. Geosc. and Rem Sens.*, Vol. 49, no. 1, Jan. 2011, p 442-450.
- Durden S.L., Z.S. Haddad and T.P. Bui, 1999: Correction of Doppler radar data for aircraft motion using surface measurements and recursive least square estimation. *J. Atmos. and Oce. Technol.*, 16.
- Durden S.L., P. R. Siqueira, and S. Tanelli, 2007: On the use of multi-antenna radars for spaceborne Doppler precipitation measurements, *IEEE Geosci. Remote Sens. Lett.*, vol. 4, no. 1, pp. 181-183.
- S.Tanelli, E. Im, S.L.Durden, L. Facheris and D. Giuli, "The effects of nonuniform beam filling on vertical rainfall velocity measurements with a spaceborne Doppler radar". *J. Atmos. Oceanic Technol.*, 19, pp. 1019-1034, 2001.
- Kobayashi, S., H. Kumagai, and H. Kuroiwa, 2002: A proposal of pulse-pair Doppler operation on a spaceborne cloud-profiling radar in W-band. *J. Atmos. Oceanic Technol.*, 19, 1294-1306.
- Kobayashi S., H. Kumagai, and T. Iguchi, 2003: Accuracy Evaluation of Doppler Velocity on a Spaceborne Weather Radar through a Random Signal Simulation. *J. Atmos. Oceanic Technol.*, 20, 944-949.
- Kobayashi S., S. Tanelli and E. Im, 2005: Second order multiple scattering theory associated with backscattering enhancement for a millimeter-wavelength weather radar with a finite beam width, *Radio Science*, 40, RS6015, doi:10.1029/2004RS003219
- Kobayashi S., S. Ito, T. Oguchi, S. Tanelli, E. Im, 2007: A time dependent multiple scattering theory for a pulsed radar with a finite beamwidth. *Radio Science*, 42, RS4001, doi:10.1029/2006RS003555.
- Kollias, P., W. Szyrmer, I. Zawadzki, and P. Joe 2007b: Considerations for spaceborne 94 GHz radar observations of precipitation, *Geophys. Res. Lett.*, 34, L21803, doi:10.1029/2007GL031536
- Kozu T., "A generalized surface echo radar equation for down-looking pencil beam radar," *IEICE Trans. Commun.*, vol. E78B, no. 8, pp. 1245–1248, 1995.
- Kumagai H., H. Kuroiwa, S. Kobayashi, T. Orikasa, "Cloud profiling radar for EarthCARE mission," *proc. of SPIE*, vol. 4894, 2003, pp. 118-125.
- Li L. et al., 2005: Measurements of ocean surface backscattering using an airborne 94-GHz cloud radar - implication for calibration of airborne and spaceborne W-band radars, *J. Atmos. Oceanic Technol.*, vol. 22, 1033-1045, 2005.
- Meneghini R. and T. Kozu, 1990: *Spaceborne Weather Radar. Artech House Ed.*
- Pazmany A.L., J.C. Galloway, J.B. Mead, I. Popstefanija, R.E. McIntosh and H. W. Bluestein, "Polarization Diversity Pulse-Pair Technique for Millimeter-Wave Doppler Radar Measurements of Severe Storm Features," *J. Atmos. Ocean. Technol.*, vol-16, 1999, pp. 1900-1910.
- Schutgens, N.A.J., 2008: Simulated Doppler Radar Observations of Inhomogeneous Clouds: Application to the EarthCARE Space Mission. *J. Atmos. Oceanic Technol.*, 25, 26–42.



# Bibliography



- Sirmans D. and B. Bumgarner, "Numerical comparison of five mean frequency estimators," *J. Appl. Meteor.*, 14, 1975, pp. 991-1003.
- Tanelli S., E. Im, S. L. Durden, L. Facheris, D. Giuli, 2002: The Effects of Nonuniform Beam Filling on Vertical Rainfall Velocity Measurements with a Spaceborne Doppler Radar. *J. Atmos. and Oce. Technol.*, *American Meteor. Society*, vol. 19, p. 1019-1034.
- Tanelli S., Eastwood Im, Luca Facheris, and Eric A. Smith, 2002b: DFT-based spectral moment estimators for spaceborne Doppler precipitation radar. *SPIE Symposium on Remote Sensing of the Atmosphere, Environment and Space, Hangzhou (RPC), Oct. 23-27 2002*. Vol. 4894.
- Tanelli S., E.Im, S.L.Durden, L.Facheris, D. Giuli and E.A. Smith, 2004, Rainfall Doppler velocity measurements from spaceborne radar: overcoming nonuniform beam filling effects. *J. Atmos. and Oce. Technol.*, *American Meteorological Society*, vol 21, 224, p. 27-44.
- Tanelli S., J. P. Meagher, S. L. Durden and E. Im, 2004b: Processing of high resolution, multiparametric radar data for the Airborne Dual-Frequency Precipitation Radar APR-2. *Proceedings of SPIE 5654*, pp. 25-32.
- Tanelli S., E.Im, R.Mascelloni, and L.Facheris, 2005: Spaceborne Doppler radar measurements of rainfall: correction of errors induced by pointing uncertainties. *J. Atmos. And Oce. Tech.*, *American Meteorological Society*, 22, , pp. 1676–1690.
- Tanelli S., S.L. Durden, and E. Im, 2006: Simultaneous Measurements of Ku- and Ka-band Sea Surface Cross Sections by and Airborne Radar, *IEEE Geosc. and Rem. Sens. Letters*, 99, 1-5.
- Tanelli S., S. L. Durden, E. Im, K. Pak, D.G Reinke, P. Partain, J.M. Haynes, R.T. Marchand: 2008: Cloudsat's Cloud Profiling Radar after 2 years in orbit: performance, calibration and processing. *IEEE Trans. on Geosc. and Rem. Sens.*,
- Tanelli S., E. Im, S. L. Durden, D. Giuli, L. Facheris, 2008b: Spaceborne Doppler Radars for atmospheric dynamics and energy budget studies, *Proc. of the IEEE Radar Conference, Rome, Italy, May 12-15 2008*.
- Testud J., P. H. Hildebrand and W.-C. Lee, 1995: A procedure to correct airborne Doppler radar data for navigation errors using the echo returned from the Earth's surface. *J. Atmos. and Oce. Technol.*, 12, pp. 800-819.
- Marshall J.S. and Hitschfeld W., "Interpretation of the fluctuating Echo for randomly distributed scatterers. Part I", *Can. J. Phys.*, **31**, pp.962-995, 1953.
- D.S. Zrnic', "Estimation of spectral moments for weather echoes", *IEEE Trans. On Geosc. Electr.*, **4**, pp.113-128, 1979.
- D. Sirmans and B. Bumgarner, "Numerical comparison of five mean frequency estimators". *J. Appl. Meteor.*, **14**, 991-1003, 1975.
- Berger T. and H.L. Groginsky, "Estimation of the spectral moments of pulse trains", presented at the *Int. Conf. On Inform. Theory*, Tel Aviv, Israel, 1973.
- K. Miller and M.M. Rochwarger , "On estimating spectral moments in the presence of colored noise", *IEEE Trans. On Inf. Theory*. **16**, pp. 303-309, 1972.